UNIVERSITY OF NAIROBI

College of Architecture and Engineering

Institute of Nuclear Science and Technology

Electrohydrodynamic Atomization of Non-Newtonian liquids with high solid content: A case study for the production of powder.

By:

Gachara Charles Waithaka

S56/71527/2014

BSc. Physics

A thesis submitted in partial fulfillment for the degree of Master of Science in Nuclear Science in the Institute of Nuclear Science & Technology in the University of Nairobi, Kenya.

@ 2020

Declaration

This thesis is my original work and has not been presented for a degree in any other university.

Sign …………………................... Date: ………………………

Mr. Gachara Charles Waithaka

Supervisors' approval

This thesis has been submitted for examination with our knowledge as university supervisors.

Supervisors

Prof. Michael J. Gatari   Sign:……………….……….

Institute of Nuclear Science and Technology   Date:……………………….

University of Nairobi, Kenya

Prof. Jan C. M. Marijnissen   Sign: ……………………….

University of Florida, USA and   Date:……………………….

University of Nairobi, Kenya

Dr. Luewton Lemos Agostinho   Sign: ………………………

NHL, University of Applied Sciences   Date: …...………………….

Leeuwarden, Netherlands

Dedication

I dedicate this work to my wife, children, and my entire family. May God bless you for your unfailing heart.

Acknowledgments

First, I would like to express my gratitude to Almighty God for his help and safeguarding me to complete my thesis. My deep gratitude is due to Prof. Michael Gatari for his humble acceptance to supervise, offer guidance, and assistance during my study and research. In a special way, I thank Dr. Luewton Lemos for his enthusiastic encouragement, willingness to support, and specifically his input in developing this research work. Also, my great appreciation goes to Prof. Jan Marijnissen for his valuable advice in the field of electrospray and constructive critiques throughout the research.

Second I like to extend my thanks to my sponsors Kenya Nuclear Electricity Board (KNEB), FB OranjeWoud, Nutricia B.V, and Centre of Expertise Water Technology (CEW) the Netherlands, for their generosity in playing the role of financing my studies. The support by International Science Programme to the Institute of Nuclear Science and Technology made my studies possible.

Finally, I wish to express my heartfelt gratitude to my dear wife Lucy Wangui for her moral support and above all taking care of my sons: Stanley Gachara and Brendan Wanjohi. Nevertheless, to my classmates and those who journeyed with me while undertaking my research, in particular, Benard Bos (NHL), Koos Venema (Venema Fijnmechaniek), Jewe Schröder (Nutricia B.V), and Nahshon Nyambane, I say thanks and God bless.

Table of Contents

List of Tables

List of Figures

List of Abbreviations, Acronyms, and Symbols

EHDA	Electrohydrodynamic atomization
ID	Internal diameter
IMF	Infant milk formula
OD	Outer diameter
R	the radius of the droplet
RSD	Relative standard deviation
ε_0	electric permittivity of vacuum
q_{lim}	Rayleigh charge limit
%w/w	Percentage weight to weight
d_j	capillary diameter
$\dot{\gamma}$	shear rate
μ_0	zero shear viscosity
μ_∞	infinite shear viscosity
τ_0	yield stress
μ	dynamic viscosity
d	droplet diameter
k	consistency factor
n	flow behavior index of the liquids
r	unperturbed jet radius
v	liquid velocity
We	liquid Weber number
γ	liquid surface tension
ρ	density of the liquid
τ	shear stress

Abstract

Electrohydrodynamic atomization (EHDA) is now a well-known technique among the researchers as a potential technique for industries. The technique uses electric fields to produce mono-dispersed charged droplets and ensures controlled production. The current work investigated the intrinsic aspects of Electrohydrodynamic atomization of non-Newtonian liquids with high solid content made from infant milk formula (IMF) powder. The aim was to determine the characteristics of sprays of IMF solutions with high solid content, compare them with characteristics of EHDA atomization of Newtonian liquids, and investigate the possibilities of out-scaling. In this context, the rheology and physical characteristics of IMF solutions at different solid content were determined. Then, a study of electrospray characteristics for each IMF solution was conducted in the dripping regime and in the jetting regime using a grounded nozzle and charged counter electrode. The visualization of the spray was done using a high-speed camera with backlight illumination. The results indicated that, in the dripping regime, an electric field influences formation of modes for solid content less than 40% w/w, which can be correlated to conventional electrospray modes. In the jetting regime, when the simple jet mode was operated at whipping break up produced small droplets compared to varicose break up. In regards to out-scaling the atomization of 55% w/w IMF solution, a thermal jacket system and a single nozzle with four orifices at 300 μm internal diameter each was manufactured. With this nozzle configuration, a throughput of ~3 L h^{-1} was achieved and droplets with broad size distribution (13 μm ≤ d ≤ 1900 μm) obtained. This was attributed to the whipping break up mechanism of the IMF electrospray jets. Further studies which should include carrying out tests in an evaporator with an aim of determining the properties of the product were recommended.

Chapter 1

INTRODUCTION

1.1. Background

Recently, most industries have shifted interest to processing products in powder form relative to liquid or solid form. Some of these industries include dairy, pharmaceutical, agriculture, and paint. Powder products are stable, and they lower storage and transportation costs (Schuck et al., 2012). To obtain the product in powder form a method known as spray drying is widely used. The technique involves atomization of concentrated feed liquids and complete or partial vaporization of water from the droplets to get the desired powder. Although the use of the high solid content is reported to be beneficial in terms of the energy input (Bouman et al.1993), it poses a major challenge with regard to efficient evaporation (Fox et al., 2010). For instance, the formation of dry patches and sugar crystallization has been attributed to the wide spectrum of droplets in the spray drying of feed liquids of high solid content (Kelly and Fox, 2016; Wu et al., 2014). Therefore, spray drying technique highly depends on the atomization process and the spray characteristics of feed liquid, in particular the droplet size, size distribution, and dispersion.

The atomizers that are mostly used in the production of dairy powders are the pressure and the swirl disk atomizers (Kelly and Fox, 2016). In contrast to the above mentioned conventional mechanical atomizers, Electrohydrodynamic atomization (EHDA) or electrospraying is well known to produce small droplets with narrow size distribution (Yurteri et al., 2010). The setup for electrospraying consists of an infusing pump connected to a charged capillary nozzle relative to a counter electrode (Scheideler and Chen, 2014). The electric field created at the nozzle exit and the counter electrode play the major role in liquid atomization.

Typically, in uncharged situation three distinct hydrodynamic regimes can be observed when a liquid is dispensed through a nozzle at different flow rates. The regimes are as follows: the dripping regime that is characterized by formation and detachment of a single droplet at the exit of the nozzle, the jetting regime that is characterized by formation of a continuous jet that originates from the capillary exit and breaks into droplets downstream, and the transition regime that occurs between the dripping and the jetting regime (Ambravaneswaran et al., 2000; Clanet and Lasheras, 1999; Agostinho et al., 2012). The application of an electric field in the dripping regime leads to obtaining conventional EHDA modes (i.e. dripping, micro-dripping, intermittent, spindle, cone jet or multi-jet) as elucidated in detail by Cloupeau and Prunet-Foch (1990) and Jaworek and Sobczyk (2008). Similarly, the application of an electric field in the jetting regime and the transition regime lead to another EHDA mode known as the simple-jet mode (Agostinho, 2013). Therefore, the electrically charged droplets enhances a good dispersion and an oppositely charged system can be implemented to control their deposition.

The characteristics of EHDA modes and the generated droplets are determined by a number of parameters that are categorized into liquid properties and the operation parameters (Chen and Pui,1997; Yurteri et al., 2010). The liquid properties include surface tension, viscosity, conductivity, and density while operation parameters are the liquid flow rate and the applied electric potential (Camelot et al., 1999). Hence, a complete description of electrospray modes entails generated droplet size, their size distribution, spray envelope, and droplet charge. In the literature, it has been demonstrated that a wide range of liquids with varying characteristics can be electrosprayed as pointed out in a review by Grace and Marijnissen (1994). This, has further enhanced the application of the EHDA technique in medicine encapsulation (Orlu-Gul et al., 2014), Micro-and nanoparticles production (Xie et al., 2006),

nanofibers production (Reneker and Yarin, 2008), thermal desalination (Agostinho et al., 2012) and remains an active area of research.

In this work, the EHDA characteristics of non-Newtonian liquids with high solid content are investigated. The study utilized formulations made by rehydrating infant milk formula (IMF) powder. To obtain results useful for realistic industrial conditions, the study used an experimental set-up consisting of a thermal jacket feed system that was connected to an electrospray system. The electrospray characteristics tests were conducted with IMF solutions containing dry solid contents varying from 10% w/w to 50% w/w and the industrial application tests investigated using the 55% w/w IMF solutions.

1.2. Problem Statement

Increased solid content in the feed liquid leads to an increase in viscosity, and, in turn, it exhibits non–Newtonian features (Bienvenue et al., 2003; Trinh et al., 2007). Additionally, concentrating the feed liquids changes the properties such as the density, surface tension, and conductivity, that are known to influence characteristics of electrospray (Chen and Pui, 1997). The ease in flow and certainty in properties foster more studies to report on electrospray modes of Newtonian liquids than about electrospray applications on non-Newtonian ones, especially those that involve increased solid content. Additionally, most of the existing droplet scaling laws that are used to characterize an electrospray system cannot be applied for other non-Newtonian liquids (Zhang et al., 2006). Since atomization of liquids with high solid content are frequently encountered in powder processing industries, and it is often difficult to obtain the required droplet size that might be obtained with EHDA, hence the success of the current study.

1.3. Objectives

1.3.1. General Objectives

The general objective is to investigate the overall characteristics of EHDA with non-Newtonian liquids formulated from high solid content and compare the function of such sprays with the current knowledge of Newtonian liquids.

1.3.2. Specific Objectives

The specific objectives are:

I.   To determine the rheology and physical properties of the IMF solutions with different solid content.

II. To study the electrospray characteristics (droplets formation, droplets sizes) of the IMF solutions in the dripping regime

III. To study the electrospray characteristics (droplets formation, droplets sizes, and spray envelope) of the IMF solutions characteristics in the jetting regime.

IV. To assess the suitability of the EHDA technique in industrial applications for IMF solutions with solid content >55% w/w.

1.4. Justification and Significance of the Study

The optimum goal of liquid atomization in every application is to create the required droplet size while minimizing energy input. An increased solid content (e.g. >50% w/w) during spray drying decreases the amount of water and consequently the energy requirement for drying (Bouman et al., 1993; Fox et al., 2010). In addition, the industrial interest is the knowledge towards the control of the atomization process during the production. Atomization and spray dispersion pattern control the size, morphology, and flowability of powder products and further determines the design of evaporators (Kelly and Fox, 2016; Schuck et al., 2012). Therefore, EHDA becomes a choice of studying such liquids with high solid contents since it is known for producing droplets with a narrow size distribution and good spray dispersion that can be controlled due to the

charged droplets. To the scientific community the study will provide valuable data about the EHDA atomization of such liquids with high solid content.

1.5. Scope and Limitation of the Study

The study makes use of infant milk formula (IMF) powder and water to formulate solutions with different solid content ranging from 10% to 55% w/w. The study of electrospray characteristics for IMF solutions and its outscaling possibilities are carried out in a laboratory scale. The analyses of the images are limited to droplets formation in the dripping regime and to droplets sizes, sizes distributions, and spray dispersion in the jetting regime.

Chapter 2
LITERATURE REVIEW

2.1 Characterization of Liquids

The study of the behavior of materials or substances under deformation is attributed to the science of Rheology (Barnes, 2000). Rheology involves characterization of the flow behavior of the materials and determination of their structure in terms of viscosity and elasticity (Larson, 1999). Rheologically, materials have been classified into either elastic, viscous or viscoelastic depending on their reaction to an applied force. For instance, ideal solids are termed elastic since when a deformation force is applied, they store the energy imposed and recover their initial state upon release of stress (Barnes, 2000). Ideal gases and liquids are described as viscous, which means the deformation energy makes them flow and the energy is transformed into heat and their state is irreversible (Barnes, 2000). Finally, some materials exhibit both elastic and viscous properties and therefore are termed as viscoelastic

For liquids, the knowledge of their flow behavior is described using rheograms. By definition, a rheogram is a plot of shear stress (τ) versus shear rate ($\acute{\gamma}$) (Chhabra and Richardson, 2008). To obtain this relationship the liquid is either confined between a cone and a plate, two coaxial cylinders, or two parallel plates and one part is slowly moved (Macosko, 1994). Because of the liquid viscosity, this movement gives rise to a frictional force that opposes the applied force (Chhabra, 2006). Eventually, the liquid is subjected into a shear flow in which the intermediate layers moves at different velocity. Figure 2.1 illustrates a shear flow of a liquid between two parallel plates when a force (F) is applied to the top plate. The plates have the same surface area (A) and are separated by a distance (dy). The resultant shear stress is expressed by the force per unit area while the shear rate is described by the velocity gradient (Chhabra, 2006). Both relations are shown in equation (2.1) and (2.2) respectively.
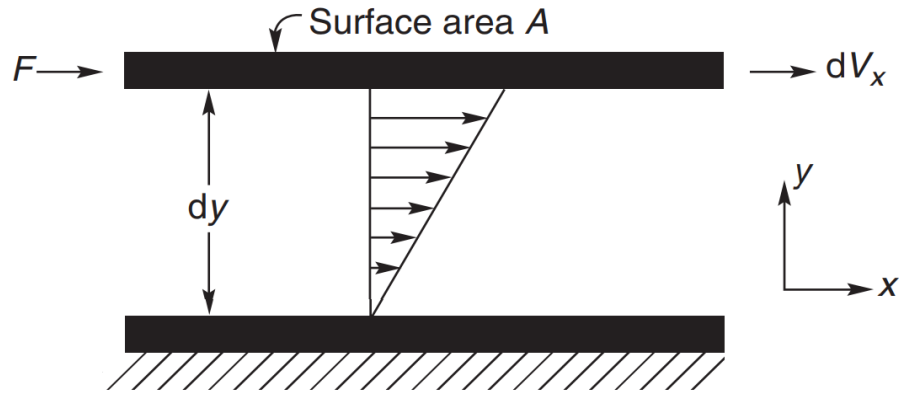
Figure 2.1: A schematic showing of shear flow of liquid between two parallel plates (Adopted from Chhabra and Richardson, 2008)

$$\tau_{yx} = \frac{Force}{Area} \left(\frac{N}{m^2} = Pa \right) \qquad \text{Eqn. 2.1}$$

$$\dot{\gamma} = \frac{dv_x}{dy} \left(\frac{m/s}{m} = s^{-1} \right) \qquad \text{Eqn. 2.2}$$

2.2. Newtonian Liquids

Most common liquids such as water, mineral oil, ethanol, and glycerol are examples of Newtonian liquids. As illustrated in the general flow curve presented in Figure 2.2, the flow behavior of Newtonian liquids shows a linear relationship between shear stress and shear rate which is described by equation (2.3) (Chhabra, 2006), where the constant of proportionality (μ) is the liquid dynamic viscosity. The dynamic viscosity describes the resistance of a liquid to flow or to deformation and depends on the liquid properties at a specified temperature (Chhabra and Richardson, 2008). In rheology, the ratio between

the shear stress and the shear rate defines the viscosity of a liquid as expressed in equation (2.4).

$$\tau = \mu \times \dot{\gamma}\,(Pa)$$
<div align="right">Eqn. 2.3</div>

$$\mu = \frac{\tau}{\dot{\gamma}}\,(Pa \bullet s)$$
<div align="right">Eqn. 2.4</div>
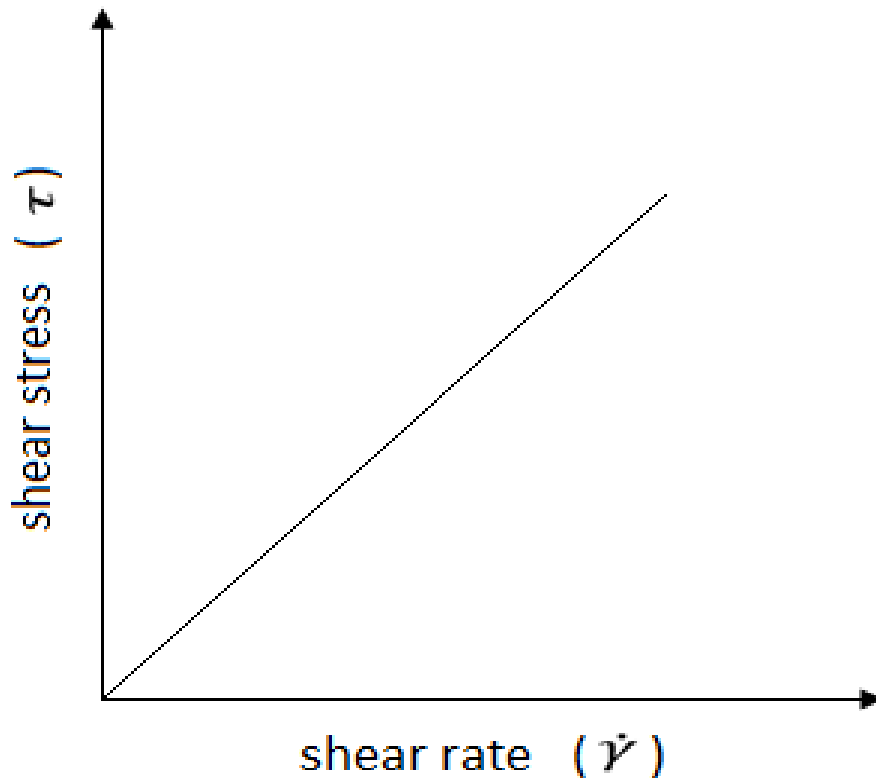
Figure 2.2: Schematic showing flow behavior of Newtonian liquids (adopted from Chhabra, 2006).

2.3. Non-Newtonian Liquids

These liquids are often encountered in industrial processes and occur in the form of emulsions, suspensions, colloids and polymer solutions (Stading, 2010). Their flow characteristics differ from those of Newtonian liquids due to their complex structure and deformation effects (Chen, 2009). One of the intrinsic aspects associated with the non-Newtonian liquid is nonlinearity between shear stress and shear rate (Chhabra and Richardson, 2008). The behavior of the non-Newtonian liquids is characterized with an apparent viscosity defined as in equation 2.4 for Newtonian liquids, but at a particular shear rate and temperature (Trinh et al., 2007). Below is a brief description of various non-Newtonian liquids.

2.3.1. Pseudoplastic Liquids or Shear Thinning Liquids

Pseudoplastic (or shear thinning liquids) are characterized by an apparent viscosity that decreases with increasing shear rate (Schramm, 1994). Examples include dilute polymer solutions, creams, salad dressings, and shampoos. It has been observed that the flow curve of some shear thinning liquids shows regions with a constant viscosity (form plateaus) at low values and high values of shear rates as shown in Figure 2.3. In this case, the corresponding values of the apparent viscosity are known as zero shear viscosity (μ_0) and infinite shear viscosity (μ_∞) respectively (Chhabra and Richardson, 2008).These values are obtained by plotting the log of the apparent viscosity versus the log of the shear rate.
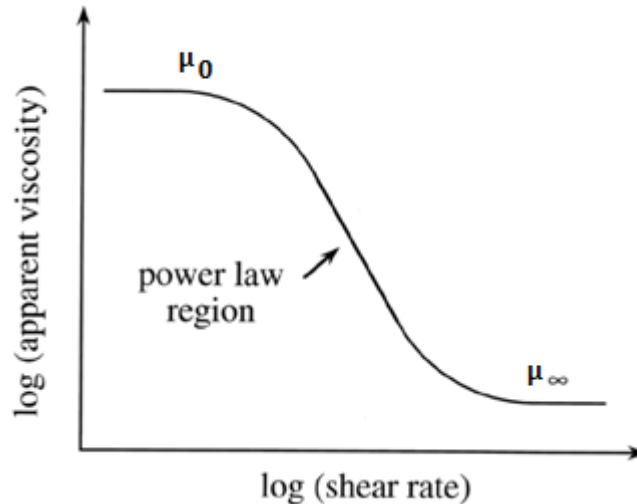
Figure 2.3: Schematic showing zero and infinite shear viscosity (adopted from Barnes, 2000).

2.3.2. Dilatants or Shear Thickening Liquids

A liquid is said to be dilatants or shear thickening if its apparent viscosity increases with increasing shear rate. The shear thickening behavior is observed in wet sand and concentrated starch or polymer solutions.

2.3.3. Viscoplastic Liquids

Viscoplastic liquids are characterized by a yield stress (τ_0) that has to be exceeded before the liquid flows. Their characteristic flow curve is either linear or nonlinear. Liquids with a yield stress and a linear flow curve are termed Bhigham-plastic, and therefore they are defined by a constant value of plastic viscosity. On the other hand, Liquids with a yield stress and a nonlinear curve are called yield pseudoplastic. Some examples of viscoplastic liquids are drilling mud, ketchup, toothpaste, yogurt, and blood. Figure 2.4 shows the characteristic flow curves for a Newtonian liquid and for the above described non-Newtonian liquids.
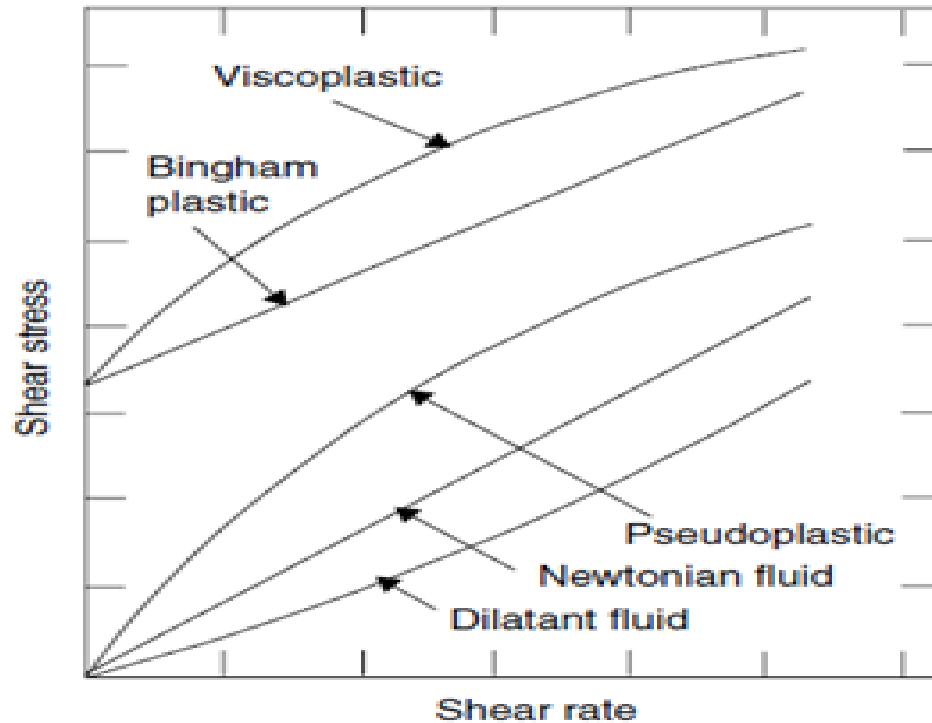
Figure 2.4: Characteristics flow curves for a Newtonian liquid and different types of non-Newtonian liquids (adopted from Chhabra, 2006).

2.3.4. Thixotropic and Rheopectic Liquids

Thixotropic liquids are defined the same as pseudoplastic liquids in the sense that, upon subjecting to a constant shear rate, its apparent viscosity decreases with time of shearing. However, their flow curve exhibits a hysteresis loop as the shear rate is decreased. Rheopectic liquids are defined same as dilatants liquids but also their flow curve shows hysteresis loop. The shape of the hysteresis loops for both the Thixotropic and rheopectic liquids depends upon the time of shearing and kinematic history of the liquid. Some examples include mayonnaise, brush paint and margarine. Figure 2.5 is a general rheogram for thixotropic and rheopectic liquids
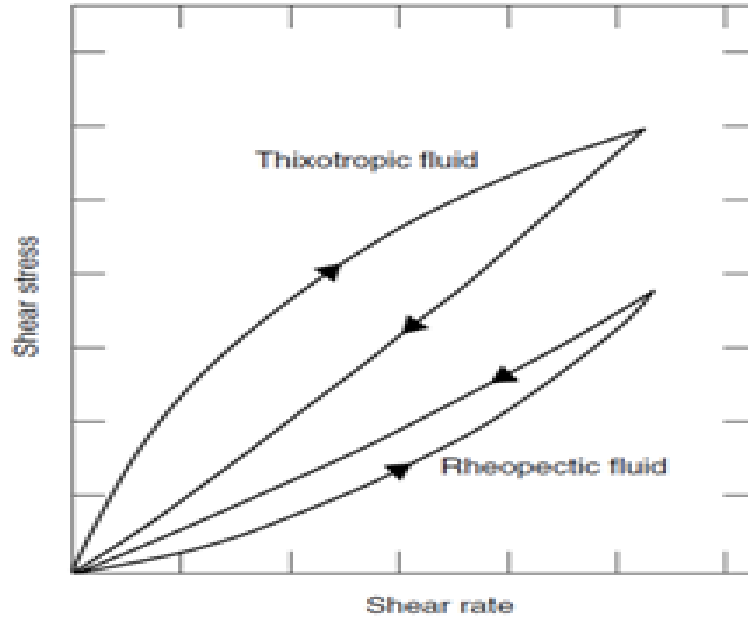
Figure 2.5: General flow curve for thixotropic and rheopectic liquids (adopted from Chhabra, 2006).

2.3.5. Other Physical Aspects of Non-Newtonian Liquids

In addition to the nonlinearity of shear stress and shear rate, other physical aspects are sometimes observed for non-Newtonian liquids. Some examples are Weissenberg effect, self-siphoning, extrusion or Barus effect (Boger and Walters, 2012). Weissenberg effect also known as rod climbing is a phenomenon where liquid climbs up a rotating rod dipped in it. The self-siphoning effect is a physical behavior that occurs when an open tube is placed inside a container with non-Newtonian liquids for the purpose of siphoning. Then, upon lifting the tube on the surface of the liquid, the siphoning action continues without deforming the structure of the surface. Extrusion or Barus effect is a phenomenon that occurs when a non-Newtonian liquid is squeezed through a nozzle and it is observed to swells as its exits.

2.4. Rheological Models

In order to interpret the liquid rheogram to useful information with regard to flow characteristics of liquids, several mathematical models have been presented in literature (Chhabra, 2006). Examples of these models include the Power law or Ostwald-De Waele model, the Herschel-Bulkley model, the Ellis and Eyring, the Casson and the Bingham models. For non-Newtonian liquids with high solid content especially that relate to reconstituted milk, the two models presented below are mostly applied (Bienvenue et al., 2003; Trinh et al., 2007).

2.4.1. Power law or Ostwald Model

This model describes the flow curve of pseudoplastic (shear thinning) liquids (Chhabra, 2006) and it takes the form:

$$\tau = k \times \dot{\gamma}^n$$

Eqn. 2.5

Where K (Pa.s^n) is the consistency factor that gives an idea of viscosity, and n is the flow behavior index of the liquid. The power law gives the flow behavior as follows: when (n=1), the equation reduces to the Newtonian equation, and thus K becomes the viscosity, when (n< 1) it describes pseudoplastic and for (n>1) it expresses dilatant behavior. It is worth noting that rheological properties for different liquids can only be compared if the liquids have the same flow behavior index.

2.4.2. Herschel-Bulkley Model

This model has three parameters namely: yield stress, consistency factor, and flow behavior index. Therefore, it is applied to fliquids with nonlinear behavior and which has a yield stress. In addition, the equation can transpose into the Power law when the

yield stress(τ_0) is zero and to the Newtonian law when n =1 and $\tau_0 = 0$. The Herschel-Buckley equation is given as:

$$\tau = \tau_0 + k \times \dot{\gamma}^n$$

Eqn. 2.6

2.5. Liquid Atomization

Liquid atomization is the mechanism under which a bulk liquid is disintegrated into a spray of small droplets (Lefebvre, 1988). The resultant spray of the fine droplets in the surrounding gas is known as aerosols (Meesters et al., 1992). Generally, the atomization process is classified depending on the energy used to create disturbances on a liquid jet. For example, pressure atomization uses pressure energy, ultrasonic atomization uses vibration energy, rotary atomization uses centrifugal energy and Electrohydrodynamic atomization uses electrostatic energy (Ashgriz and Yarin, 2011). Among these, Electrohydrodynamic atomization or electrospray is known for its ability to produce droplets in the nano and micrometer size range (Marijnissen, 2004). With regard to dairy powder production, most of the atomizers used are pressure and swirl disk atomizers (Kelly and Fox, 2016).

2.5.1. Background of Liquid Break-up

The first work to report on jet break-up probably dates back to the 15th century by Leonardo da Vinci in his book 'the *Codex Leicester'*. da Vinci noted that the detachment of the droplets from a stream of water was governed by droplet inertia overcoming the surface tension (Eggers and Villermaux, 2008). Later in 1849, Plateau established that cylindrical jets were unstable to surface instabilities which had a wavelength larger than the jet radius by a factor of 2π. In 1879, Rayleigh extended this description for an inviscid liquid jet subjected to small axis symmetric varicose instabilities. The scholar demonstrated that the disintegration of the liquid jet into droplets was governed by the fastest growing varicose instabilities (Hartman et al., 1999). The wavelength of the

fastest growing instabilities, which is often termed as the optimal or dominant wavelength, was shown to be $4.51d_j$ (Lin and Reitz, 1998). After break up, this liquid ligament of length $4.51d_j$ forms a spherical droplet in which the size can be predicted on the basis of a sphere of equal volume as in the relation below:

$$4.51d_j \times \left(\frac{\pi}{4}\right)d_i^2 = \left(\frac{\pi}{6}\right) \times d^3 \qquad\qquad \text{Eqn. 2.7}$$

$$d = 1.89d_j \qquad\qquad \text{Eqn. 2.8}$$

Where d is the droplet diameter and d_j is the jet diameter.

According to Lin and Reitz (1998), the works of Rayleigh form the basis on the study of axis-symmetric capillary jet break up or Rayleigh regime at the liquid-gas interface.

2.5.2. Droplets Formation Regimes

When a liquid is dispensed from the end of a capillary nozzle into a quiescent gas, at low velocity, a drop grows quasi-statically until its weight overcomes the surface tension forces and adhesion forces (with capillary nozzle if applicable). This mechanism of a single droplet breaking up or dripping from the nozzle exit is referred to as dripping regime (Ambravaneswaran et al., 2000). If the jet velocity is increased beyond a certain value, a continuous jet is formed at the nozzle tip which breaks-up into droplets downstream (Agostinho et al., 2012; Clanet and Lasheras, 1999). The above descibed droplet formation mechanism is known as the jetting regime. The transition from dripping into jetting regime is referred to as transition or dripping faucet regime ((Ambravaneswaran et al., 2004). Figure 2.6 below shows the physical distinction between the three regimes using a water jet (adopted from Agostinho et al., 2012.
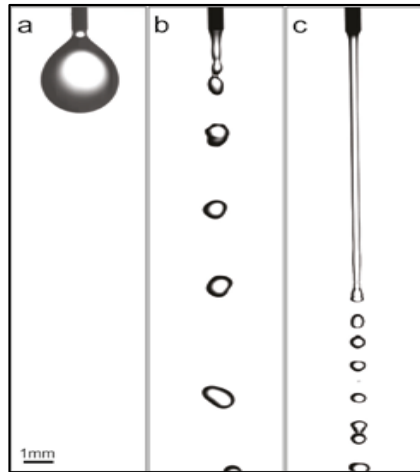
Figure 2.6: Schematic showing droplet formation in dripping regime (a), transition regime (b), and jetting regime (c) using water (adopted from Agostinho et al., 2012).

Clanet and Lasheras (1999) distinguished the transition from dripping to the jetting regime by considering the jetting to occur when the intact length was about twenty times the nozzle radius. Van Hoeve et al. (2010) observed that the lower critical velocity (v) for transition from dripping to jetting can be determined by the ratio of kinetic energy and surface tension of the liquid known as the liquid Weber number (We) given by below formula:

$$We = \frac{\rho v^2 r}{\gamma}$$
<div align="right">Eqn. 2.9</div>

Where r is the unperturbed jet radius, γ is the surface tension of the liquid and ρ is the density of the liquid.

The jetting regime was found to occur at:

$$We = \frac{\rho v^2 r}{\gamma} \succ 4 \qquad\qquad \text{Eqn. 2.10}$$

Agostinho et al. (2012) experimentally found that using water the three regimes occur at We < 1 for dripping, 1≤ We< 4 for the transition regime and We ≥ 4 for the jetting regime.

Other regimes that account for aerodynamic effects have been reported in the literature (Chigier and Reitz, 1996). These include first wind induced regime, second wind induced regime, and atomization regime (Lin, 2003). These regimes are not going to be considered in this work and therefore it will not be discussed in detail. For further reading the reader is referred to the work of Lefebvre (1988).

2.5.3. Non-Newtonian Effects on Liquids Jets

There is vast literature mentioning the different aspects of atomization of the non-Newtonian liquid. Some of these aspects which could be relevant for this work are covered here. The pioneering work of Middleman (1965), Goldin et al. (1969), and Bousfield et al. (1986) showed that dilute polymer jets are stable with respect to capillary disturbances in relation to Newtonian liquids. Such characteristics has been attributed to the damping effect caused by polymer additives to the propagation of capillary disturbances (Mun et al., 1998). Other studies have shown that with a high concentration of polymer additives, the jet can transform from varicose break-up to droplets interconnected by a thin thread known as 'beads on a string' morphology (Bhat et al., 2010; Christanti and Walker, 2002). A review of the effects of visco-elasto–plastic on capillary instabilities was presented by Mckinley (2005). A numerical study on the dripping regime for polymer solution performed by Yildrim and Basaran (2006) demonstrated that for a particular liquid rheology (i.e. pseudoplastic or dilatant) there exists a range of flow rates (or Weber numbers) in which satellite droplet does not occur. For the case of transition from dripping to the jetting regime, Clasen et al. (2009)

developed a dynamic theory and explained how elastic effects modify this transition due to a phenomenon they called 'gobbling'. Gobbling was shown to be a situation where the terminal drop 'greedily' swallows several small successive droplets before it detaches.

2.6. Electrohydrodynamic Atomization (EHDA)

Electrohydrodynamic atomization or electrospray is a process where a liquid jet is broken-up into mono-dispersed droplets under the influence of implemented electric stress (Jaworek and Sobczyk, 2008). The above mentioned phenomenon was first studied experimentally using water and glycerol by Zeleny in 1917. With the aid of photographic images, fine droplet formation from a conically shaped meniscus were observed (Zeleny, 1917). Later, Taylor (1964) provided a theoretical description of the conical meniscus shape of the electrified droplet. The above mentioned functional mode was then named as the 'Taylor cone' in honor of the contribution (Cloupeau and Prunet-Foch, 1989).

Extensive studies have been conducted with the aim of understanding the control parameters of the electrospray. For example, Mutoh et al. (1979) investigated a range of feed liquid conductivity. Smith (1986) reported on effects of liquid properties and operation parameters, De la Mora and Loscertales (1994) and Ganan-Calvo et al. (1997) presented scaling laws with regard to droplet size and emitted current, and Hartman et al. (1999) took another approach to develop scaling laws and a model to calculate the shape of a cone in cone-jet mode, electric field in and outside the cone, and the surface charge density on the cone and jet.

The EHDA technique has been employed in various applications such as mass spectroscopy (Fenn et al., 1989), propulsion systems (Gamero and Hruby, 2001; Hendricks, 1962), drug delivery (Ijsebaert et al., 2001), and encapsulation (Xie and

Wang, 2007). It has been possible to apply EHDA in various field due to the use of different functional modes that have been described and explained by Cloupeau and Prunet-Foch (1990), Grace and Marijnissen (1994), Jaworeck and Krupa (1999), and Jaworek and Sobczyk (2008). The most observed mode is the cone-jet mode. Other known modes are the dripping, micro-dripping, spindle jet, intermittent cone-jet, and multi-jet (Yurteri et. al, 2010).

Even though former works have reported about a functional mode associated with high flow rate known as the simple-jet mode, it was not sufficiently characterized till the recently published by Agostinho (2013). The author established its operation window and characterized the mode in terms of droplet size, size distribution droplet charge, spray envelope and break-up length. The author showed that the mode can be applied successfully in desalination and in processes that require large throughput.

Most of the reports found in the literature involves electrospray characteristic of low viscous or viscous Newtonian liquids (i.e. water, ethanol and glycerol). The interest in the technique has led to researchers reporting on the characteristics and functioning of EHDA with non-Newtonian liquids. Examples are Zhang et al. (2006) who used high viscous silicone oil with viscosity ~58,560 mPa s (in literature considered as pseudoplastic) and electrical conductivity ~10^{-9} S m^{-1} to obtain micro threads of size range 9≤d≤170 µm, Pancholi et al. (2009) electrosprayed a chitosan suspension on a stable cone jet and they reported about the effects of liquid viscosity and surface tension on particle diameter, Moghadam et al. (2010) used different high viscous, pseudoplastic (shear thinning) non-Newtonian polymer solutions, and derived scaling laws relating the produced droplet size with the Weber and the Reynolds numbers and the electric field intensity. Such interest is justified by the fact that many industrial/commercial processes are based on non-Newtonian liquids, e.g. drug or food encapsulation, spray drying, spray

painting, etc. However, the literature reporting the intrinsic aspects of the application of EHDA atomization of solutions with high solid content (>30% w/w) is lacking.

2.6.1. EHDA Principles

A simple setup for electrospraying consist an infusing pump, a syringe connected to capillary nozzle, a counter electrode, and a high voltage power supply as shown in Figure 2.7.
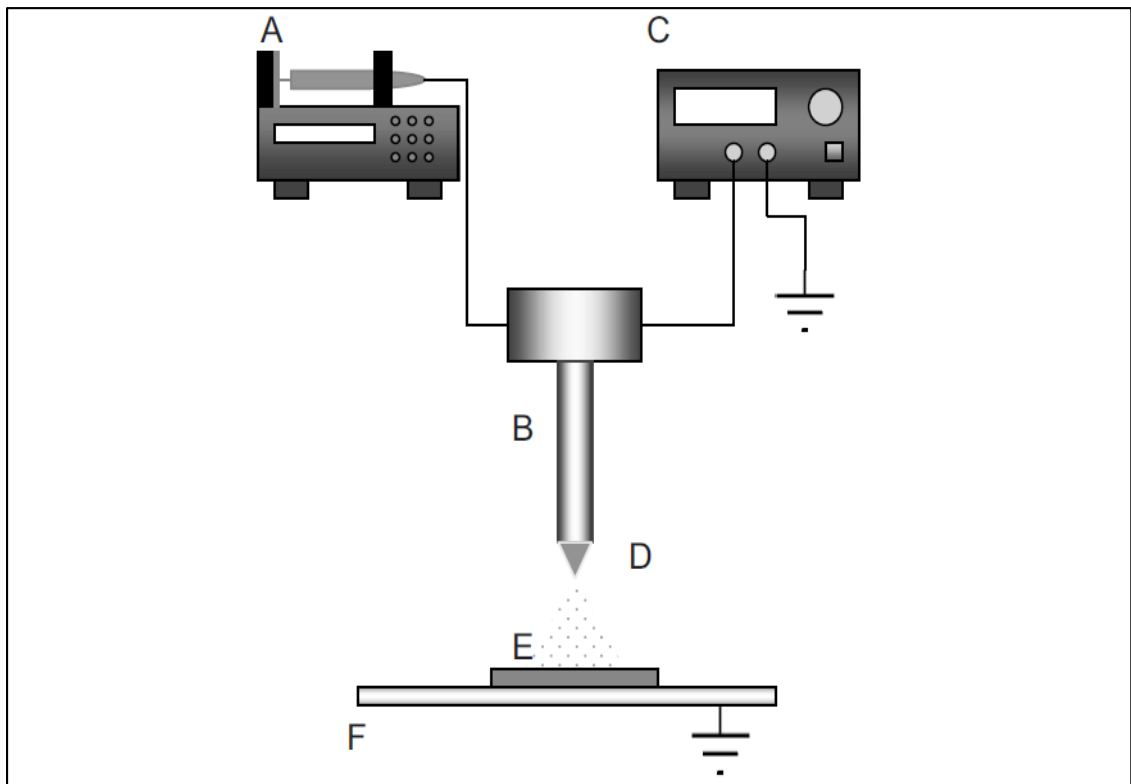
Figure 2.7: EHDA set-up A) An infusing pump fitted with a syringe, B) Capillary nozzle, C) A high voltage power supply, D) A Taylor cone and spray of droplets, E) Earthed counter electrode, and F) Earthed support (Adopted from Yurteri et al., 2010).

The liquid is discharged through the nozzle at a flow rate of the order mL h^{-1} while an electric potential in the range of 1-10 kV is applied between the nozzle and counter

electrode (Yurteri et al. 2010). The applied electric potential creates an electric field as well as induces surface charge around the tip of the nozzle. As the liquid discharges at the tip, it experiences an electric stress. Depending on the flow rate and the electric field strength, a balance between electric normal stress and the liquid surface tension can result in the formation of a Taylor cone (Hartman et al. 2000) The formation of a cone causes the acceleration of the liquid and the concertation of surface charge at the apex of the cone and an eventual emergence of jet at the tip of the cone (Camelot et al. 1999). The jet proceeds downward and breaks into charged droplets. The size of the produced droplets and the liquid surface tension governs the maximum charge that a droplet can attain, which is known as Rayleigh limit defined in equation (2.12). Droplet charge limit causes instability of the droplets and further spontaneous evaporation of the droplets with different sizes.

$$q_{\lim} = 8\pi (\varepsilon_0 \gamma)^{1/2} R^{3/2}$$
<div align="right">Eqn. 2.11</div>

Where $q_{\lim}$ is the Rayleigh charge limit, ε_0 is electric permittivity of vacuum, γ is the liquid surface tension, and R is the radius of the droplet.

The above discussed functional EHDA mode is known as the cone jet mode. Other functional modes are discussed in the next section.

2.6.2. Electrospray Modes

For a particular liquid, different combinations of electric field and flow rate result in different spray modes with different droplet size characteristics (Yurteri et al., 2010). As pointed out earlier, Cloupeau and Prunet-foch (1990) were probably the first authors to describe and explain the different electrospray modes observed. Different authors have extended the description of modes by developing a stability map relating to potential and flow rate where the modes can be realized, and they include Agostinho (2013) and Grace and Marijnissen (1994). Figure 2.8 shows an example of such diagram.
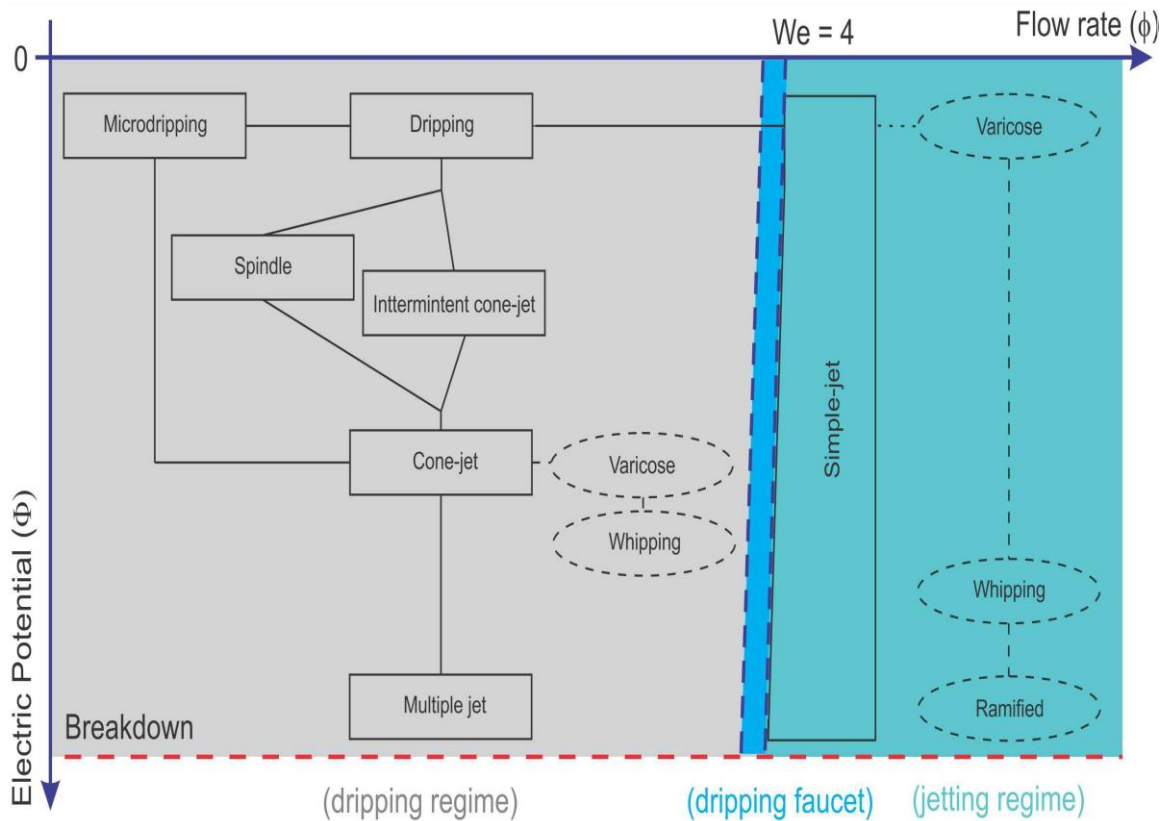
Figure 2.8: Electrospray modes at different droplet formation mechanism versus the applied potential (adopted from Agostinho, 2013).

Agostinho (2013) observed that the EHDA modes are realized at three different droplet formation mechanisms which can be differentiated by liquid Weber number (We). Namely the dripping regime (We< 1), the dripping faucet regime (1≤ We <4), and finally the jetting regime (We≥4).

In the dripping regime, the dripping mode is observed when an applied electric potential is sufficient enough to accelerate the emission of the droplet from the tip of the nozzle (Notz and Basaran, 1999). The mode constitutes the production of droplets larger than the nozzle diameter at regular time intervals (i.e. low frequency till 500 Hz). If the flow

rate of the liquid is lowered and the applied potential is increased the micro-dripping mode is observed, in which the applied electric potential tends to strip droplets from the apex (Shiryaeva and Grigor'ev, 1995). The droplet size ranges from nano to micro size range and their size distribution is often monodispersed (Jaworek and Krupa, 1999). If flow rates and applied potential are increased, either spindle mode or intermittent cone-jet mode can be observed. The spindle mode is characterized by a cycle that starts with a relaxed meniscus, followed by transformation of the meniscus into a conical shape with a jet emanating from the apex, the jet breaking into fine droplets, the detachment of a spindle-like ligament from the cone and finally the meniscus retracting while the ligament proceeds to break up into a large droplet and several small droplets (Yurteri et al., 2010). Further, the authors note that in the intermittent cone-jet mode the cycle starts with a hemispherical meniscus that transforms into a cone, followed by formation of a stable jet and finally a cone relaxing into a meniscus. The jet forms a spray of fine droplets while the recovery of the meniscus causes the jet to collapse into several large droplets.

If the electric potential is increased, a balance between the normal electric field force and the surface tension of the droplet may be achieved. As a result, the droplet meniscus is deformed into a conical shape with a jet emanating from its tip which consequently breaks up into a spray (Meesters et al., 1992). The mode is referred to as cone-jet mode and is known by producing droplets much smaller than the nozzle diameter with narrow size distribution (Marijnissen, 2001). The magnitude of the applied electric potential influences the breakup of the jet, whereby the jet can either undergo a varicose or whipping break-up (Cloupeau, 1990; Hartman et al., 2000). With higher electric potential, several jets emanating from the meniscus may form and multi-jet mode occurs.

An EHDA mode that has been characterized starting at a point where We = 3 in the transition regime to point where We = 21 in the jetting regime, is the simple jet mode (Agostinho et al., 2012). Starting with uncharged jet, the liquid flow rate is increased till a permanent jet is formed directly from the nozzle exit which breaks up due to Rayleigh-Plateau instabilities. An application of an electric field result in an EHDA mode known as the simple jet mode (Agostinho, 2013). According to the author, the simple jet mode is associated with several characteristics. First, in comparison to uncharged jets the action of the electric field result into a reduction of the droplets average diameter of about 20% of the primary droplet. Second, for a particular flow rate, the applied potential causes the droplets to disperse forming a spray envelope (a dispersion angle of 10° was considered as the initial point of reference). Third, increasing the flow rate and applied potential the jet was observed to change from the varicose break up into the whipping break up with the production of poly-dispersed droplets. Lastly, the simple jet mode can produce monodispersed sprays when operated in the transition regime and at an appropriate electric potential. However, in relation to the cone-jet mode, the droplet size in the simple jet is in the range of the nozzle diameter. Furthermore, due to increased flow rate and well-developed spray envelope, this mode was recommended for evaporation applications that require massive production such as desalination and spray drying.

Chapter 3

METHODOLOGY

3.1 Materials and Methods

This chapter highlights the methods used to conduct the experiments in this work. Basically, it can be divided into IMF solution preparation, IMF solution characterization, the electrospray experiment set up, and analysis.

3.2 IMF Solutions Preparation

Solutions with different solid content were prepared by dissolving the IMF powder in water at temperature of 50 °C. The mixture was mechanically stirred using a magnetic stirrer until the powder was evenly dissolved. Heating was done for 8 to10 minutes to mimic pasteurization and ensure complete dissolution of lactose. A re-circulating hot water bath was used to maintain the IMF solution at the specified temperature and heating process. The solution was then transferred into a solution chamber maintained at 55 °C to allow long storage and avoid denaturing of protein.

3.3 IMF Solution Characterization

The physical properties of the IMF solutions were carried out at 70 °C which presents the real temperature for atomization.

3.3.1 Rheology

The rheology of the solutions was determined using rotational viscometer (RM100, Lamy®). The system consists a rotating bob of a diameter 25 mm and cylinder with a holding capacity of 20 mL. The viscosity range for this system is 5-150,000 mPa s and a shear rate range of 0.38 s^{-1} to 1500 s^{-1}. The rheomat is coupled with a temperature probe PT100 and a thermostating hot water bath that ensured the solution was kept at constant temperature during measurement. The IMF solutions were subjected to a shear rate ranging of from 0.38 s^{-1} to 1340 s^{-1} and the apparent viscosity at each shear rate was

recorded. The observed data was used to draw the flow curves. The Power law model was transformed into logarithmic as in equation (3.1) and data was fitted to determine the consistency coefficient (K) and the flow behavior index (n).

$$\log_{10}(\tau) = \log_{10} k + n \log_{10} \dot{\gamma}$$
Eqn. 3.1

3.3.2 Other Physical Properties

The surface tension of the IMF solutions at different solid content was measured using with K6 Kruss tensiometer (kruss GmbH, Germany), which employs the Du Nouy ring method. The tensiometer consisted of a platinum ring (R10111) as a measuring probe and a 50 mL beaker. The measuring range was1 to 90 mN/m with a resolution of 0.5 mN/m. The surface tension was determined by submerging the tensiometer ring in the IMF solutions and pulling it slowly out of the solution. The force required to raise the ring from the solution surface (just before the breaking of lamella) was measured and recorded. Three measurements were carried using fresh IMF solutions and the average is reported. The tensiometer was Calibrated using tap water (71 mN/m).

The conductivity of IMF solutions at different solid content was determined directly with a CDC401 (Hach®) conductivity probe. The conductivity probe is coupled with a temperature sensor. The measurement range is 0.01 μS/cm -200 mS/cm with an accuracy of 0.5% of the reading. The probe is designed to measure the resistance of the solution between electrodes, which are 1 cm apart. The measurements were recorded after the readings stabilized. This was repeated three times and the average value was reported. The probe was calibrated using milli-Q water (18 MΩ cm).

The density of the IMF solutions was determined by constant volume method; the measurements were done using a standard density flask of 50 mL. The mass of an empty

and filled density flask was measured using a precision balance (model Kern 572-35) with accuracy of (0.01 g). The measurements were done in triplicate and the average value was reported.

3.4 Electrospray Experiment

Figure 3.1, shows the experiment set up used. The setup contains two chambers maintained at different temperature, an EHDA system, and a computerized data acquisition system. The chamber maintained at 55 $^{\circ}$C, is the IMF solution chamber whose purpose is to allow long spraying period without flocculation and denaturing of the protein. The compressed air channel connected to the solution chamber was used to provide a positive pressure to aid the flow of the solution. The stirrer was used to prevent the thickening of the IMF solution, and the temperature probe monitored the temperature of the solution. The second chamber maintained at 75 $^{\circ}$C was used to ease the flow and allow the IMF solution to attain atomization temperature. The EHDA system consisted a grounded nozzle (I.D = 0.51 mm, O.D = 0.82 mm), and counter electrode. For dripping regime, a negatively charged plate with a diameter of 600mm was used and for jetting regime a negatively charged ring (I.D = 480 mm, O.D = 540 mm) was used. The negative high voltage was delivered using HPC 35-35000 (FUG®). Where necessary, Comsol multiphysics® software was used to model the electric field in the system.
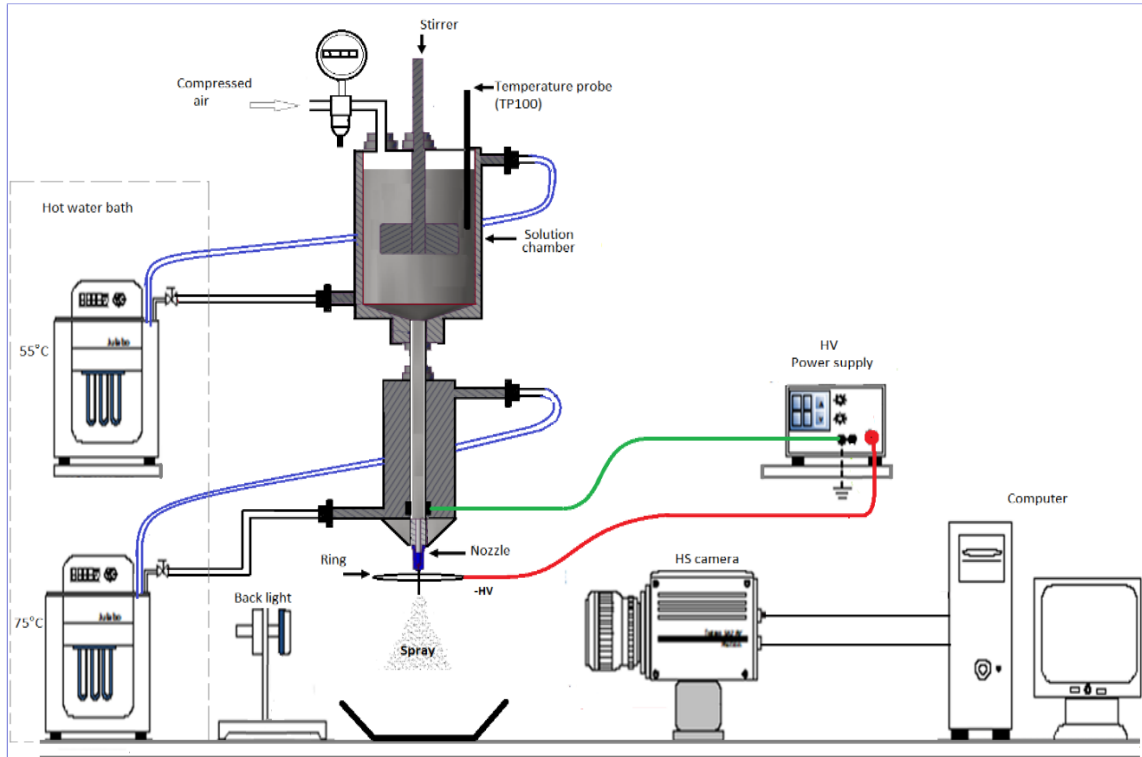
Figure 3.1: Experiment Setup

The experimental study involved identifying the EHDA modes in the dripping regime (i.e. dripping, micro dripping, intermittent cone jet, cone jet or multi- jet) and in the jetting regime (i.e. The simple jet mode with varicose break up and the simple jet mode with whipping break up). The electrospraying process was recorded using a computerized imaging system which comprised *SAX2* high speed camera (Photron[®]) with back illumination. For each mode, the corresponding droplet size, size distribution and spatial dispersion was determined by analyzing the captured images using Image J[®] (image processing software). The parameters to define the droplets were the feret diameter and circularity. The Feret diameter is the measure of the longest distance between two parallel tangents of the droplet while circularity describes how close the droplet is to a sphere (Olson, 2011). To ensure correct measurement in the software (ImageJ[®]), the outer diameter of the nozzle was used to calibrate the images.

3.4.1 Non Dimensionless Number

As rule of thumb, it is necessary to evaluate the importance of different forces governing droplet formation as well as relate to other work (Grace and Marijnissen, 1994). In this study Weber number was used to define the droplet regimes; an approach similar to that by Agostinho (2013). The Weber number given in the equation (3.2) below was used to define the droplet formation regime (i.e. dripping, transition or jetting regime) for different solid content IMF solution.

$$We = \frac{\rho v^2 r}{\gamma}$$
Eqn. 3.2

Where the liquid surface tension (γ), density (ρ), the nozzle's inner radius (r), and the liquid flow rate (Q) were the parameters considered.

RESULTS AND DISCUSSION

4.1 Rheology of IMF Solutions

Using the current rheometer configuration (i.e. bob and the cylinder), it was not possible to determine the dependency of viscosity on the shear rate for 10% w/w and 20% w/w IMF solutions. In addition, for 30% and 40% w/w IMF solutions the measurements could be obtained at shear rates ranging from 258 to 1032 s^{-1}. For, 50% w/w and 55% w/w IMF solutions their flow characteristics were determined at shear rates ranging from 25 to 1000 s^{-1}. Figure 4.1 below, shows flow curves obtained for IMF solutions with solid content 30% w/w, 40% w/w, 50% w/w and 55% w/w.
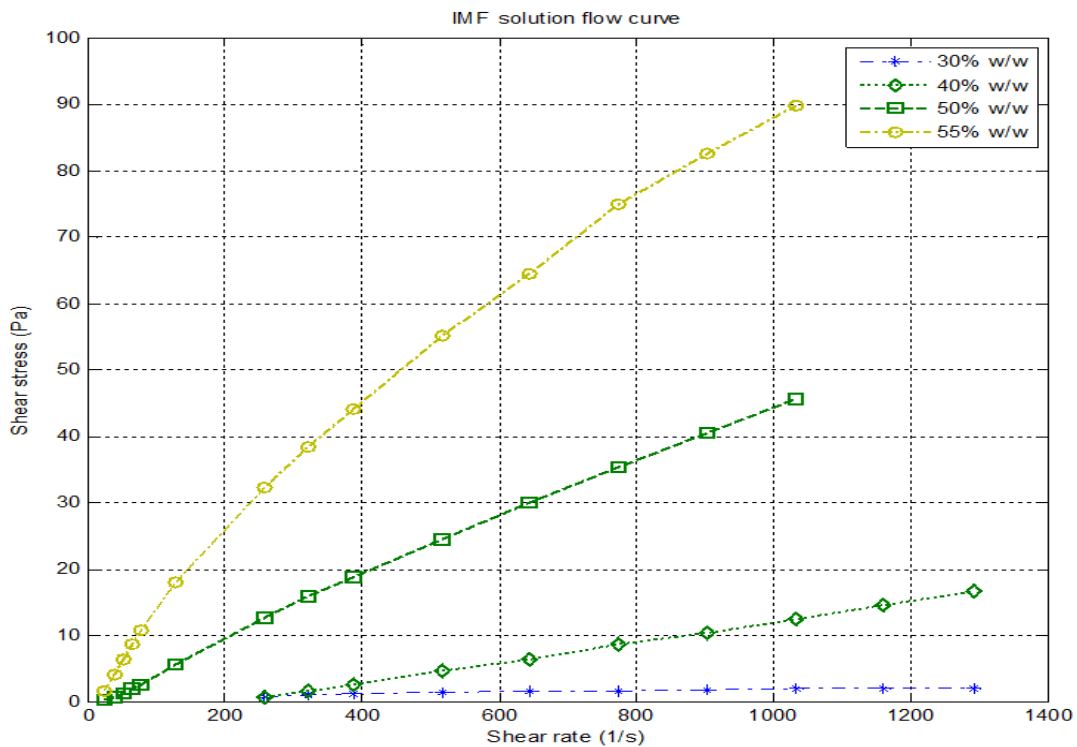
Figure 4.1: IMF solutions flow curves.

From the flow curves, a linear relationship between the shear stress and shear rate was obtained for 30% w/w and 40% w/w which depict a Newtonian behavior. Therefore, the

10% w/w and 20% w/w IMF solutions were considered Newtonian liquids. For 50% w/w and 55% w/w, their flow curves showed a ramp at low shear rates (this is well portrayed in Figure 4.2). The ramp was followed by a curve that showed a Pseudoplastic or Shear thinning characteristic. The stress ramp shows the maximum apparent viscosity exhibited by each solution. Therefore, the stress at the maximum apparent viscosity is considered to be the yield stress (Franck, 2004). This indicates that the solutions required overcoming of a yield stress when pumping.
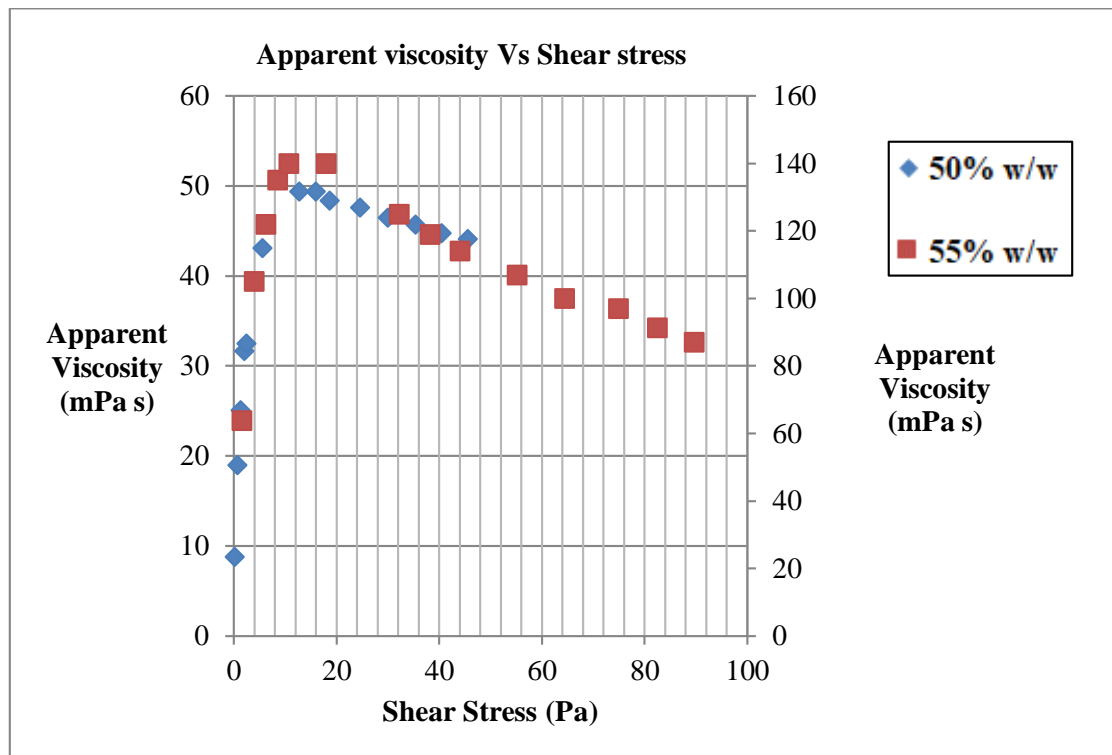
Figure 4.2: Yield stress determination for 50% w/w and 55% w/w using a graph of apparent viscosity versus shear stress. The primary y-axis is for 50% w/w curve and the secondary y-axis is for 55% w/w curve.

The data with the straight curve was fitted into the Power law model and the flow characteristic parameters: consistency coefficient (K) and flow behavior index (n) were obtained. These parameters are listed in Table 4.1.

Table 4.1:Flow characteristics parameters for different IMF solutions: yield stress, flow index (n), and consistency index (K).

Powder concentration (%w/w)	Yield stess (Pa)	Flow index,n	Consistency index, K (Pa s^n)
30	-	1.00	2.80×10^{-3}
40	-	1.01	9.20×10^{-3}
50	12.74	0.99	4.99×10^{-2}
55	18.06	0.97	1.22×10^{-1}

From the results, it is clear that the IMF solutions with 30% w/w and 40% w/w at 70 °C were Newtonian liquid. In this case, their apparent viscosity is 2.8 mPa s and 9.2 mPa.s respectively. On the other hand, the 50% w/w and 55% w/w IMF solution were non-Newtonian liquid with the flow characteristic exhibiting Pseudo plastic and with yield stress.

4.2 Other Physical Properties

Table 4.2 shows the average of the measured physical properties of the different IMF solutions i.e. the density, the surface tension, and the conductivity.

Table 4.2: The summary of the physical properties of different IMF solution.

Powder concentration (% w/w)	Density (kg m^{-3})	surface tension (N m^{-1})	Conductivity (S m^{-1})
10	1009	3.5×10^{-2}	2.66×10^{-4}
20	1034	3.9×10^{-2}	4.66×10^{-4}
30	1068	4.4×10^{-2}	4.61×10^{-4}
40	1098	4.5×10^{-2}	4.74×10^{-4}
50	1128	4.6×10^{-2}	4.16×10^{-4}
55	1142	4.6×10^{-2}	3.48×10^{-4}

It can be seen that an increase in solid content leads to an increase in density and surface tension. However, conductivity at high solid content (i.e. 55% w/w) was seen to decrease. The decrease in conductivity can be attributed to the fact that the ion mobility in that solution is limited due to low water concentration. Otherwise, it is expected to increase due to the high concentration of solid content.

4.3 Regimes Definition

Based on the nozzle diameter and the physical properties of IMF solutions, it was found that the regimes obtained occurred at different Weber number as tabulated below.

Table 4.3: Regimes definition for different IMF solutions.

Dripping Regime		
Solid content (% w/w)	Weber Number (We)	Flow rate, Q (mL h^{-1})
10 and 20	We < 2.1	Q < 420
30,40, and 50	We < 2.1	Q < 420
Transition Regime		
10 and 20	$2.1 \leq$ We < 3.1	$420 \leq$ Q< 480
30	$2.1 \leq$ We < 2.4	$415 \leq$ Q< 480
40 and 50	$2.1 \leq$ We < 2.4	$415 \leq$ Q< 450
Jetting Regime		
10 and 20	We$\geq$3.1	Q$\geq$480
30	We $\geq$ 2.4	Q$\geq$480
40 and 50	We $\geq$ 2.4	Q$\geq$450

The tests were carried using water which showed that, for water, the regimes occurred as was defined in Agostinho (2013) i.e. dripping at We< 2.1(Q = 570 mL h^{-1}), the transition at $2.1 \leq$ We < 4, and jetting We $\geq$ 4 (Q = 780 mL h^{-1}). This shows that the regimes are defined at lower values of Weber number using IMF solution especially the jetting regime. Figure 4.3 provides an insight into the observable differences between the three domains using solutions with 50% w/w content at: (a) the dripping regime at a flow rate

of 5mL h⁻¹, (b) the transition regime at a flow rate of 450 mL h⁻¹, and (c) the jetting regime at a flow rate of 520 mL h⁻¹.

.
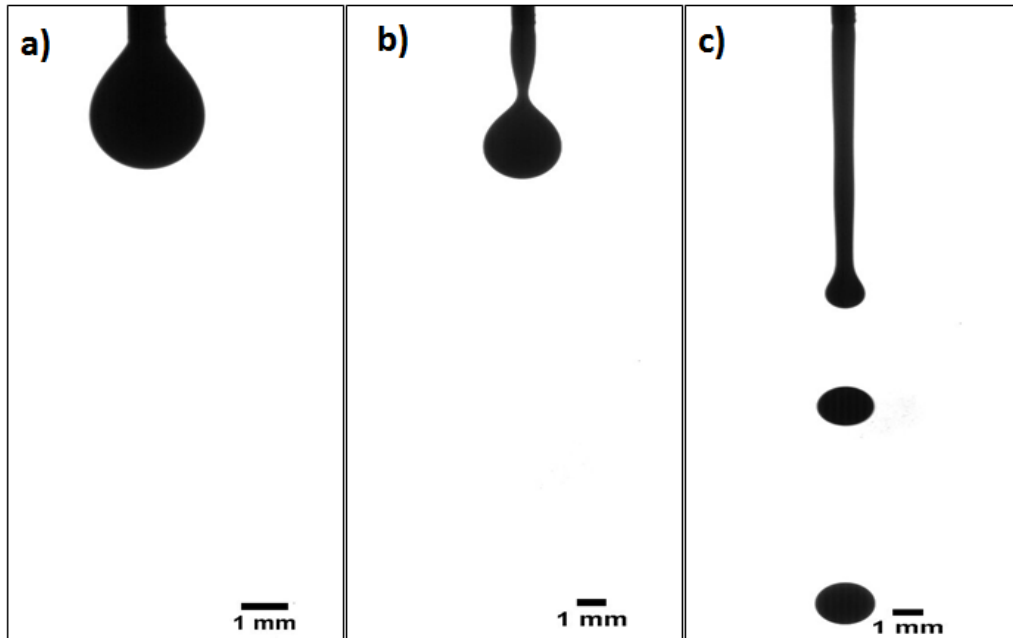
Figure 4.3: Regimes definition using IMF solutions with 50% w/w content where a) is the dripping regime at a flow rate of 5 mL h⁻¹, b) the transition regime at flow rate of 450 mL h⁻¹ and c) the jetting regime at flow rate of 520 mL h⁻¹.

4.4 Electrospray

The electrospray experimental results about the spray characteristics for each solid content, flow rate, and applied potential are discussed in this section. The first section presents the electrospray characteristics observed in the dripping regime and the second section discusses electrospray results in the jetting regime.

4.4.1 Electrospray Characteristics in the Dripping Regime

This first section discusses the electrospray characteristics of IMF solution in the dripping regime. The experiments were undertaken using IMF solutions with a solid content of 30% w/w, 40% w/w, and 50% w/w.

4.4.1.1 Electrospray Characteristics of IMF Solution with Solid Content 30% w/w

The behavior and electrospray characteristics were investigated at a flow rate of 1 mL h^{-1}, 5 mL h^{-1}, and 10 mL h^{-1}. After establishing a stable flow of the solution, the application of electric potential started at 0 kV and gradually increased to consider the influence of electric field on droplet formation. In all the above flow rates, it was noted that an electric potential at the range of 0 kV to 6 kV resulted into the enhanced dripping mode. A notable difference was eminent between 1mLh and the other two flow rates at electric potential beyond 6 kV.

In the case of 1 mL h^{-1}, at 7 kV and 10 kV the action of the electric field on the meniscus of the pendant droplet resulted in pinching off of a single droplet from the tip without alteration of the shape of the meniscus. An EHDA mode associated with the pinching of small droplets at a low flow rate is referred to as micro dripping. As it can be seen in Figure 4.4, small droplets are generated. At a further increase of the electric potential to 13 kV, it was observed that the meniscus was pulled into a thin ligament which then proceeded to break up into several droplets of different sizes.
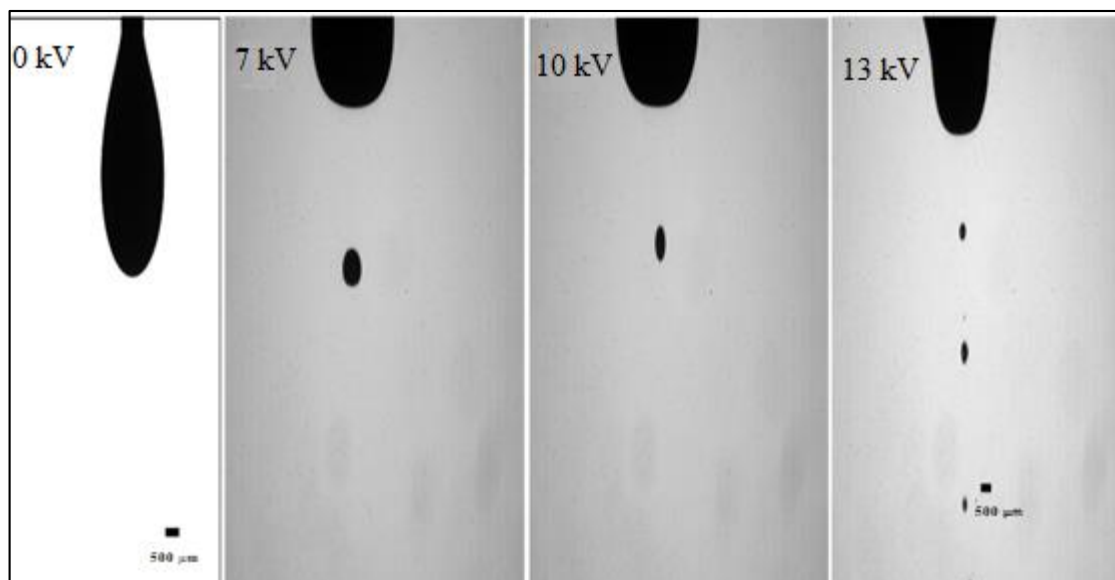
Figure 4.4: Snapshots showing droplet formation at the different electric potential for a flow rate of 1 mL h^{-1}.

In the case of 5 mL h^{-1} and 10 mL h^{-1}, application of an electric potential of 8 kV to 10 kV produced a behavior depicted in Figure 4.5. The sequence starts with a rounded meniscus (i), then stretches out into a conical shape in which it was observed a spray of fine droplets proceeded (not visible in the image) (ii, iii, and iv), after which the base of the stretched ligament pinches off forming one or more droplets with varying size depending on the length of the stretched filament (v). After the detachment of the ligament, the sequence is repeated by the meniscus restoring back into the initial state (i). The EHDA mode in which the meniscus is periodically transformed into a conical shape, followed by formation of a jet which sprays fine droplets and then stretching into a ligament that detached and proceeds to form several droplets is described in the literature as the spindle mode. Thus, the observed EHDA mode with IMF solutions with solid content 30% w/w operated at flow rates 5 mL h^{-1} and 10 mL h^{-1}and an applied potential ranging 8-10 kV was associated with the spindle mode observed in electrospraying of Newtonian liquids such as ethanol and water. However, a liquid jet is

visible for Newtonian liquids operating in the spindle mode, but in this work it was is not. This can be attributed to the presence of powder particles.
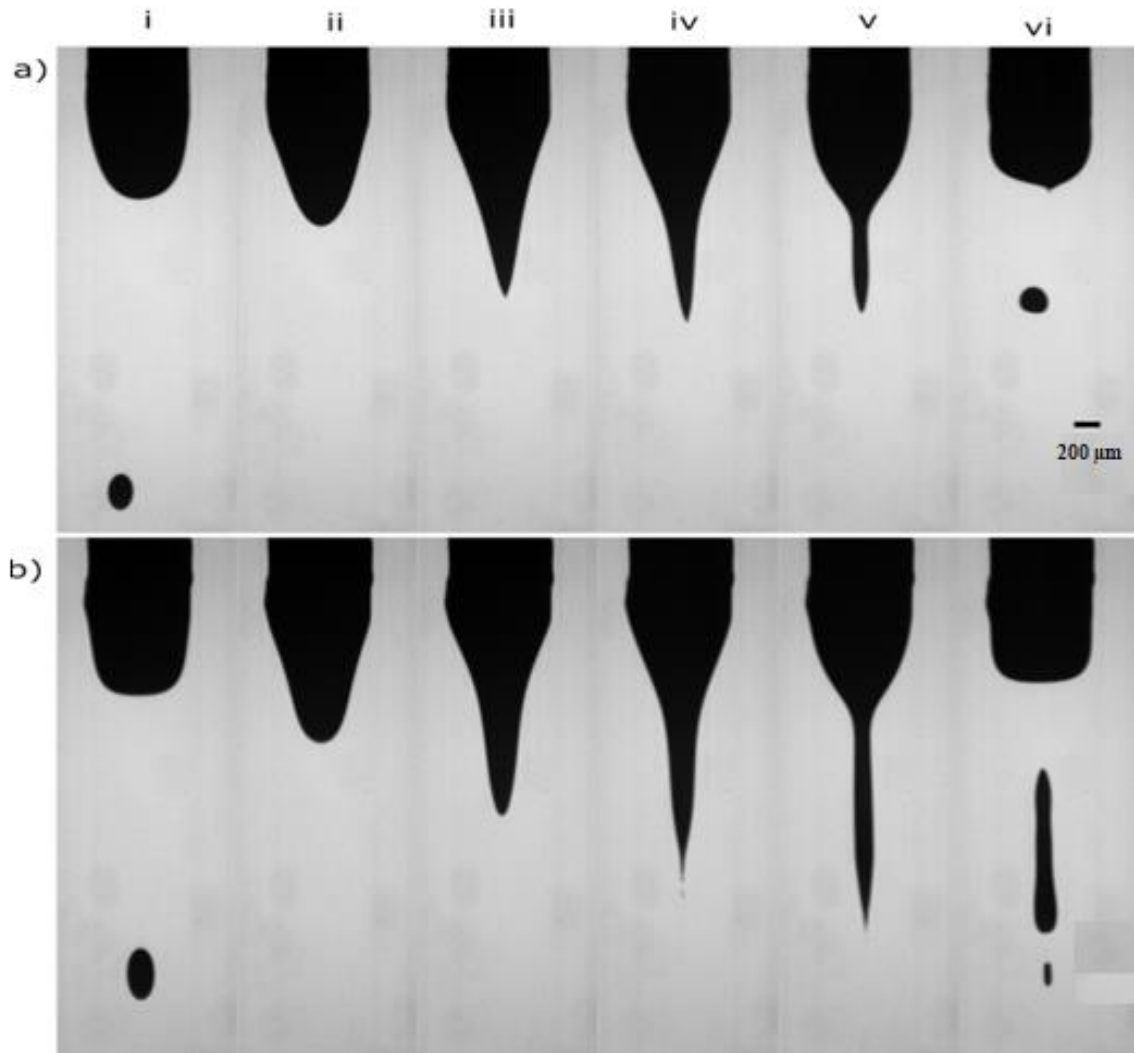
Figure 4.5: Spindle mode sequence for IMF solution with 30% w/w solid content at a flow rate of (a) 5 mL h^{-1} (b) 10 mL h^{-1} and applied an electric potential of 8 kV. The frequency of the two cycles is ~4 ms (250 droplets per second) and ~3 ms (333 droplets per second).

For a flow rate of 5 mL h^{-1}, the potential was increased till 13 kV see Figure 4.6. It can be seen that there was no major difference in terms of the electrospray cycle except that the strong electric field, caused the detachment of a filament that experienced horizontal displacement as it proceeded to break up into droplets of different sizes.

Figure 4.6: Electrospray sequence for IMF solution with 30% w/w solid content at a flow rate of 5 mL h^{-1} and an electric potential of 13 kV. The frequency of the mode is ~2.3 ms.

With the studied flow rates and applied potentials using 30% w/w IMF solutions, the cone-jet mode was not observed as commonly obtained in Newtonian liquids such as ethanol.

4.4.1.2 Electrospray Characteristics of IMF Solutions with Solid Content 40% w/w
The electrospray characteristics were studied with similar operational conditions as those in 30% w/w: flow rates of 1 mL h^{-1}, 5 mL h^{-1}, and 10 mL h^{-1} and range of applied potentials of 0 kV to 13 kV. Starting with a flow rate of 1 mL h^{-1} and applying the

electric potential in the range of 0- 6.5 kV, there was the minimal influence of the applied potential on droplet formation in terms of frequency. Increasing the potential to 7 kV see Figure 4.7, it was observed that the pendant droplet starts with a rounded meniscus that is transformed into a conical shape. As the tip prolongs, it thins out and detaches forming small and big droplets. The meniscus would then relax into a spherical shape and the cycle starts.
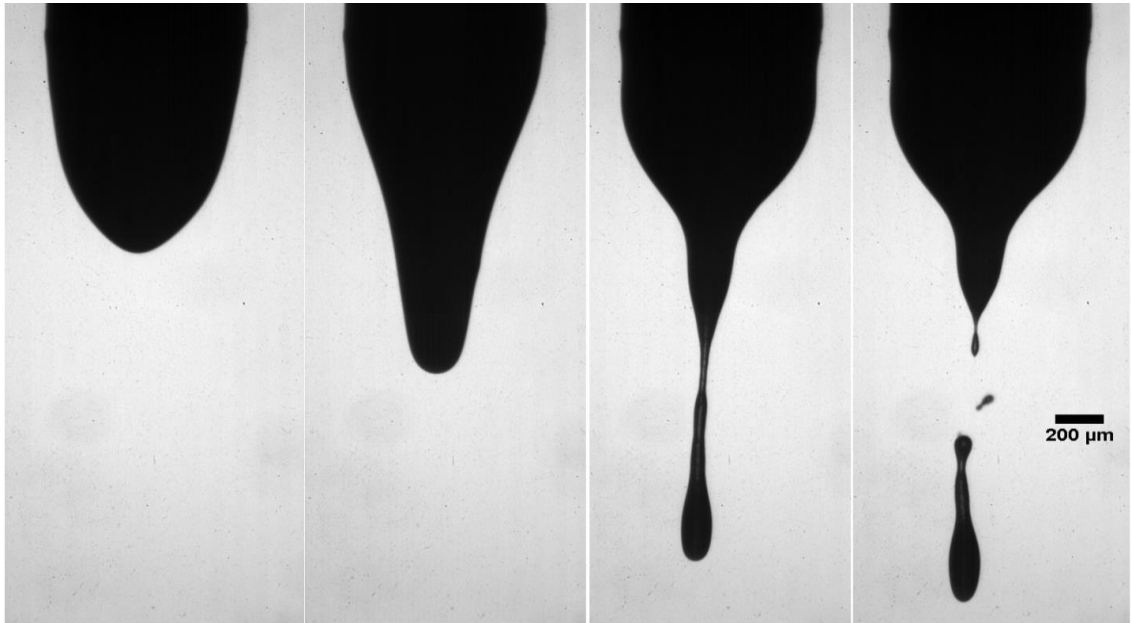
Figure 4.7: Electrospray sequence for IMF solution with 40% w/w solid content at a flow rate of 1 mL h^{-1} and applied the electric potential of 7 kV. The total time for the sequence is ~13 ms.

A cycle similar to that of 7 kV was observed when the electric potential was increased to 10 kV and 13 kV see Figure 4.8 and 4.9 respectively.
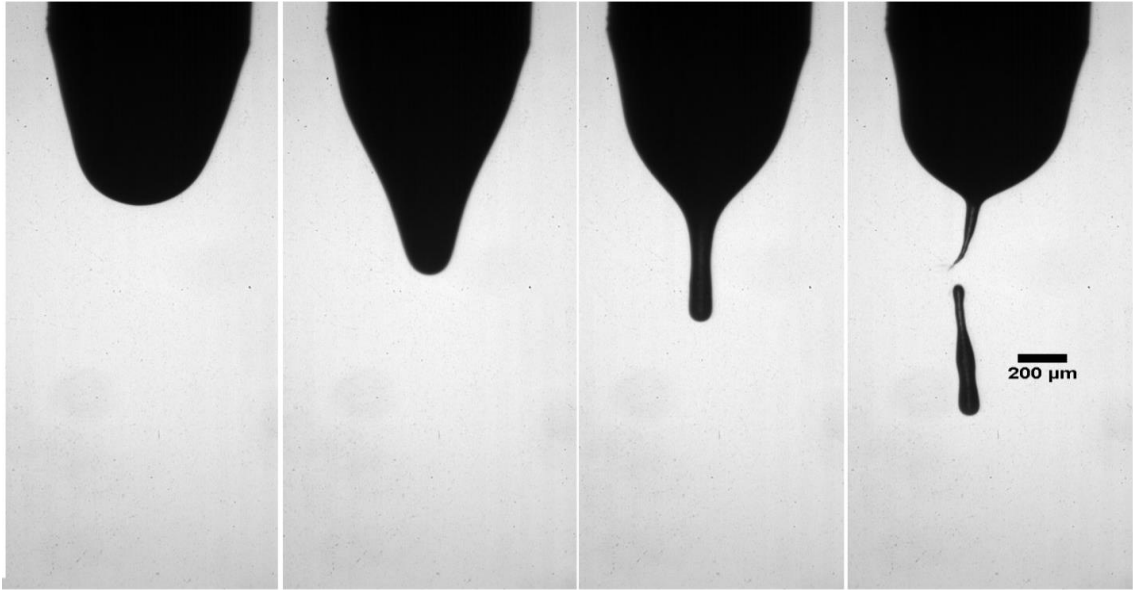
Figure 4.8: Electrospray sequence for IMF solution with 40% w/w solid content at a flow rate of 1 mL h^{-1} and applied an electric potential of 10 kV. The total time for the sequence is 7 ms.
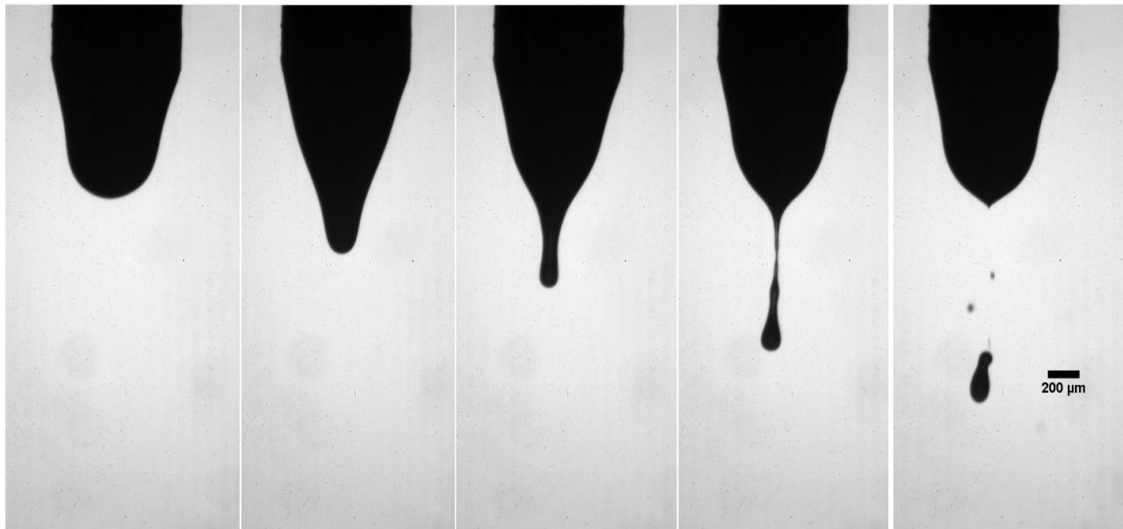
Figure 4.9: Electrospray sequence for IMF solution with 40% w/w solid content at a flow rate of 1 mL h^{-1} and applied the electric potential of 13 kV. The total time for the sequence is 5.3 ms.

At a flow rate of 5 mL h^{-1} and an applied electric potential of 8 kV the characteristics shown in Figure 4.10 were obtained. The sequence is similar to that obtained in the electrospraying IMF solution with a solid content of 30% w/w at 8 kV. As said earlier, such sequence is associated with the spindle mode.
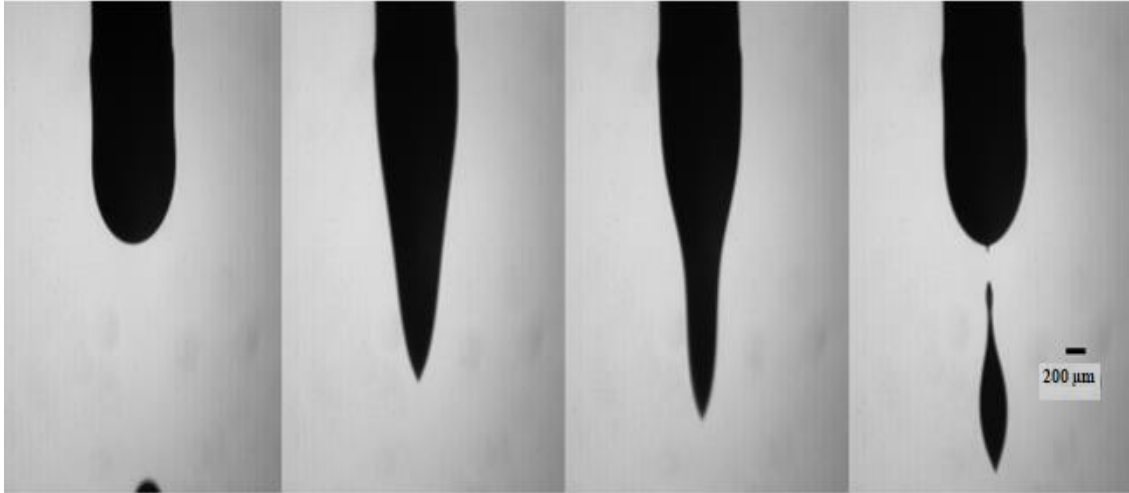
Figure 4.10: The spindle mode electrospray sequence for IMF solution with 40% w/w solid content at a flow rate of 5 mL h^{-1} and applied an electric potential of 8 kV. The total time for the sequence is 11.3 ms.

Figure 4.11 (a) and (b) shows the sequence obtained when the applied potential was increased to 10 kV and 13 kV respectively. It was observed that the droplet formation cycle resembled that for an applied potential of 8 kV discussed above. However, a spray of very small droplets was observed at the apex of the meniscus (see second snapshot in Figure 4.11 (a)). In other cases, the tip was elongated into a thin filament, sprayed at the head, and finally collapsed into a single droplet.
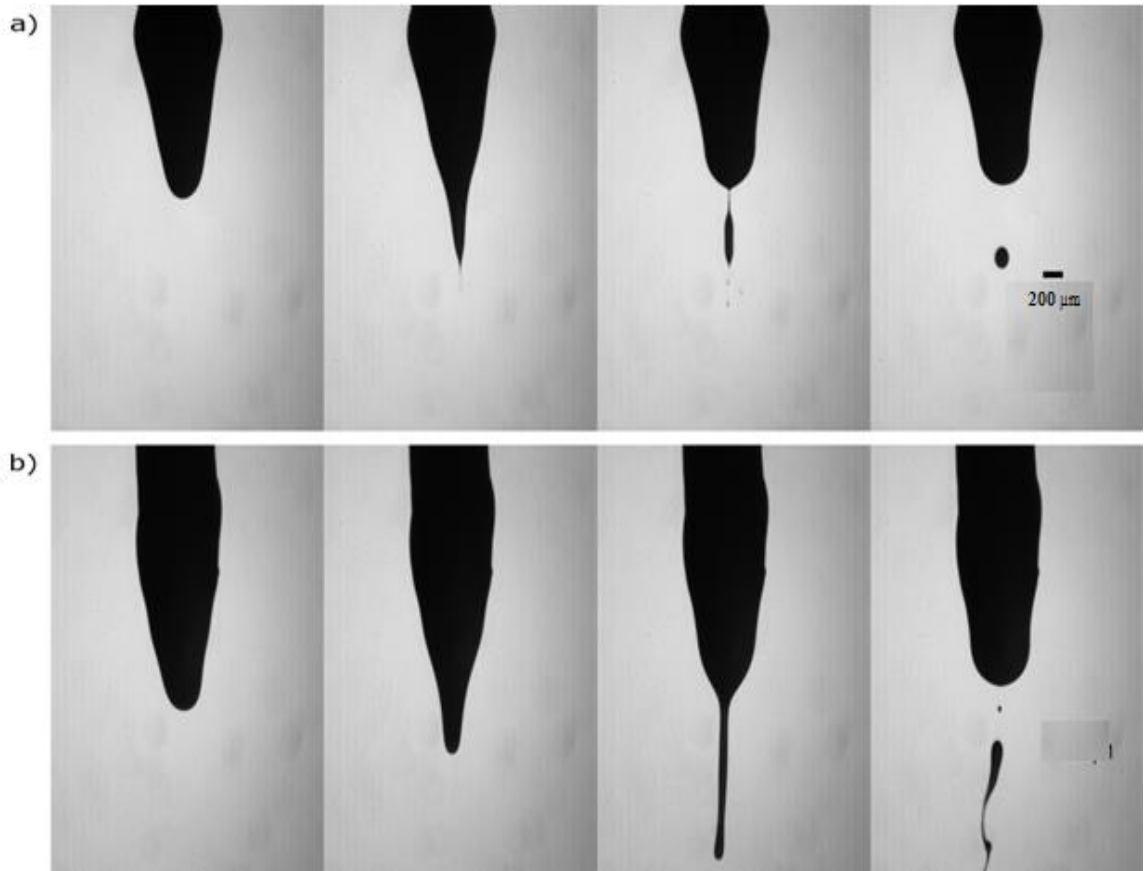
Figure 4.11: Electrospray sequence for IMF solution with 40% w/w solid content at a flow rate of 5 mL h^{-1} and an applied electric potential of (a) 10 kV and (b) 13 kV. In both case, the frequency of droplet formation was 240 droplets per second (i.e. the time for both sequences was ~4.2 ms).

Figure 4.12 shows the sequence obtained with an increased flow rate of 10 mL h^{-1} and an applied potential of 8 kV. The pendant droplet starts with a rounded meniscus which is transformed into a conical shape, and then a spray of fine droplets emerges at the tip (not visible in the image but was noticeable in form of deposition at the charged plate). Due to flow rate and spray mass imbalance, the droplet elongated downward, then thinned out at a point, and eventually, a large droplet detached. The trailing end also disintegrated into other small droplets and the sequence restarts.
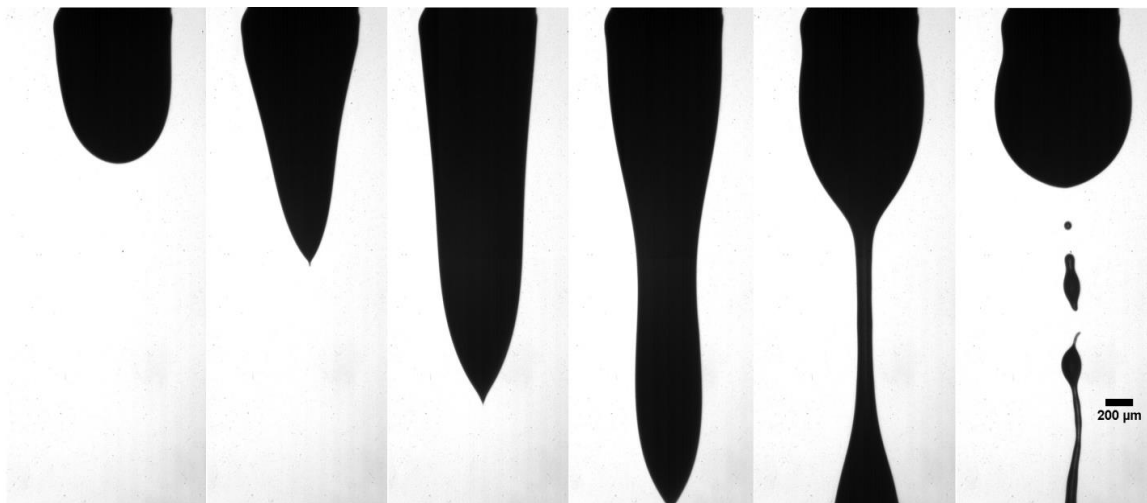
Figure 4.12: Electrospray sequence with 40% w/w IMF solutions at a flow rate of 10 mL h^{-1} and applied the electric potential of 8 kV. The time for the sequence is ~18.7 ms.

Increasing the applied potential to 13 kV, it can be seen in Figure 4.13 the cycle starts with a conical shape (i), followed by spraying at the tip (ii and iii) that lasts for a period of 8 ms while spraying, the meniscus is then prolonged into a ligament (iv) that thins and detaches at the base (v). After detachment, the ligament proceeds to form a big droplet followed by several small droplets disintegrating from the thinned part (vi). Such electrospray characteristics have not been observed in electrospraying of Newtonian liquid. This diverse characteristic shows how the presence of solid content can modify the known EHDA modes.
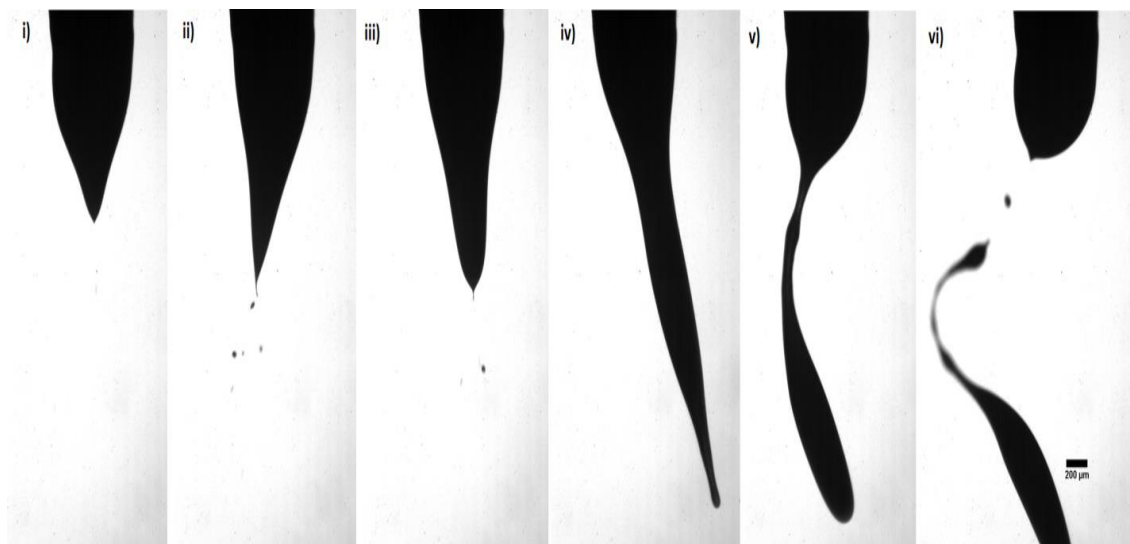
Figure 4.13: Electrospray sequence with 40% w/w IMF solutions at a flow rate of 10 mL h^{-1} and applied an electric potential of 13 kV. The spraying in i to iii lasts for ~ 8 ms then inhibited by formation of the big ligament.

4.4.1.3 Electrospray Characteristics of IMF Solution with Solid Content 50% w/w

For the 50% w/w IMF solutions, electrospray characteristics were investigated only with flow rates of 5 mL h^{-1}. The observed behavior and electrospray characteristics at 8 kV is as shown in Figure 4.14. The sequence started with a conical meniscus, then elongated downward, and due to surface tension started to neck. Consequently, an oval shaped head with a thin filament as a tail was formed in which it breaks off. After detaching, only the tail and the pointed tip were seen to break into small particles.
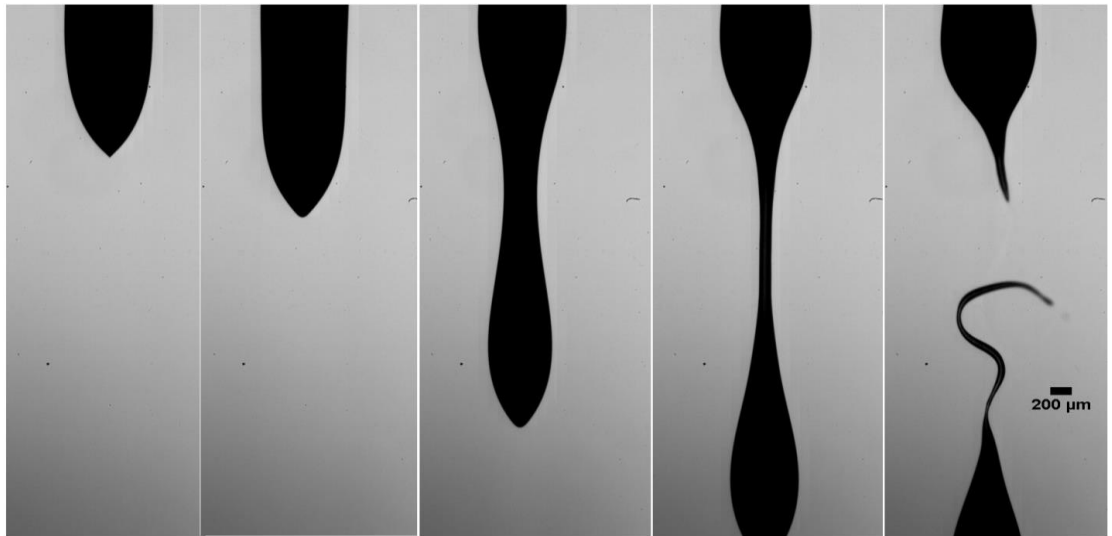
Figure 4.14: Electrospray sequence with 50% w/w IMF solutions at a flow rate of 5 mL h^{-1} and applied an electric potential of 8 kV. Time for the sequence is 0.5 s.

When an applied potential was increased to 13 kV see Figure 4.15, the hanging droplet was transformed into a conical shape (i). In this case, parcels or particles were seen to be stripped off from the tip (iii). The tip was observed to lengthen at the tip, forming a thin liquid filament (v). The filament was observed to undergo horizontal oscillations that resulted in the filament breaking to small pieces (iv) and the cycle started.
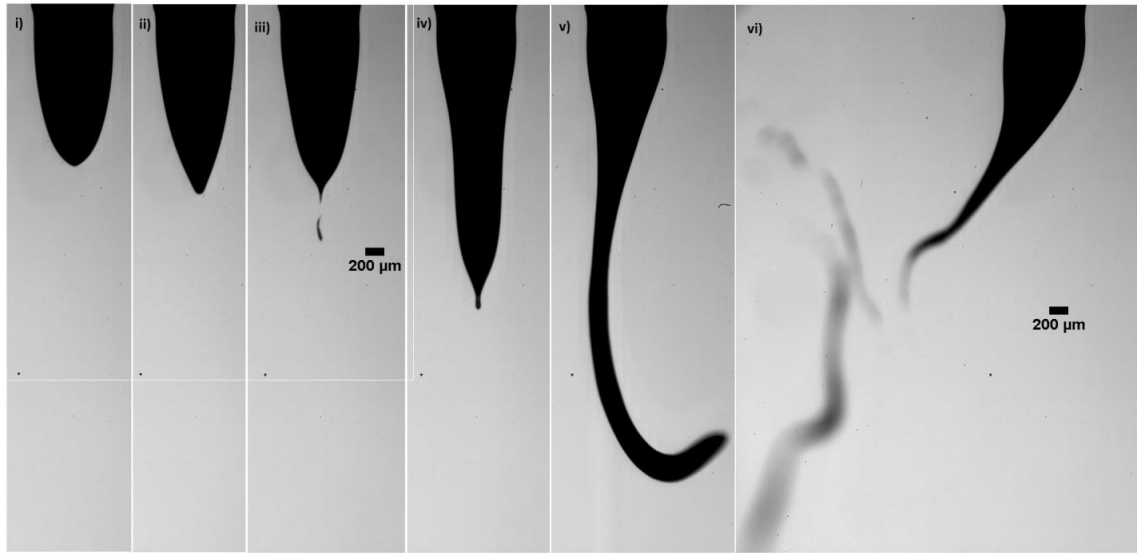
Figure 4.15: Electrospray sequence with 50% w/w IMF solutions at a flow rate of 10 mL h^{-1} and applied an electric potential of 13 kV. The ligament was observed to reappear after a period 0.44 s.

The above described behavior and characteristics can only be associated with the solution having high solid content, which led to entanglement of powder particles as the solution flow. However, this entanglement is different from the observed characteristic exhibited in electrospraying of polymer solutions in a technique known as electro-spinning (Reneker and Yarin, 2008).

In general, it can be observed that in the dripping regime the presence of powder affects the observation and realization of EHDA modes. And the effect is more pronounced in solution with high solid content. This is an indication that in the process which requires a higher throughput the EHDA cannot be operated in the dripping regime. Considering that the ultimate goal for this work is to provide characteristics necessary for industrial use, a study for electrospray at the jetting regime is presented next.

4.4.2 Electrospray Characteristics in the Jetting Regime

This section presents the spray characteristics of IMF solutions with solid content 10%, 20%, 30%, 40%, and 50% w/w. The investigations were carried using flow rates of 500, 520 and 550 mL h^{-1} and an applied potential was varied from 0 to 17 kV for each flow. All the experiments involving electrospraying of IMF solution with 10% w/w to 50% w/w, a nozzle with ID = 0.51 mm and O.D = 0.82 mm was used.

4.4.2.1 Electrospray Characteristics of 10% w/w IMF Solutions

Figure 4.16 below shows snapshots of break up processes at different electric potentials for 10% w/w IMF solutions operated at a flow rate of 500 mL h^{-1}. From the images it can be observed that the jets for the uncharged situation (0 kV) and 9 kV undergo varicose break up while for 11 kV and 15 kV undergo whipping break-up.
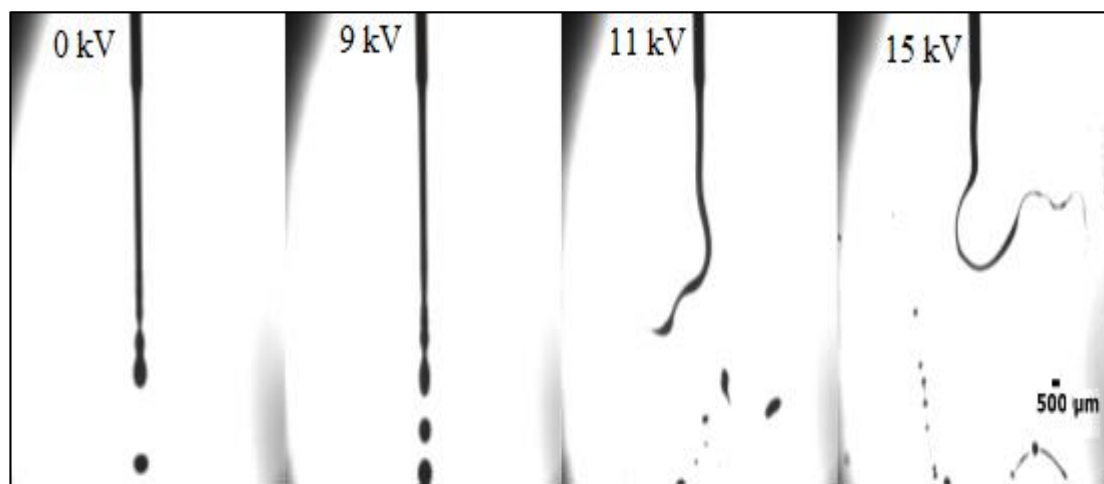
 Figure 4.16: Snapshots showing droplet formation processes at different applied potential using 10% w/w IMF solution at a flow rate of 500 mL h^{-1}.

During movie analyses, more characteristics were observed in each situation with regard to the droplet formation process. At 0 kV, it was observed that three categories of droplet size were generated during the jet break up process. From Figure 4.17 (i) the

droplet labeled (a) is attributed to the main droplet in which its size is approximately twice the inner diameter of the nozzle. In the same caption, the hanging droplet (b) is about to pinch off and a development of incoming droplet. But, in (ii), it can be observed that the hanging droplet opens up before pinching off and swallows the incoming droplet. The two droplets merge as they pinch off from the jet (iii and iv). They eventually collapse into a single droplet as in (v). In such a scenario, the droplet formed has a volume that is twice that of the main droplet. In addition, coalescence of two primary droplets after breaking off was observed and also resulted into a big droplet. In other instances, it was seen that three droplets could merge to form a big droplet before breaking off from the jet. Then, the formed droplet would have a volume which is thrice that of the main droplet.
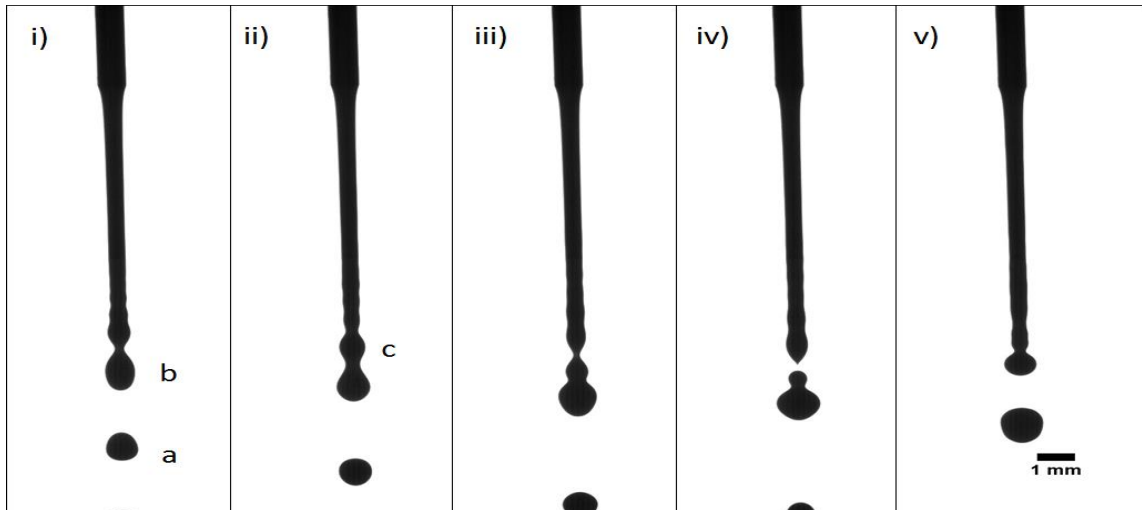
Figure 4.17: Droplet formation at 0 kV with 10% w/w IMF solution. The flow rate is 500 mL h^{-1}.

According to Shinjo and Umemura (2010), the generation of main droplets happens as a result of the downward growth of unstable long wave that is created at the nozzle exit while the swallowing of the incoming droplet is caused by an upward propagation of short capillary wave created by contraction of the tip after a droplet pinch-off.

The third category of droplets is small droplets, d, in Figure 4.18. These droplets were formed from a contraction of a filament connecting two big droplets as shown in sequence i to ii.
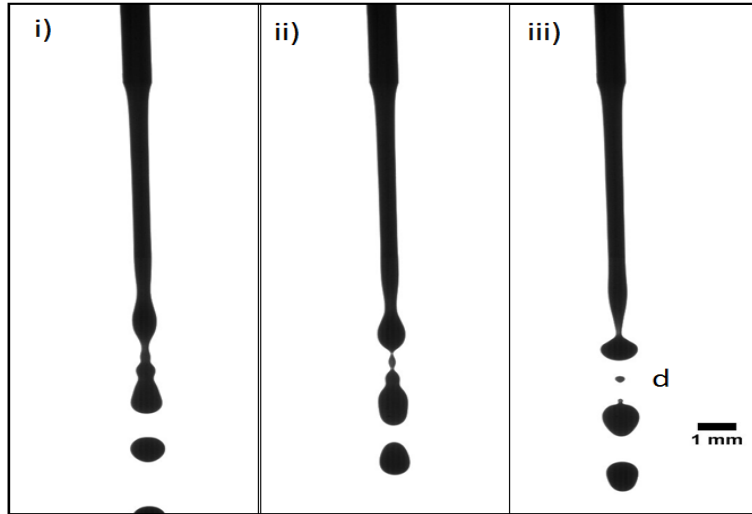
Figure 4.18: Formation of satellite droplet at 0 kV with 10% w/w IMF solution. The flow rate is 500 mL h^{-1}.

Upon applying an electric potential of 9 kV, the spray contained the main droplets, big droplets, and satellite. However, there was a minimal coalescence of droplets. Such occurrence is attributed to the charged droplets produced during atomization (Agostinho et al., 2012).

At 11 kV, the jet developed a whipping motion. During the whipping motion, a liquid filament could form between two successful droplets [see Figure 4.19 (i and ii)]. Then both the leading droplet and the filament break off from the jet (iii). Where the droplet either forms a single droplet or sprays small droplets, while the filament breaks up into many small droplets of different sizes (iv).
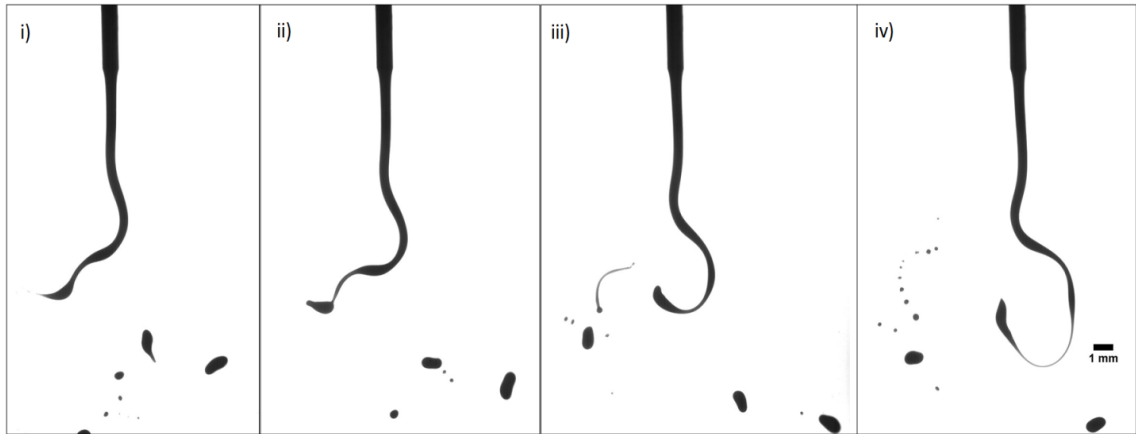
Figure 4.19: Jet breaks up process and droplets formation at 11 kV with a flow rate of 500 mL h^{-1} using 10% w/w IMF solution.

At 15 kV, compared to the case for 11 kV, the whipping motion was violent in that the jet tends to shorten and thins out at the leading tip see Figure 4.20 (i). Then, during whipping motion, the thinned part of the jet breaks off as a whole to form a ligament (ii and iii). The ligament proceeds to disintegrate into small droplets of different sizes through a varicose break-up (iv).
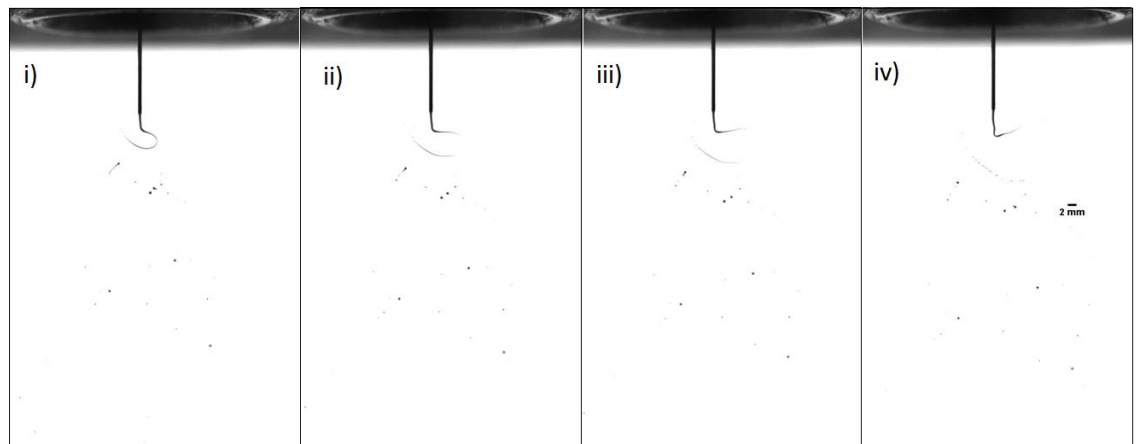
Figure 4.20: Jet break up process and droplets formation at 15 kV with a flow rate of 500 mL h^{-1} using 10% w/w IMF solution.

In the literature, most works have identified such characteristics of the breaking up process. For instance, in the dissertation of Hartman (1998), established a production of droplets with different sizes during the breakup process. The droplets were categorized into the main droplets, the secondary droplets, and the satellite droplets, whereby both the secondary and satellite droplets were formed from a liquid filament connecting the main droplets. Thus, the secondary droplets were smaller than the main droplets but bigger than the satellite droplets.

The droplets size distribution generated for the 10% w/w solution, corresponding to the above-mentioned conditions are shown in Figure 4.21. From the figure, at 0 kV, there are four distinct peaks which represent main droplets located at1.1 mm, big droplets at 1.4 mm and 1.6 mm, and the satellite droplets peak at 0.4 mm. This corresponds to the observation made from the movies of the breaking process. In that, the position of the main droplets equals twice the inner nozzle diameter (i.e. 0.51 mm). While the position of the big droplets peaks corresponded to the diameter of droplets with double or triple the volume of the main droplets (referred as doubles and triples respectively).

Upon applying an electric potential, several observations were drawn from the distribution curves with regard to the influence of applied electric potential. At 9 kV, the main peak remained constant and there was a tendency to reduce the generation of doubles and triple. From the movie analyses, it was noted that the satellite droplets were deflected off the axis by the main droplets and the interaction of charged droplets led to few droplets coalescing causing droplet segregation. This phenomenon is among the advantage of EHDA in atomization of liquids.

At 11 kV, the droplet size distribution is broad. This is expected since in break up process, most big droplets with different sizes were formed as the jet was displaced from

the axis-symmetric position. The small droplets resulted from the spraying of the big droplets and fragmentation of the liquid filaments. Hartman (1998) observed that the size distribution can be used to tell the breakup process of the jet. At this applied electric potential, it represents the initial characteristic of whipping break up.

At 15 kV, the size distribution becomes broad and skewed to the right. The explanation of this can be drawn from the images of the breaking process. The radial fluctuation of the jet was much wide resulting to the jet breaking off as a ligament. The ligament further disintegrated into small droplets of different sizes. From the spectra of 15 kV (at Figure 4.21), it can be noted that the modal size is located at 0.3 mm. However, cross-checking in movies, it was found that the modal class ought to be in the range of 0.4 to 0.6 mm. The reason behind this was that the analyses software (Image J) recorded the diameter of the ligaments produced during whipping motion (i.e. ligaments diameter measured 0.3 mm). Another aspect noted from the movie is that very small droplets (less than 10 µm) were generated though not counted due to color thresholding of the images during analyses while eliminating the noise introduced by the strobe light.
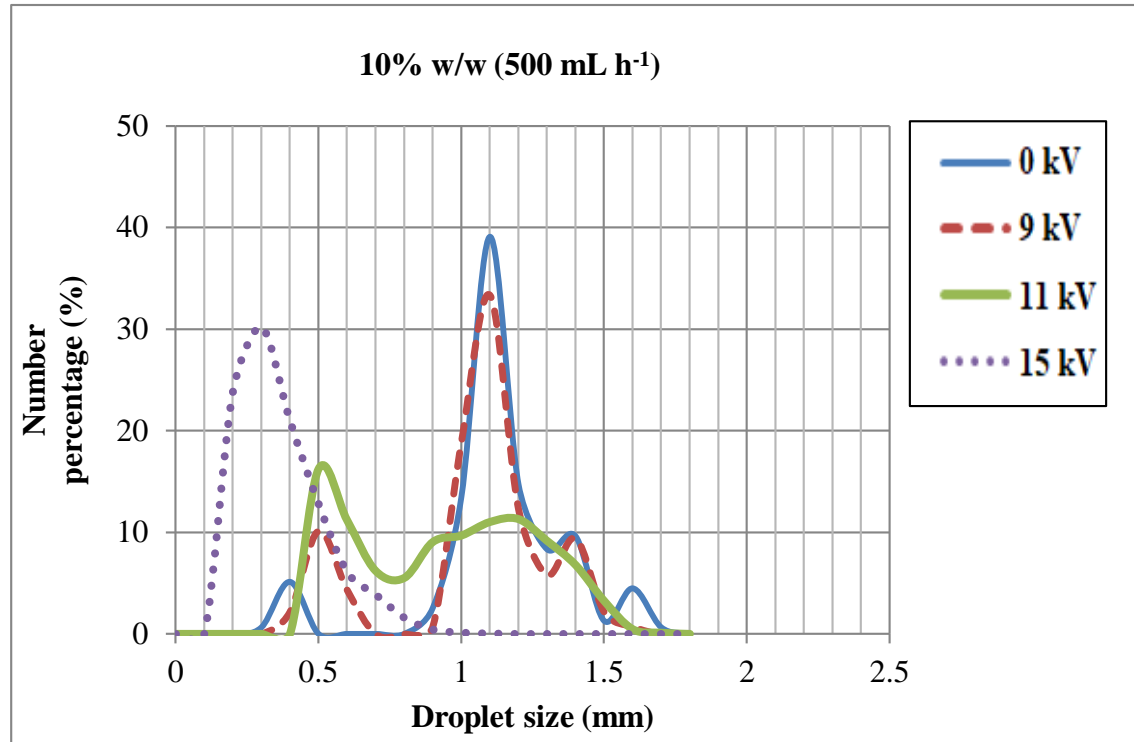
Figure 4.21: Droplets size distribution curves for 10% w/w IMF solution at different electric potential operated at 500 mL h^{-1}.

When the flow rate was increased to 520 mL h^{-1} and 550 mL h^{-1}, similar physical characteristics were observed with respect to breaking process as discussed for 500 mL h^{-1}. The droplet formation under varicose break up was observed at 0 to 10.8 kV and due to whipping break up it was realized for applied electric potential above 10.8 kV. Therefore, the size distribution of the generated droplets at 0 kV, 9 kV, 11 kV, and 15 kV are shown in Figure 4.22.

In both flow rates, the spectra for 0 kV had well-defined peaks of the main droplets and the satellite droplets. A close look revealed a hump in each case positioned to the right of the main peak. This was an indication of the presence of doubles or triples that are, however, few in this case. Such an observation can be attributed to the fact that at increased flow rate the jet radius is expected to reduce resulting in relatively smaller droplets.

At 9 kV, the spectrum shows the presence of the main droplets, doubles and the satellite droplets. Also, was noted that the position of the main droplets peak remained constant while the distribution was constricted toward the center. The resultant was a narrow span of the distribution compared to that for 0 kV. This indicated that, in both flows, the application of an electric potential led to the dominance of a single wavelength. According to the literature, the electric stress tends to reduce the jet radius (Hartman et al., 2000) and as a consequence the wavelength of the dominant disturbance shortens generating smaller droplets (Agostinho et al., 2012).

At 11 kV, the droplets size is bimodal with a broad distribution. It was clear from the obtained images that the spray comprised big droplets of different sizes and small droplets as a result of whipping motion of the jet.

At 15 kV, in both cases, a broad distribution was obtained which is a characteristic of whipping break up. As stated earlier, the modal class shown in the distribution curve (i.e. 0.3 mm) comprised a number of droplets and diameter of the ligament, increasing the number in this size.
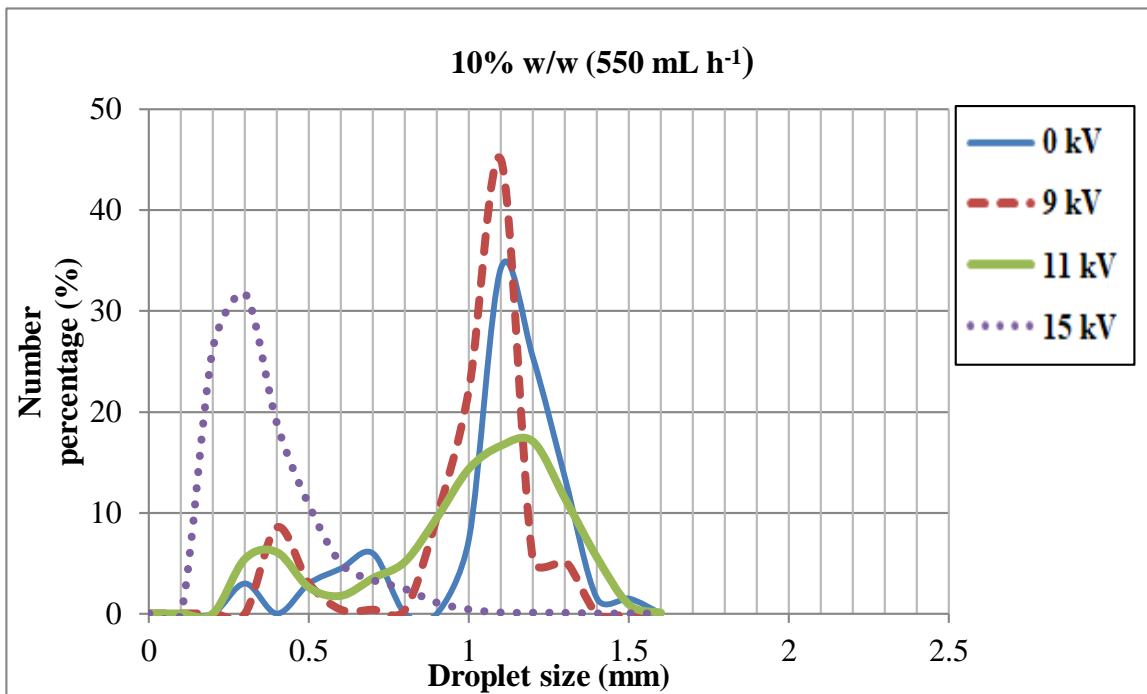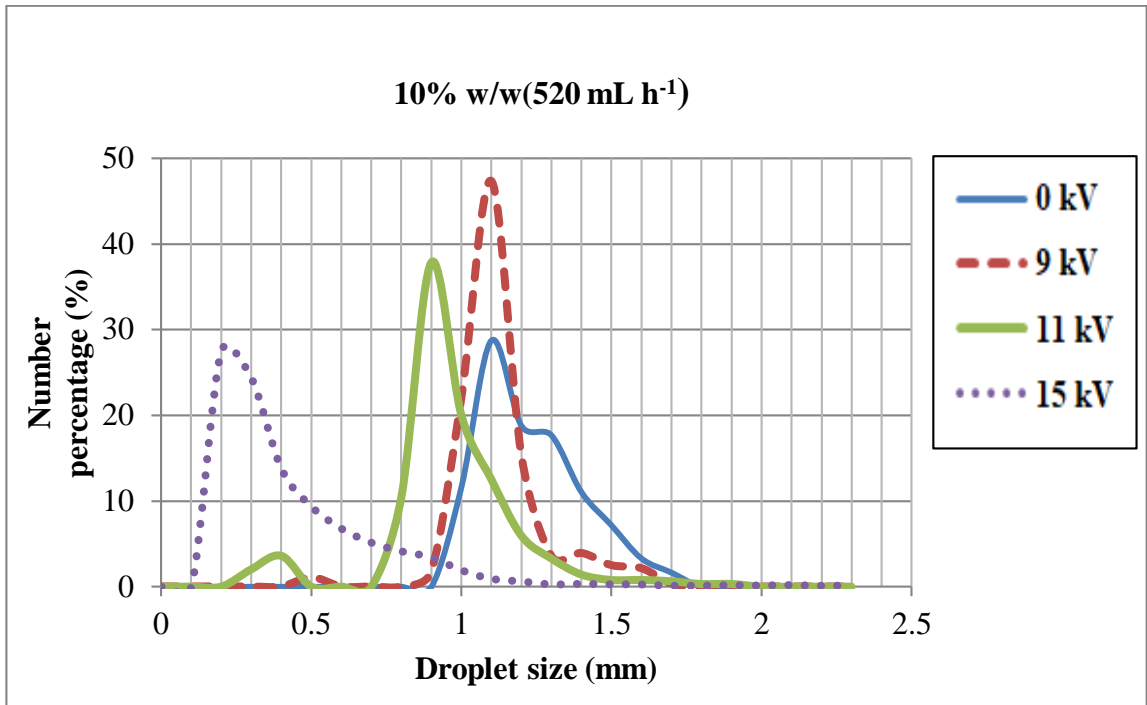
Figure 4.22: Showing the droplets size distribution for 10% w/w IMF solution at different electric potential operated at 520 mL h^{-1} (above) and 550 mL h^{-1} (below).

In an effort to quantify the influence of an applied potential on the droplet size distribution especially in determining mono-dispersed spray, most studies in electrospray utilize relative standard deviation (RSD). Some examples include the works of Agostinho et al. (2013), Loscertales et al. (2002), and Tang and Gomez (1995) among others. Therefore, the RSD was evaluated to determine the tendency of droplets size generated at the three flow rates and the effect of applied potential and shown below.
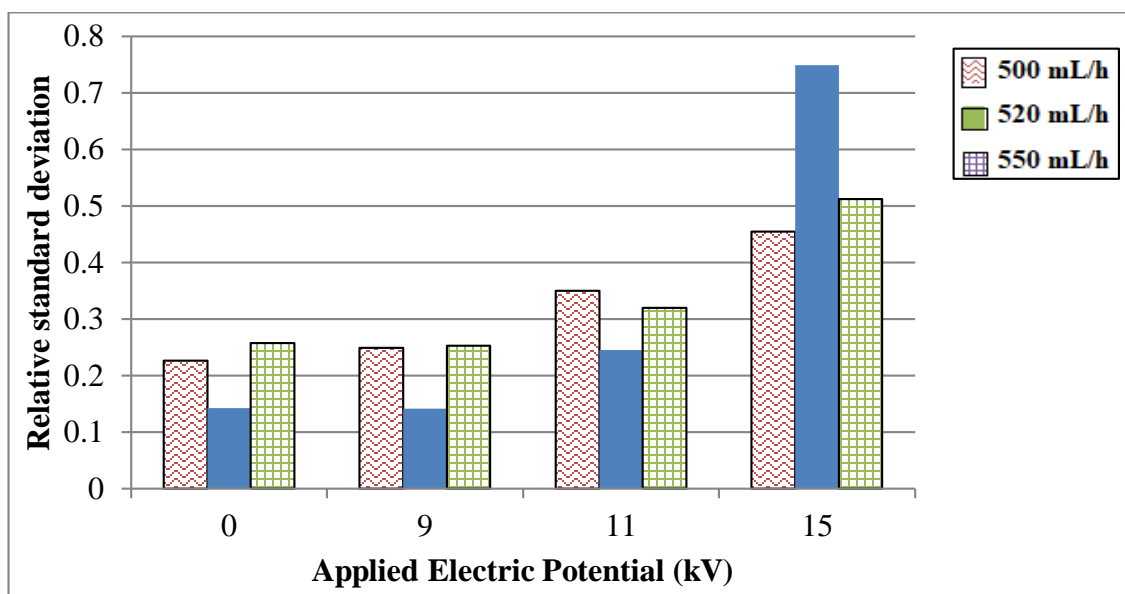
Figure 4.23: Relative standard deviation of droplet size generated at a different flow rate at each applied potential for 10% w/w IMF solution.

Figure 4.23 showed that in each flow rate the droplets size distribution at 0 kV and 9 kV presents a relatively similar distribution with an RSD of approximate 0.25 and below. In the literature, distributions with RSD less than 0.2 are considered to be mono-dispersed spays (Agostinho et al., 2012). Therefore, the distributions for 0 kV and 9 kV at 520 mL h^{-1} can be considered to have mono-dispersed droplets. In the case spray of 11 kV and 15 kV, the distributions are broad giving an RSD greater than 4. This is in line with the

study of Agostinho et al. (2012), in which they found that whipping break up resulted in a higher RSD.

4.4.2.2 Electrospray Characteristics of 20% w/w IMF Solutions

As shown in Figure 4.24 below, the droplet formation mechanism at 0 kV to 9 kV was due to varicose break up and that for 11 kV and 15 kV was due to whipping breakup.
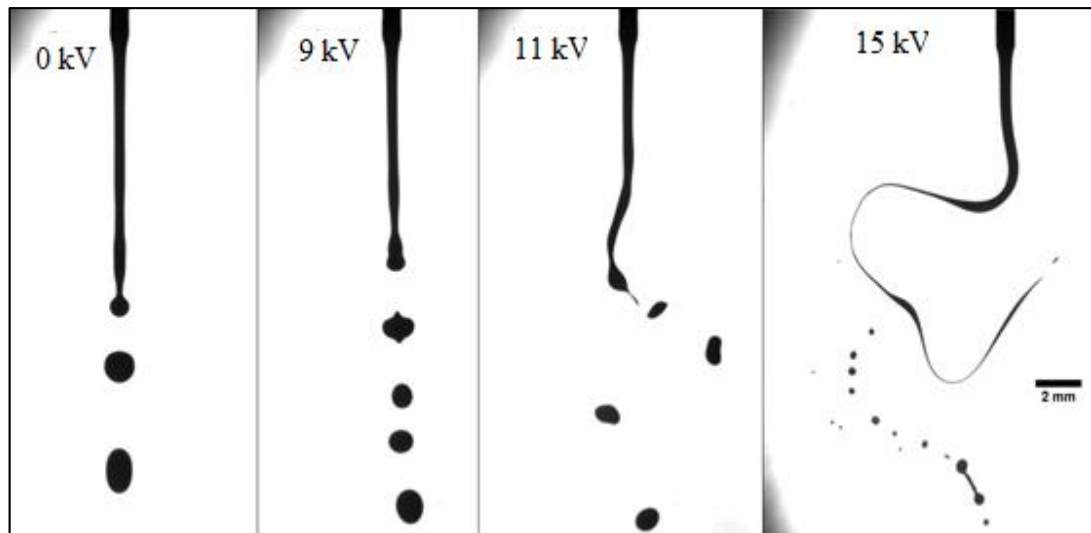
Figure 4.24: Snapshots showing droplet formation processes at different applied potential using 20% w/w IMF solution with a flow rate of 500 mL h^{-1}.

As discussed in case of 10% w/w solutions with regard to breaking processes, the movie analyses for this solution also showed that the spray comprised the main droplets, doubles, triples, and the satellite droplets. However, there was a peculiar characteristic observed for the 20% w/w solution. The droplets had pronounced deformations, in that, they deformed into prolate and oblate spheroids as they progressed downward. Considering the size quantification for this work was carried using Feret's diameter, such movement affected the shape of size distributions. This is because the Feret's diameter gives the particle size along the defined reference line (Hinds 1999). In our

case, the reference was the outer diameter of the nozzle (oriented horizontally). Another possible way was to quantify the size using the equivalent diameter of the projected area (Hinds, 1999), however, almost a similar distribution was obtained.

Figure 4.25 presents size distribution curves for 500 mL h^{-1}, 520 mL h^{-1}, and 550 mL h^{-1} at different applied potential. Starting with the size distribution for 500 mL h^{-1}, the 0 kV spectrum has three modes with the first mode positioned at 1.1 mm, and it is attributed to the main droplets, the second mode positioned at 1.4 mm and attributed to doubles, and the third mode at 1.8 mm that represent four droplets merging together. In the movies analyses, satellite droplets of size 0.5 mm were present in the spray, though they are not depicted in the distribution.

At 9 kV, the spectrum has the peak associated two peaks, one that attributed to the main droplets and a small peak associated with satellite droplets. It can be noted that the main droplet peak trails to the right and shifts to the left to 1.0 mm. The trailing is an indication that the spray comprised doubles and triples droplets which correspond to the movies. The shifting to the left is attributed to the effect of electric stress in the reduction of droplet size as explained earlier.

At 11 kV, the distribution assumes more or less a broadened mono-distribution, though compromised by the small peak to the left. It was clear from the movies that a broad size of droplets was generated during the oscillation of the jet. Also unlike the case of 10% w/w, it was observed that now and then a ligament between the leading droplet and the tip of the jet collapsed into a small single droplet.

At 15 kV, the breakup mechanism resembled that of 10% w/w IMF solution. Therefore, the spray consisted of more small droplets and a few big droplets. Similarly, the ligaments' diameter introduced an additional number to the droplets sizes.

At an increased flow rate of 520 mL h^{-1} and 550 mL h^{-1} it is evident that the droplets generated in the case of 0 kV can still be categorized into the main droplets (at 1.1 mm), doubles (1.4 mm), triples (1.6 mm) and the satellite droplets (~0.5 mm). From the movie analyses, it was observed that most droplets coalesce after breaking especially when a big droplet pinched from the jet.

At 9k, the distribution is more or less similar to the case of 500 mL h^{-1}. The main peak trails to the right and there is the presence of a peak associated to the satellite droplet. The only discernible difference is the position of the main peak. However, the effect of the applied potential tends to reduce the size of the generated droplets.

At 11 kV, the breakup process is as discussed for 500 mL h^{-1}; thus, it shows a similar distribution. In which the main peak represents a broad size distribution with the mode positioned at 1.1 mm while the small peak to the left represents small droplets generated with its mode at 0.4 mm. At 15 kV, the applied potential had resulted into a wide distribution, a characteristic of whipping break-up.

Figure 4.25: Different droplets size distribution curves for 20% w/w IMF solution at different electric potential operated at 500 mL h^{-1} (above), 520 mL h^{-1} (middle), and 550 mL h^{-1} (below).

In order to quantify the droplets size distributions for 20% w/w IMF solution at the three flow rate, Figure 4.26 presents the RSD at each applied potential. The figure shows that for each flow rate the uncharged spray generated more or less mono-dispersed droplets. In each case, upon application of the electric potential, the RSD increased with an increase in applied potential. Therefore, this indicated that the spray for charged jets produced a poly dispersed spray.

Figure 4.26: Relative standard deviation of droplet size generated at a different flow rate at each applied potential for 20% w/w IMF solution.

4.4.2.3 Electrospray Characteristics of 30% w/w IMF Solutions

Figure 4.27 shows droplets formation at the different applied potential for 30% w/w IMF solution operated at 500 mL h^{-1}. In this case, the droplet formation at 0 kV and 9 kV was due to varicose breakup and that for 11 kV and 15 kV whipping break up. In addition, the breaking up processes at each applied potential showed characteristics that were discussed earlier in section 4.4.2.1.

Figure 4.27: Snapshots showing droplet formation processes at different applied potential using 30% w/w IMF solution with a flow rate of 500 mL h^{-1}.

Figures 4.28, 4.29, and 4.30 are size distribution curves for 500 mL h^{-1}, 520 mL h^{-1} and 550 mL h^{-1} respectively. Looking across them it was noticed that the main droplets peak was positioned at 1.1mm for 500 mL h^{-1} and 520 mL h^{-1}, but positioned to the left at 1.0 mm for 550 mL h^{-1}. The distributions also show the presence of doubles and triples, but the satellite droplets were only observed in 550 mL h^{-1}.

Upon application of an electric potential, it was observed that at 9 kV the three distributions assume a normal distribution. Notably, the position of main peak for both 500 mL h^{-1} and 550 mL h^{-1} shifts to the left but, that for 520 mL h^{-1} remained constant with a narrow span. These two situations show production of smaller main droplets than their respective 0 kV situation as discussed earlier in section 4.4.2.1.

Further increase of applied potential to 11 kV and 15 kV the effect was the production of droplets with a wide spectrum, where, the width increased with increase in applied potential.

Figure 4.28: Showing different droplets size distribution curves for 30% w/w IMF solution at different electric potential operated at 500 mL h^{-1}
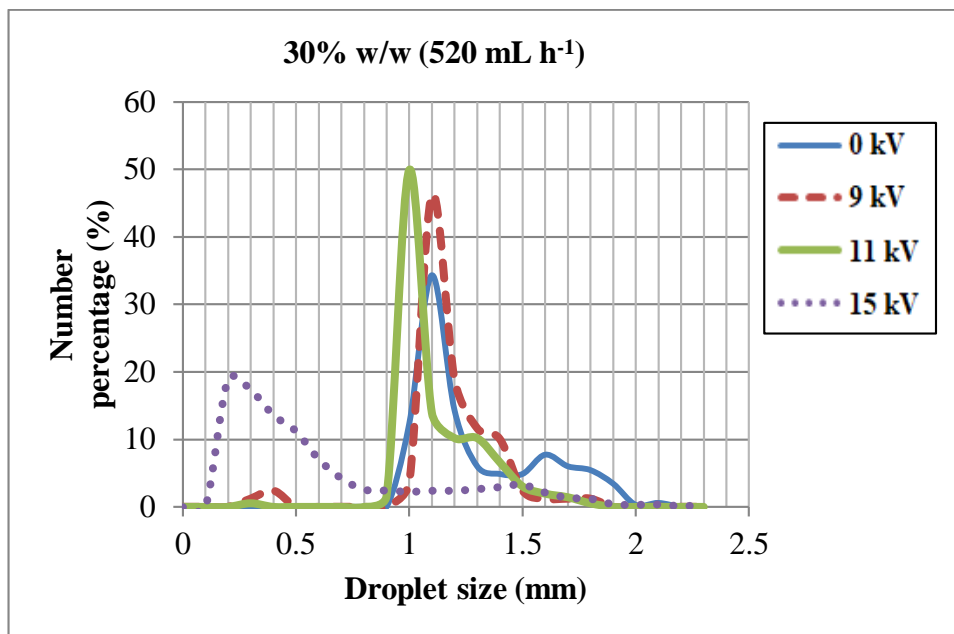
Figure 4.29: Showing different droplets size distribution curves for 30% w/w IMF solution at different electric potential operated at 520 mL h^{-1}.
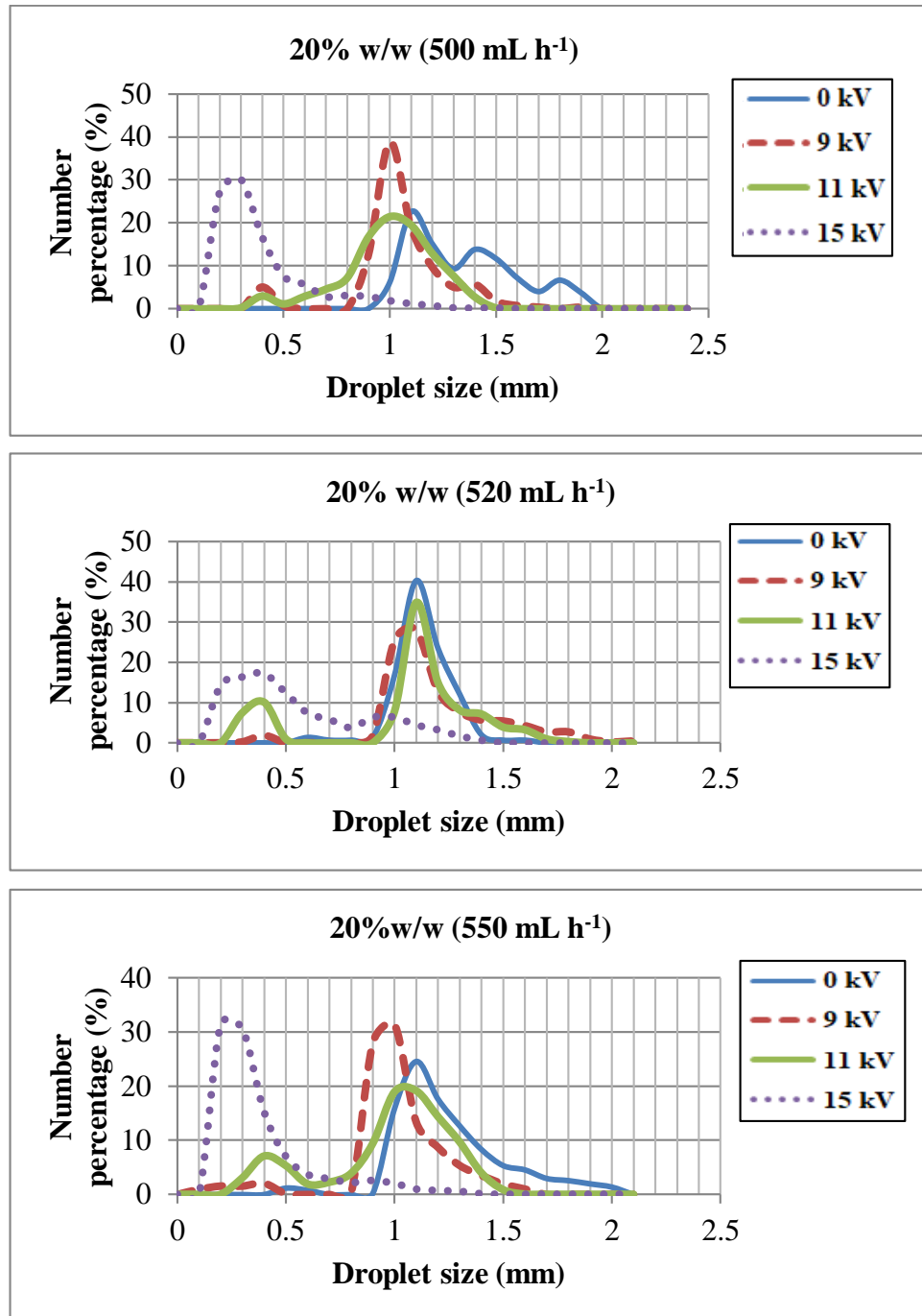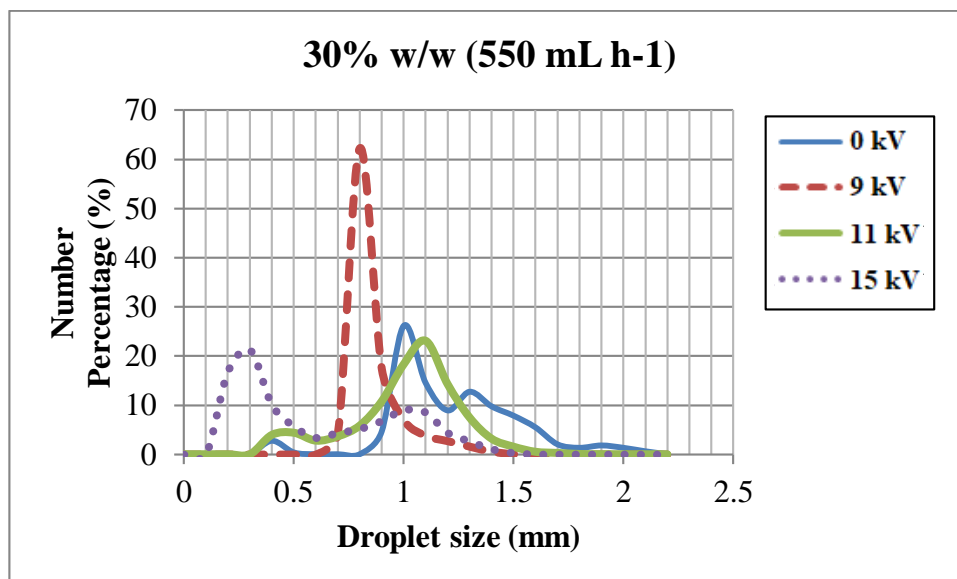

Figure 4.30: Showing different droplets size distribution curves for 30% w/w IMF solution at different electric potential operated at 550 mL h^{-1}.

Figure 4.31 shows the RSD of the size distribution obtained at the three flow rates at different applied electric potential. In this case, it was seen that the sprays for 9 kV comprised monodispersed droplets. This was also depicted in their size distribution curves. This shows that the application of the electric potential reduced the formation of upward short waves generated by the pinching of a droplet. The onset of whipping break-up at 11 kV resulted in a broad distribution which widens even more at 15 kV.
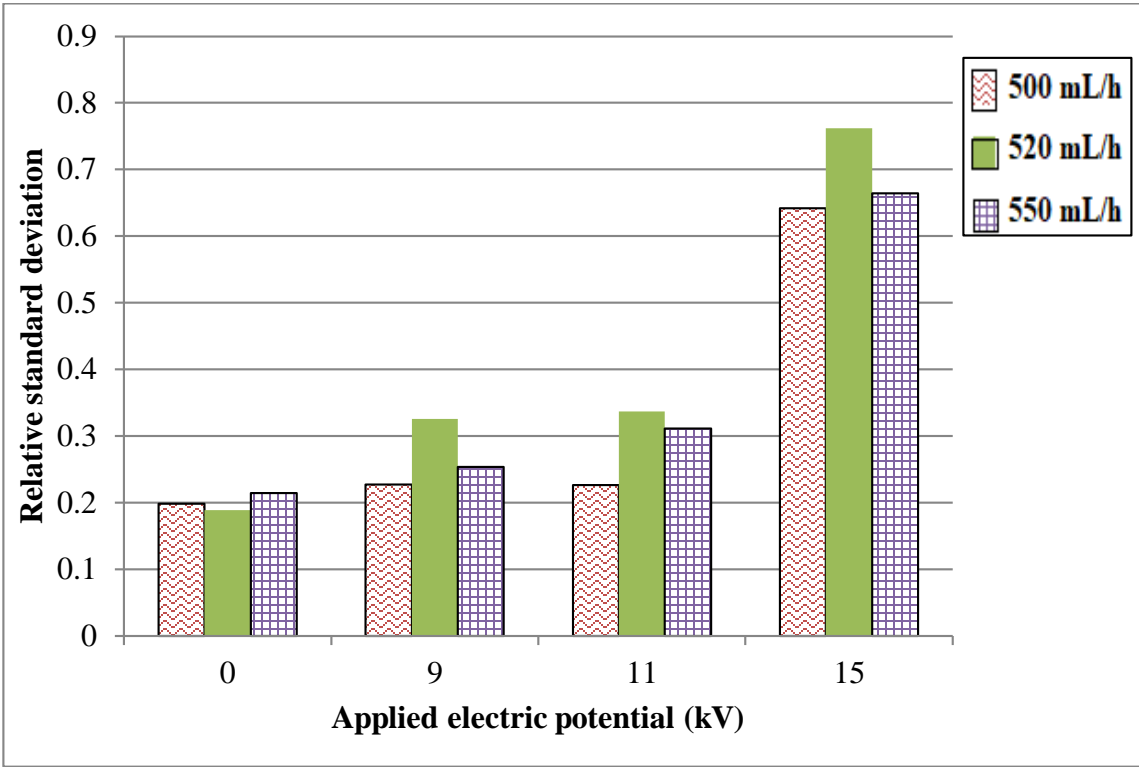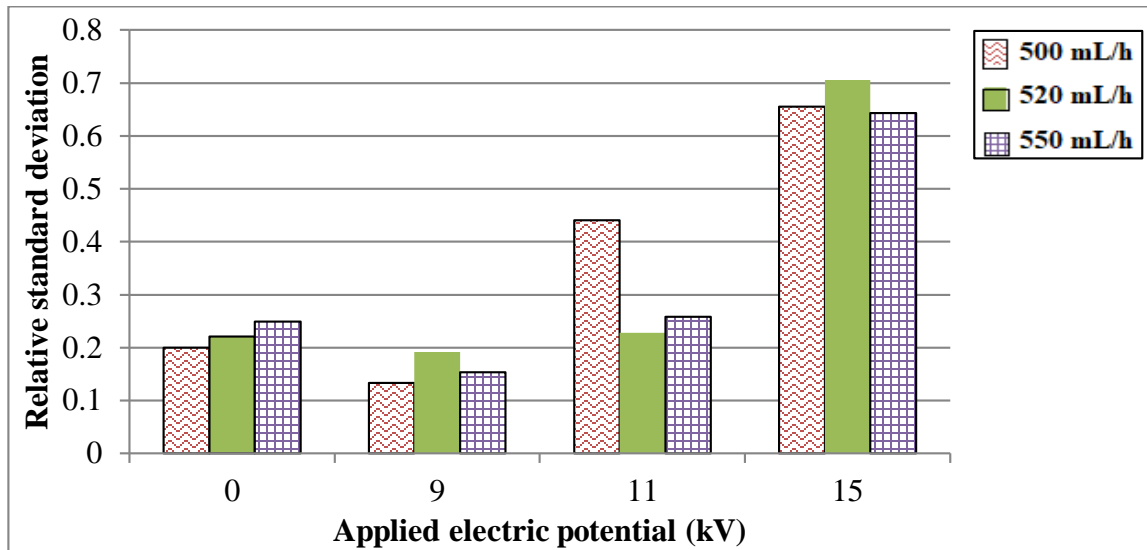

Figure 4.31: Relative standard deviation of droplet size generated at a different flow rate at each applied potential for 30% w/w IMF solution.

4.4.2.1 Electrospray Characteristics of 40% w/w IMF Solutions

Figure 4.32 is the physical appearance of droplet formation mechanism for 40% w/w IMF solution at different potential when operated at 500 mL h^{-1}.
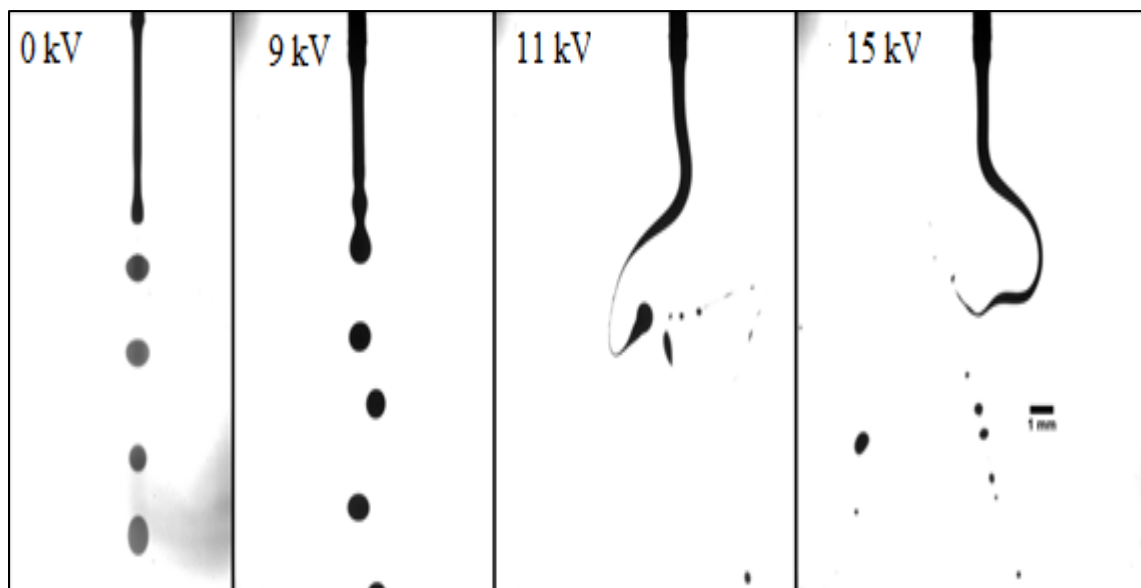

Figure 4.32: Snapshots showing droplet formation processes at different applied potential using 40% w/w IMF solution with a flow rate of 500 mL h^{-1}.

Figure 4.33 shows the size distribution obtained at the different applied potential for the three flow rates (i.e. 500, 520 and 550 mL h^{-1}). As it can be seen, at 0 kV, the generated droplets are primarily the main droplets and the big droplets. With the current solution, there was the presence of the satellite droplets but they were not that pronounced compared to the 10% w/w and 20% w/w solutions. Like in 30% w/w, the position of the peak associated with the main droplets remains almost equal at 1.2 mm in 500 mL h^{-1} and 520 mL h^{-1} and also positioned left at 1.1 mm for 550 mL h^{-1}. A comparison to the previous solutions, the results indicates production of larger droplets using 40% w/w solution with 500 mL h^{-1} and 520 mL h^{-1}.

At 9 kV, a normal size distribution was obtained in the case of 500 mL h^{-1} and 550 mL h^{-1} while three modes in case of 520 mL h^{-1} were obtained.

In the case of 11 kV, the size distribution shows a broad bimodal distribution. The mode to the right was attributed to big droplets while that to the left was attributed to the small-sized droplet. Considering that the breakup process was due to whipping, it was not possible to categorize the droplets as done in 9 kV.

At 15 kV, the droplets generated took the form of a wide distribution which is a characteristic of whipping break up.
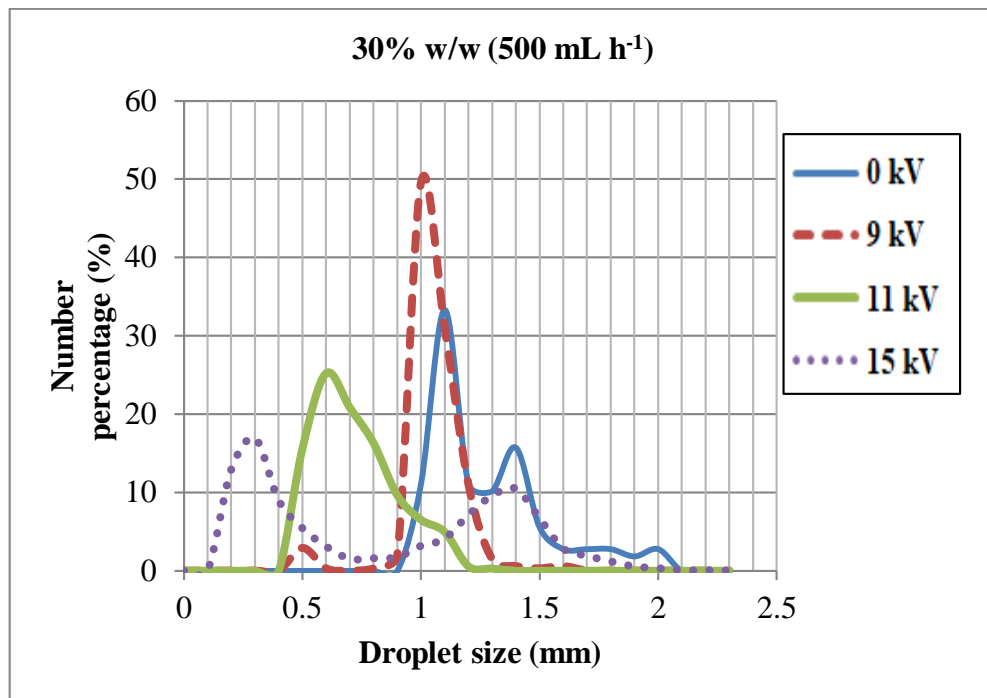
Figure 4.33: Different droplets size distribution curves for 40% w/w IMF solution at different electric potential operated at 500 mL h⁻¹ (above), 520 mL h⁻¹ (middle), and 550 mL h⁻¹ (below).

The quantification on the effect of applied potential on the droplet size by use of RSD is shown in Figure 4.34. The results show that the uncharged spray had rather monodispersed droplets. Application of an applied potential of 9 kV resulted to decrease in RSD in particular for 500 mL h^{-1} and 550 mL h^{-1}. Further increase of an applied potential led to the production of polydispersed droplets.

Figure 4.34: Relative standard deviation of droplet size generated at a different flow rate at each applied potential for 40% w/w IMF solution.

4.4.2.2 Electrospray Characteristics of 50% w/w IMF Solutions

Figure 4.35 shows the physical appearance for 50% IMF solutions at a different potential with a flow rate of 500 mL h^{-1}. It was noted that with the 50% w/w IMF solutions, the droplet formation at 0 kV and 9 kV was due to varicose break-up, at 11 kV due to whipping, and at 15 kV break up of a ligament through whipping that disintegrated into droplets through a varicose breakup. Consequently, from the movies,

it was noted that for the same flow rate, the 50% w/w jets had breakup length longer than that of 10%, 20%, 30% and 40% w/w.
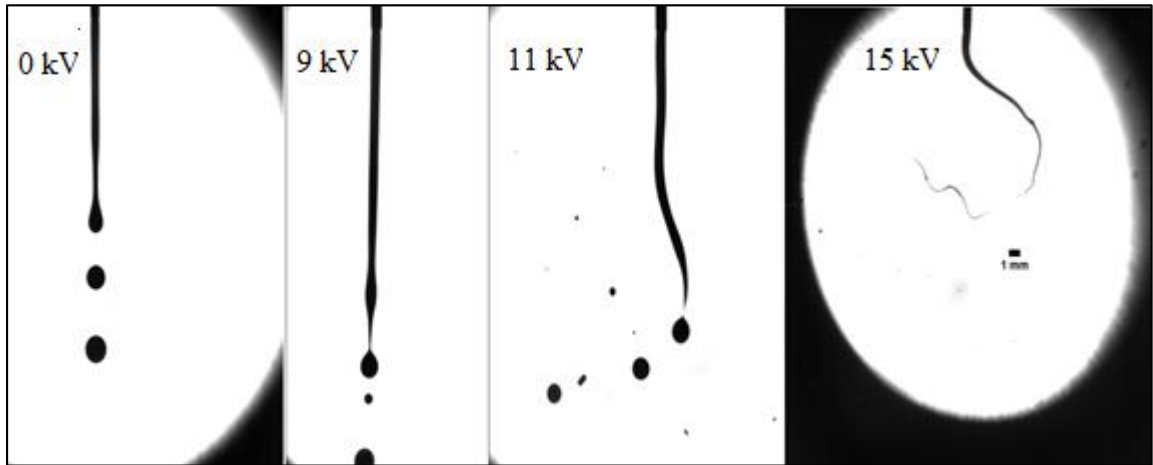
Figure 4.35: Snapshots showing droplet formation processes at different applied potential using 50% w/w IMF solution with a flow rate of 500 mL h^{-1}.
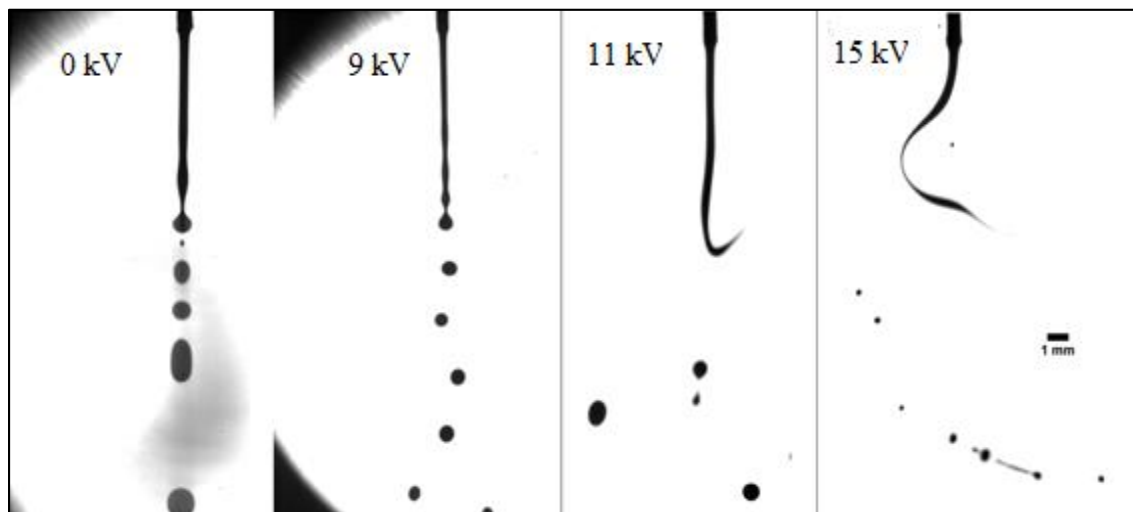
Figure 4.36 shows the droplet size distribution at for 0 kV, 9 kV and 11 kV. For this solution, the analyses for 15 kV posed a challenge since the whipping was so violent that the generated droplets were out of focus on the microscopic lens. By using the wide view lens, the results only gave an indication of jet break up process and was not possible to quantify generated size (see Figure 4.37).

From the three graphs in Figure 4.36, the profile of the generated droplets at 0 kV was multimodal. The main peak was positioned at 1.5 mm, 1.6 mm, and 1.7 mm for 500 mL h^{-1}, 520 mL h^{-1}, and 550 mL h^{-1} respectively. From the movies, it was observed that the peaks to the right of the main peak resulted from the hanging droplet swallowing an incoming droplet. The incoming droplets were seen to vary in size. For instance, in the graph of 500 mL h^{-1}, the peak positioned at 1.9 mm represented doubles (i.e. droplets

with volume twice that of the main droplet). The generation of a wide range of droplets shows that the solution poses a unique characteristic.

On application of an electric potential, at 9 kV, there was a tendency to reduce the polydispersion of the droplets. For 500 and 520 mL h^{-1}, the distribution assumed a bimodal distribution in which the big peaks represented main droplets and small peaks the satellite droplets. For 550 mL h^{-1}, the spectra assumed a normal distribution, and looking at the movies the few small and big droplets were observed.

At 11 kV, the profiles show a bimodal distribution which comprises big droplets and small droplets. From the movie analyses, it was seen that the breakup process that was as discussed earlier in section 4.3.2.1. During the whipping motion a liquid filament was formed in between a hanging droplet and the tip of the jet, which after detaching and pinching off from the jet, the droplet collapsed to a single droplet and the filament disintegrated into small droplets of different sizes. No spraying of the individual droplet was observed in this case.
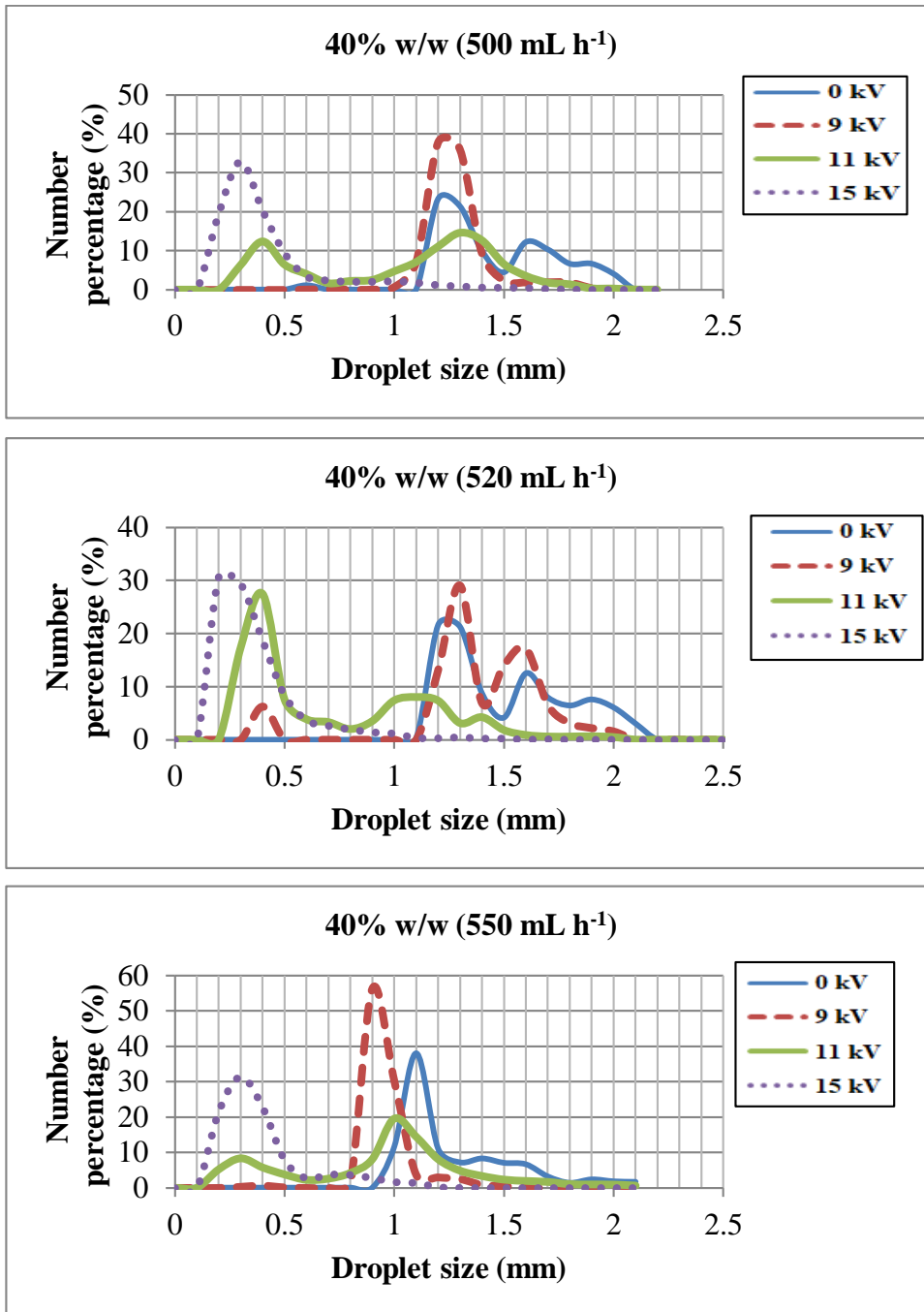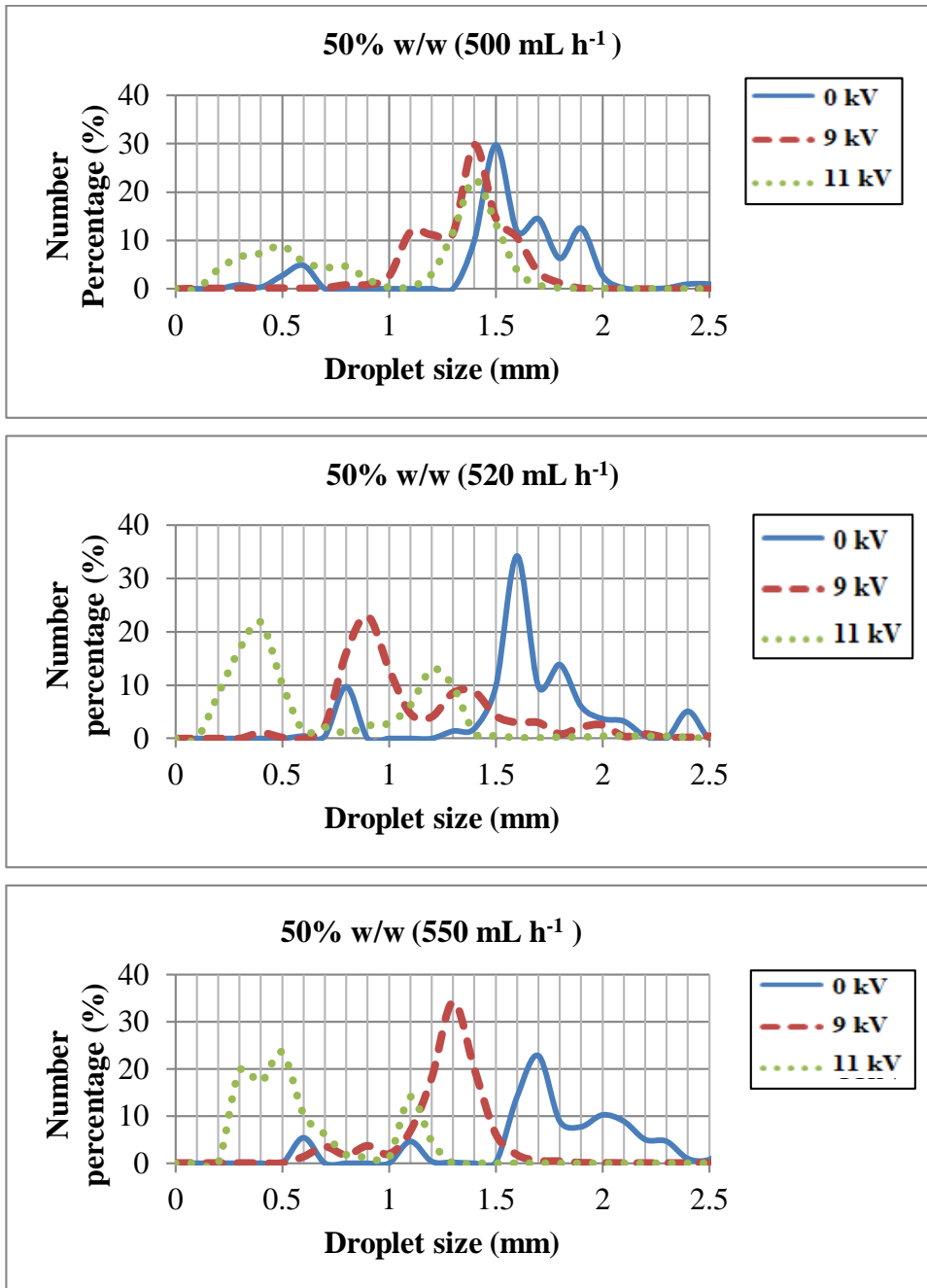
Figure 4.36: Different droplets size distribution curves for 50% w/w IMF solution at different electric potential operated at 500 mL h^{-1} (above), 520 mL h^{-1} (middle), and 550 mL h^{-1} (below).
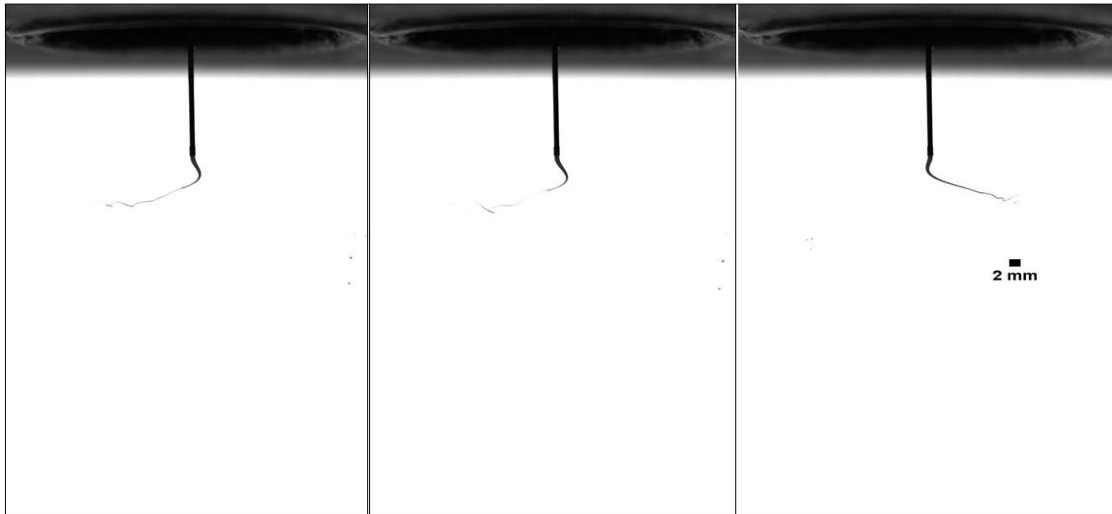
Figure 4.37: Snapshot taken with a wide lens showing droplets formation at 15 kV for 50% w/w with a flow rate 520 mL h^{-1}.

Figure 4.38 shows the RSD of droplets obtained in each flow at different applied potential. It can be observed that monodispersed spray was obtained at 9 kV and with flow rates of 500 mL h^{-1} and 550 mL h^{-1}. From the size distribution curve, it is clear that the presence of a wide size distribution resulted to increase in RSD.
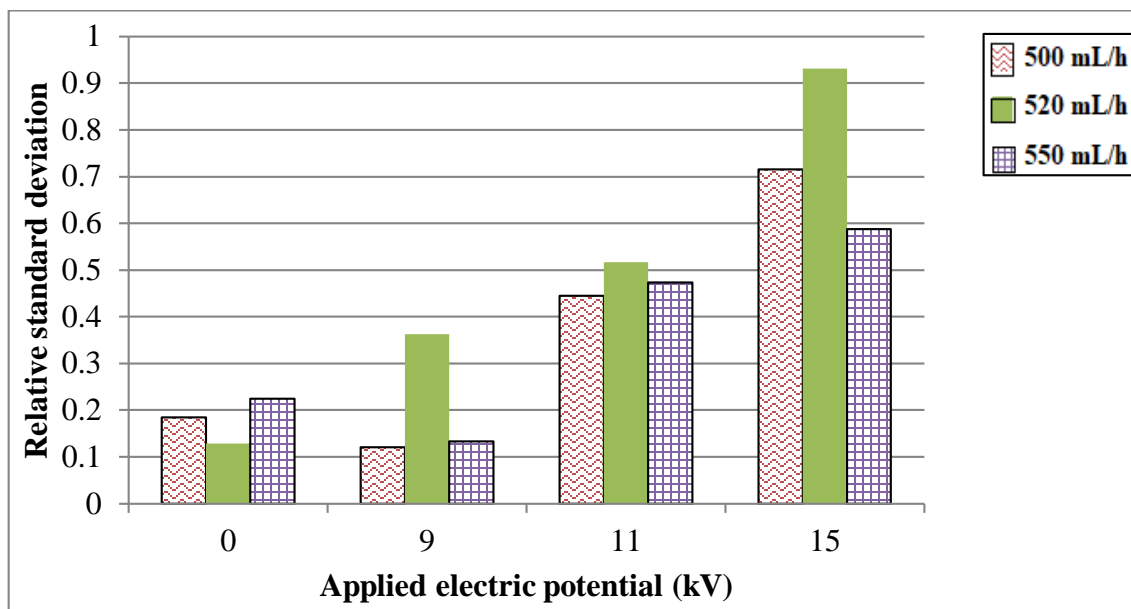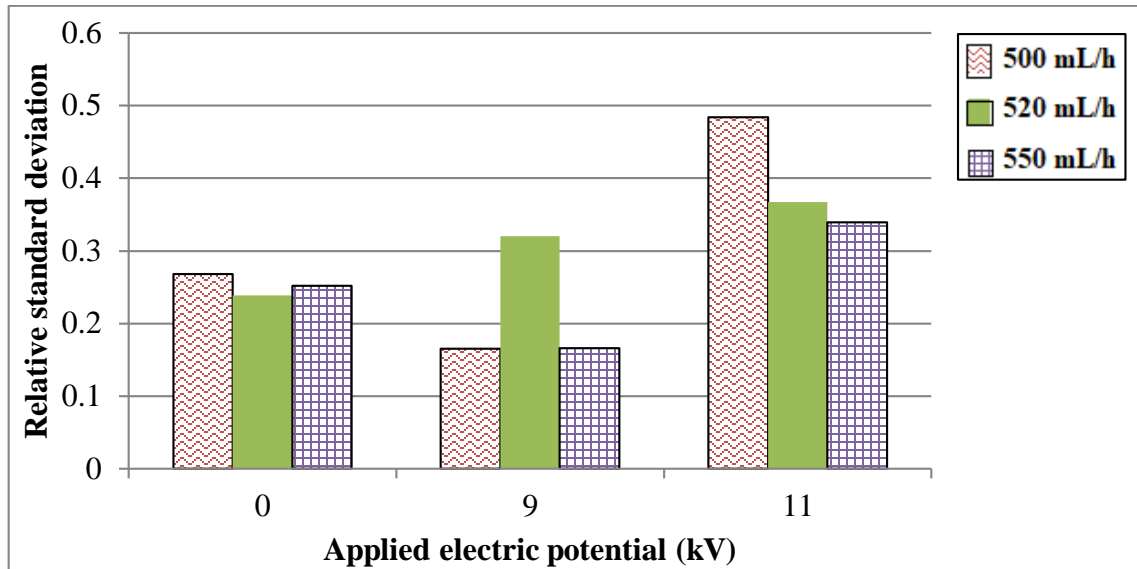
Figure 4.38: Relative standard deviation of droplet size generated at a different flow rate at each applied potential for 50% w/w IMF solution.

4.4.3 The Tendency in Droplets Sizes Across the Solid Content

Having looked at the tendency for each IMF solution at a different flow rate and different applied potential, this section draws a comparison based on solid content at each flow rate. As noted earlier, in the analyses of movies regarding the breaking process, different droplets with different volume were generated. As a result, these droplets were termed as the main droplets, doubles, and triples. Another category that was identified was the satellite droplet. Therefore, such intrinsic characteristic was found necessary to investigate across IMF solutions with different solid content at same flow rate.

The movie analyses for 0 kV, 9 kV, and 11 kV considered those droplets generated as a result of jet break up and not those that formed due to coalescence. For 15 kV, the modal sizes of the generated droplets from a breaking ligament were considered. For that

reason, the main droplets were selected to draw the comparison across the variant IMF solutions and the presence of the other categories of droplets was indicated.

Figure 4.39 shows a comparison of the main droplets obtained at a different applied potential with a flow rate of 500 mL h^{-1} for different solid content. Along with, it is a key showing the other categories present in the spray at different applied potential. It was observed that in the uncharged situation, the solutions with 10%, 20%, and 30% w/w generated primary droplets of size 1.1 mm, those with 40% w/w generated primary droplets of size 1.2 mm and with 50% w/w generated primary droplets of size 1.7 mm. In all the solutions there was the presence of doubles, triples and satellite droplets.

On applying the electric potential of 9 kV, there was a minimal size reduction for 10 to 40% w/w solution, but a big change was noted for 50% w/w solution. The applied potential also minimized the production of doubles and triples while satellite droplets were observed in all the solutions. By increasing the applied potential to 11 kV, the size of the droplets breaking from the jet remains more or less constant. It is plausible to state that there was the production of small droplets which could not be referred as satellite and big droplets which could not be categorized as doubles or triples since they formed through the breaking of a ligament. Further, an increase of applied potential to 15 kV led to a tremendous decrease in droplet size for all solid content.
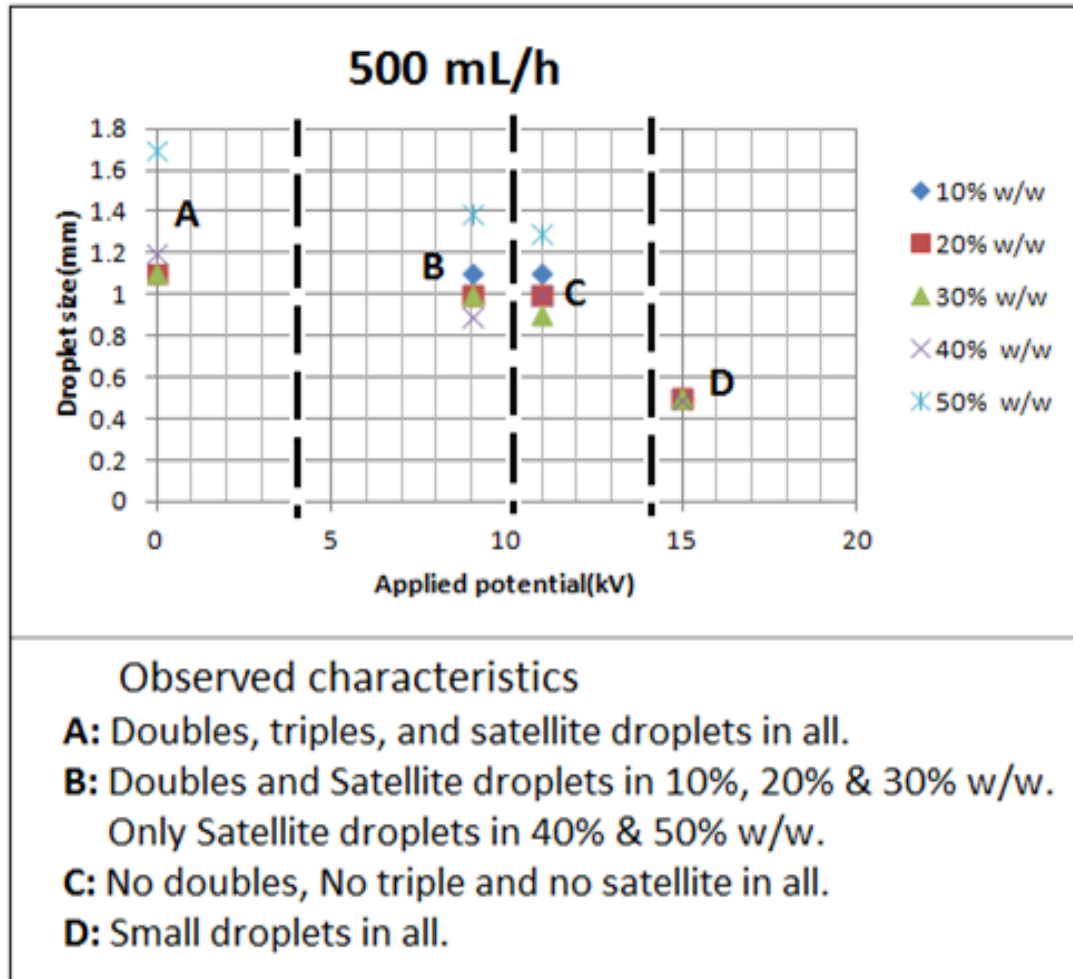
Figure 4.39: Showing primary droplets and other generated droplets for different solid content at a flow rate of 500 mL h^{-1}.

As it can be seen in Figure 4.40 and 4.41, at an increased flow rate had the overall effect of an applied potential in the generation of the small size of droplets. Also, all doubles and triples vanish at 11 kV. Because of large number of small droplets, it was not possible to differentiate them with satellite droplets.
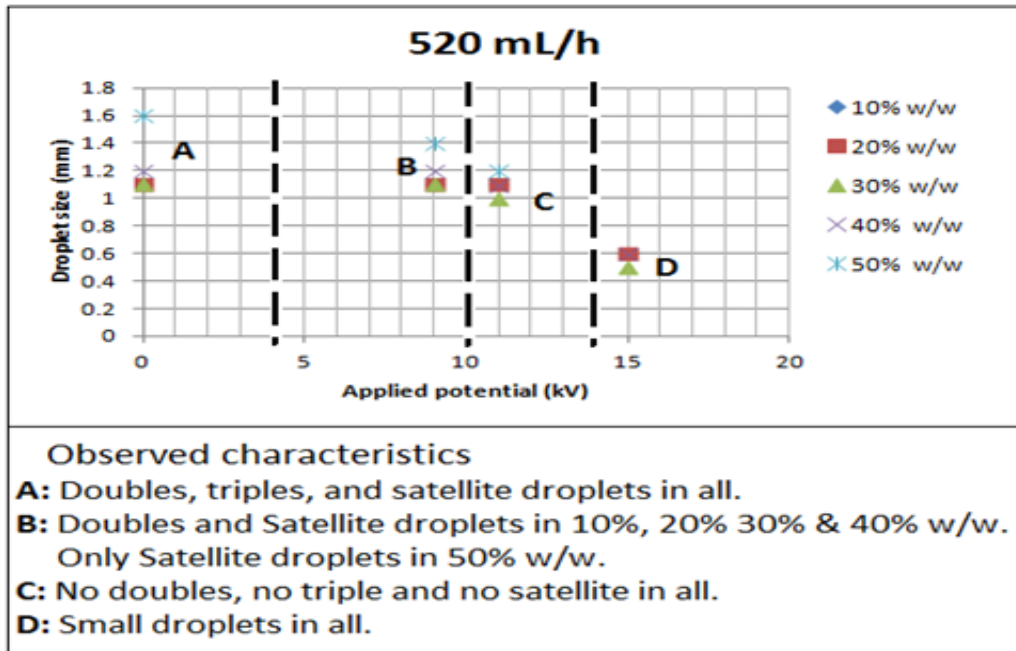
Figure 4.40: Showing primary droplets and other generated droplets for different solid content at a flow rate of 520 mL h^{-1}.
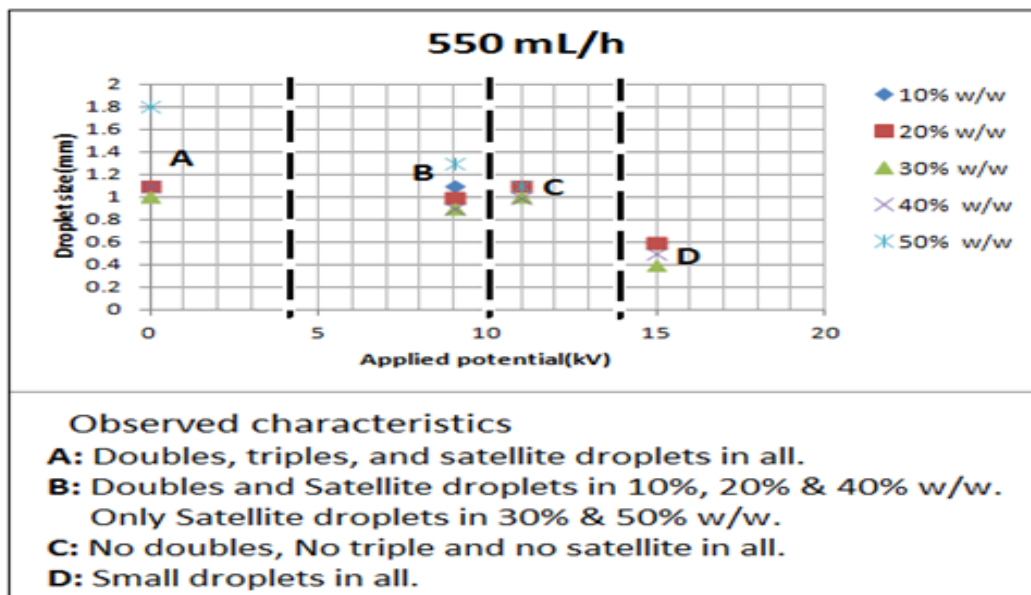
Figure 4.41: Showing primary droplets and other generated droplets for different solid content at a flow rate of 550 mL h^{-1}.

4.4.4 Droplet Spatial Distribution

In addition to the production of small droplets, another effect of the applied potential in electrospray is the spray dispersion. This is attributed to the production of charged droplets in which the action of an electric field force and Coulombic interaction causes the droplets to repel that lead to spray dispersion. Such aspect is necessary during the design for an evaporator during the spray drying process. In all IMF solutions used, by increasing the applied potential droplets dispersion was eminent see Figure 4.42 (i), (ii) and (iii). The set of images (i) were obtained with 20% w/w, ii) with 40% w/w and iii) with 50% w/w all operated at a flow rate of 520 mL h^{-1}. The images for 0 kV are a single frame from the respective movies while those for 6 to 15 kV were obtained by stacking together 200 frames.
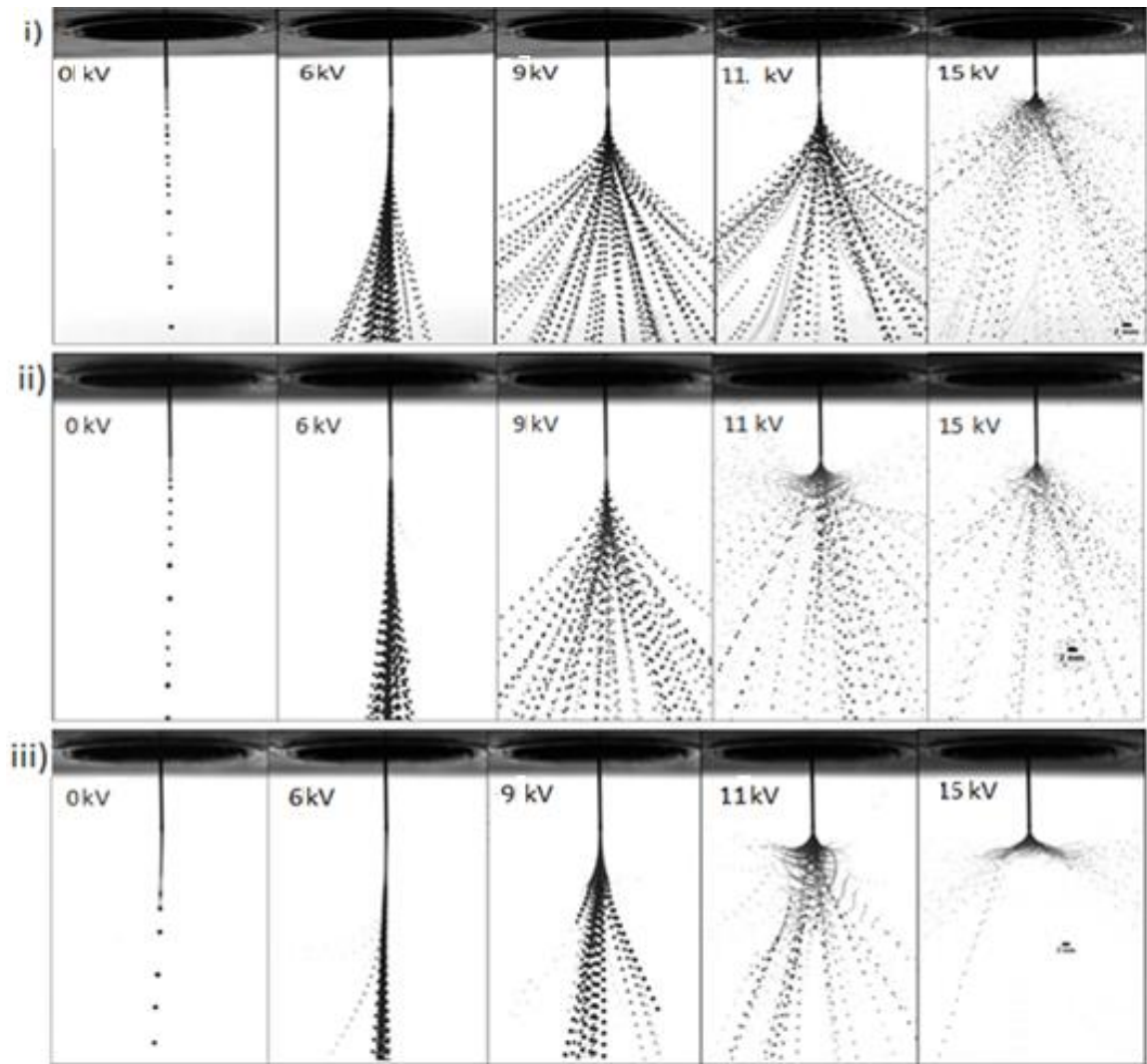
Figure 4.42: Showing droplets dispersion at different potentials and at a flow rate of 520 mL h^{-1} for different solid content i) 20% w/w, ii) 40% w/w, and iii) 50% w/w.

Figure 4.42 shows that as the applied potential increases the droplets disperses to form a spray envelope. Additionally, the IMF solutions with 20% and 40 % had broader spray envelopes that those with 50% w/w at same applied potential. At an increased applied potential (i.e. 15 kV), the 50% w/w IMF solution presented a different spray envelope. This was also observed for the other flow rates see Figure 4.43. The set of images a)

shows a flow rate of 500 mL h^{-1} b) a flow rate of 520 mL h^{-1} while a set of images i), ii) and iii) are for 30% w/w, 40% w/w and 50% w/w IMF solutions respectively. Even though, relatively small droplets were obtained at 15 kV, the droplets tracks show that the droplets are uncontrollable, especially for 50% w/w since it showed an open cone or "umbrella effect."
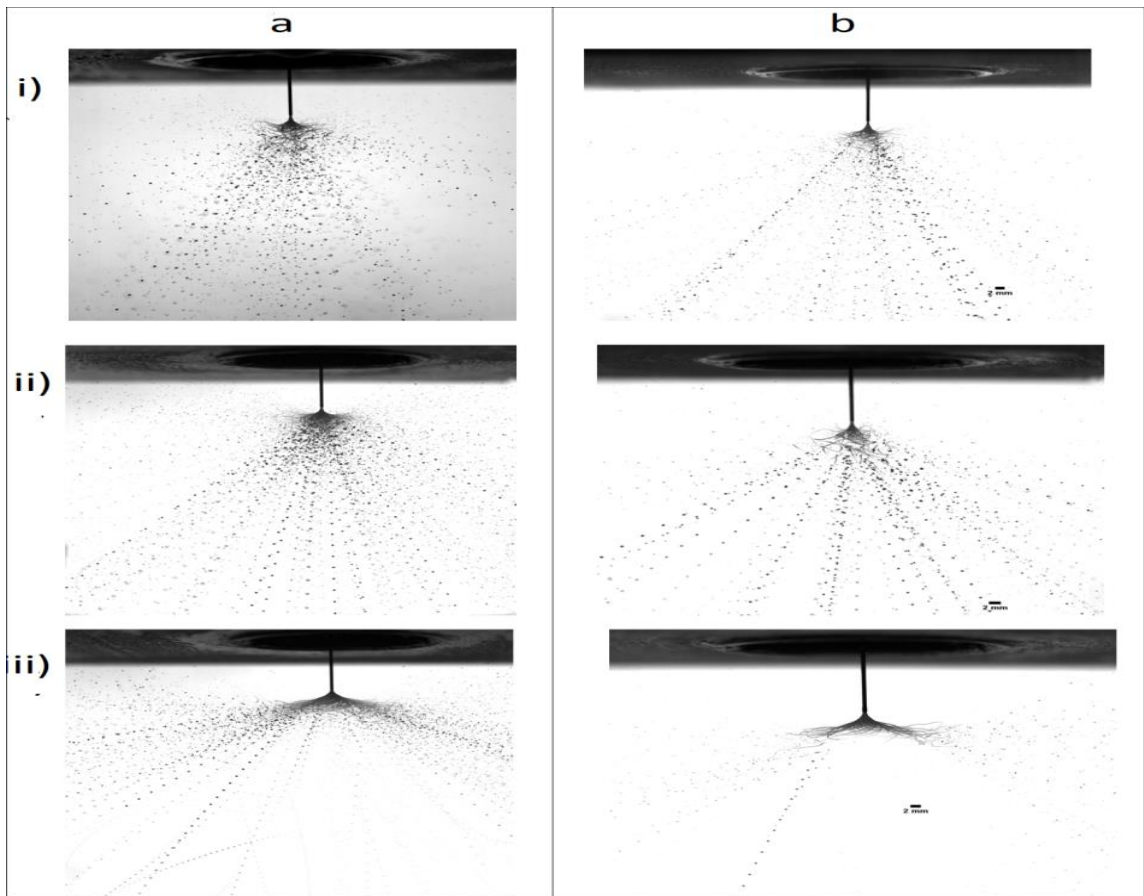
Figure 4.43: Spray envelope at flow rate of 500 mL h^{-1} (a) and 520 mL h^{-1} (b) for 30% w/w (i), 40% w/w (ii) and 50% w/w at an applied potential of 15 kV.

4.5 Application of EHDA on IMF Solution with 55% w/w Solid Content

As elucidated in the first part of this chapter regarding the rheology characterization of IMF solutions, it was illustrated that IMF solutions with 55% w/w solid content are a Non-Newtonian liquid with a flow behavior described as Pseudoplastic or shear thinning liquid. In the second part regarding electrospraying, it was shown that the IMF solutions with solid content equal to or greater than 40% w/w pose a challenge while electrospraying in the dripping regime. However, with such IMF solutions, it was possible to electrospray in the jetting regime in a mode described as the simple jet mode. In addition, relatively small droplets were obtained in the simple jet mode with whipping break up. Therefore, EHDA operated in the simple jet mode with whipping break up was chosen as suitable to apply on IMF solutions with a solid content of 55% w/w

The first part of the following section presents investigations carried out using different nozzle geometries in search of a suitable nozzle configuration. Characteristics of the electric field around the nozzle is modeled using COMSOL Multiphysics® 4.4. Subsequently, using the selected nozzle which has four orifices the results on spray characteristics obtained at different total flow rates and different applied potentials are discussed.

4.5.1 Nozzle Configuration Investigation

The reason that prompted this investigation is that, unlike the IMF solutions with 50% w/w and lower in which had a continuous jet while pumping through a capillary nozzle, for 55% w/w IMF solutions parcels or ligaments were obtained instead. Therefore, upon application of the electric field, such parcels produced particles in the range of 8mm. In addition, a nozzle with large throughput was required since such solid content is of interest in the industrial processing of infant powder milk production. The nozzle development started with the serrated nozzle, a nozzle with a grooved insert and lastly a nozzle with four orifices.

4.5.1.1 Serrated Nozzle

The design of serrated nozzle was inspired by the works of Almekinders and Jones (1999). In their work, they showed the use of serration to achieve a multi-nozzle as means of achieving high throughput. In our case, the saw tooth dents were created at the end of a capillary nozzle of ID =1.54 mm and OD = 1.83 mm. Figure 4.44 shows a picture of the serrated nozzle design (magnification x40). The idea behind this design of the nozzle was to obtain several jets using a single nozzle by creating points with high electric fields using the sharp points of saw-tooth dents.

Figure 4.44: A photo of the serrated nozzle

Preliminary experiments were carried out using ethanol as a test liquid, and upon applying an electric potential liquid jets were obtained in each dent as shown in Figure 4.45 (a). Then, using IMF solutions with 55% w/w solid content, it was observed that the solution could not be manipulated to flow through the dents and a normal flow was obtained as shown in Figure 4.45 (b).
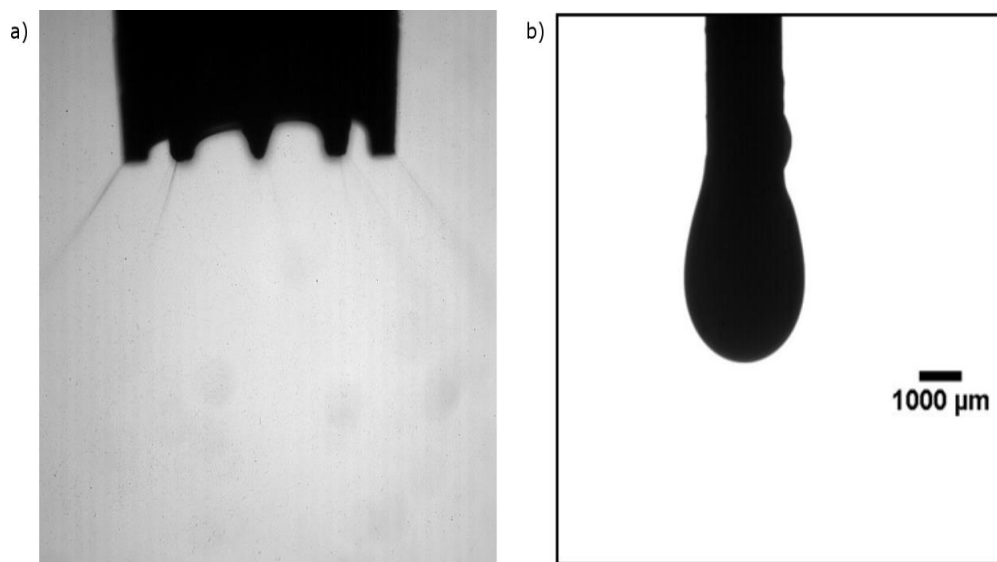
Figure 4.45: Ethanol electrospray jets using the serrated nozzle with a flow rate of 1 mL h^{-1} and an applied electric potential of 12 kV, b) IMF solution with solid content 55% w/w issuing from the serrated nozzle at a flow rate of 200 mL h^{-1}.

4.5.1.2 Nozzle with a Grooved Insert

Figure 4.46 shows the picture of a nozzle with a grooved insert design and a top and side view (this is meant to aid visualization of the design for lack of a good photograph of the design and both are not to the same scale). Six semi-circular grooves were milled on a surface of a piece of brass rod designed in a manner that when inserted in the nozzle an opening with an internal diameter of 250 μm was formed. This design was inspired by the observation that 55% w/w IMF solution required a physical separation during a flow. It was expected that grooves on the surface of an insert could serve the purpose (i.e. to obtain several jets and increase the throughput).
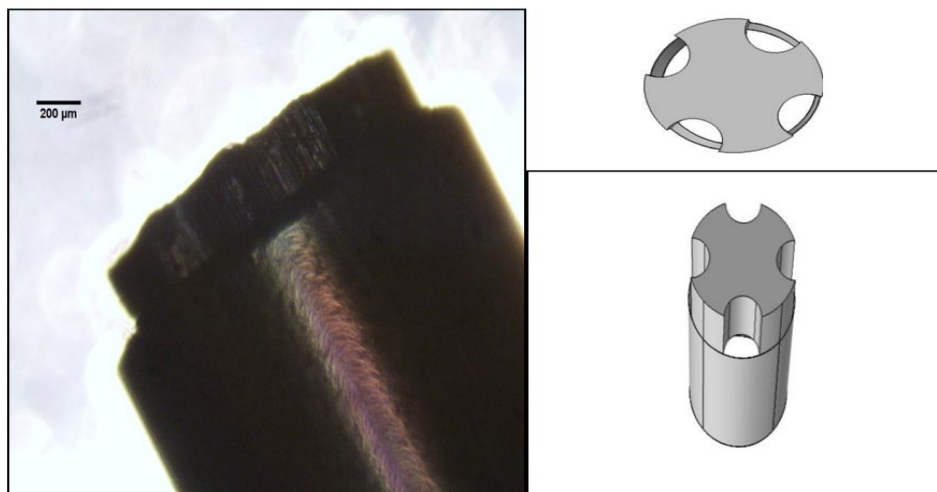
Figure 4.46: A picture of a nozzle with an insert and a top and a side view (to aid visualization).

The preliminary tests using 55% w/w IMF solution proved difficult to pump the solution through due to clogging of the openings after some time. It was observed that the different flows joined at the nozzle exit instead of running separately. Also, the insert posed challenges with regard to spraying as it could detach during the run.

4.5.1.3 Single Nozzle with Four Orifices

The development of this nozzle resulted from the many tests that were carried out using a capillary nozzle with I.D of 0.51, 0.41, 0.33, 0.25 and 0.20 mm. These are blunt end EFD® nozzle gauge 21, 22, 23, 25, and 27 respectively. From the tests carried out, it was noted that the least nozzle size that could allow the solution to pass through with ease was 330 µm. It was also noted that wetting at the nozzle exit was much pronounced. Therefore, a nozzle that could fit the existing electrospray chamber was designed and some factors such as wetting, ease flow of the solution, pressure, and cleaning were considered. A capillary nozzle with I.D = 1.83 mm and O.D = 1.54 mm was fabricated to ease flow for IMF solution and connected to four orifices that were milled on piece of brass mimicking cows' udder. Figure 4.47 shows photos of a single nozzle with four

orifices. The orifices had an I.D = 0.3 mm and separation of 2.65 mm. The orifices are short and their tips are conically shaped to ease the flow without clogging and avoid wetting at the nozzle exit respectively (for detailed dimensions see Appendix).

Figure 4.47: Photos showing a single nozzle with four orifices.

Figure 4.48 shows a snapshot of the nozzle in action. The size of the four jets are in the same range with the internal diameter of the orifice.
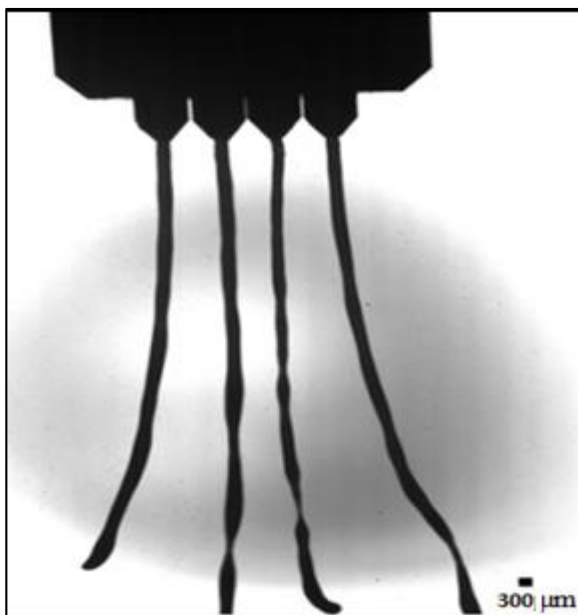
Figure 4.48: A snapshot of 55% w/w IMF solution jets using a single nozzle with four orifices operated at a total flow rate of 1.6 L h^{-1} at no potential.

With four orifices, the design was aimed at achieving a high throughput since it acts like a multi-nozzle system. An advantage of this design compared to other multi-nozzle designs is its simplicity, in that, only a single ring was used as a counter electrode while other designs use several rings (i.e. Agostinho 2013; Bocanegra et al., 2005; Brouwer 2011; Mwangi 2013; Tatemoto et al., 2007). The electric field distribution of this nozzle was investigated using Comsol Multiphysics® software and its comparison was drawn with two configurations; a configuration of a single nozzle with a ring up (as presented by Agostinho, 2013) and a configuration with two nozzles with a ring-up for a multi-nozzle design as developed by Mwangi, 2013. The results are shown and discussed below.

4.5.1.4 Comsol Model and Electric Field Characteristics

As stated above, characteristics of the electric field for the single nozzle design with four orifices were investigated using Comsol Multiphysics® software. A comparison was drawn between this nozzle design and a nozzle with a ring up configuration and a multi-nozzle design configuration as developed by Mwangi (2013). The model gave a prediction on the magnitude of the axial and radial electric field at the nozzle tip. Using an electrostatic (AC/DC) module, a 2D space dimension was used to represent a cross-section of each design. The applied boundaries conditions were the same, i.e. grounded nozzle and charged ring (-7 kV). Table 4.4 below, shows the dimensions of the ring, nozzle and the distance between them for the three designs modeled.

Table 4.4: Dimensions of the modeled nozzles designs.

Design	Ring diameter(cm)			Nozzle diameter (mm)	Nozzle to plate distance (cm)
	Inner	outer	thickness		
Single nozzle	1.7	2	0.01	0.3	1.7
Multi Nozzle	1.7	2	0.01	0.3	1.7
Single Nozzle with Four orifices	4.8	5.4	0.05	(As per appendix II)	1.7

Figure 4.49 below shows the 2D model geometry, the axial and radial electric field plots (versus distance).
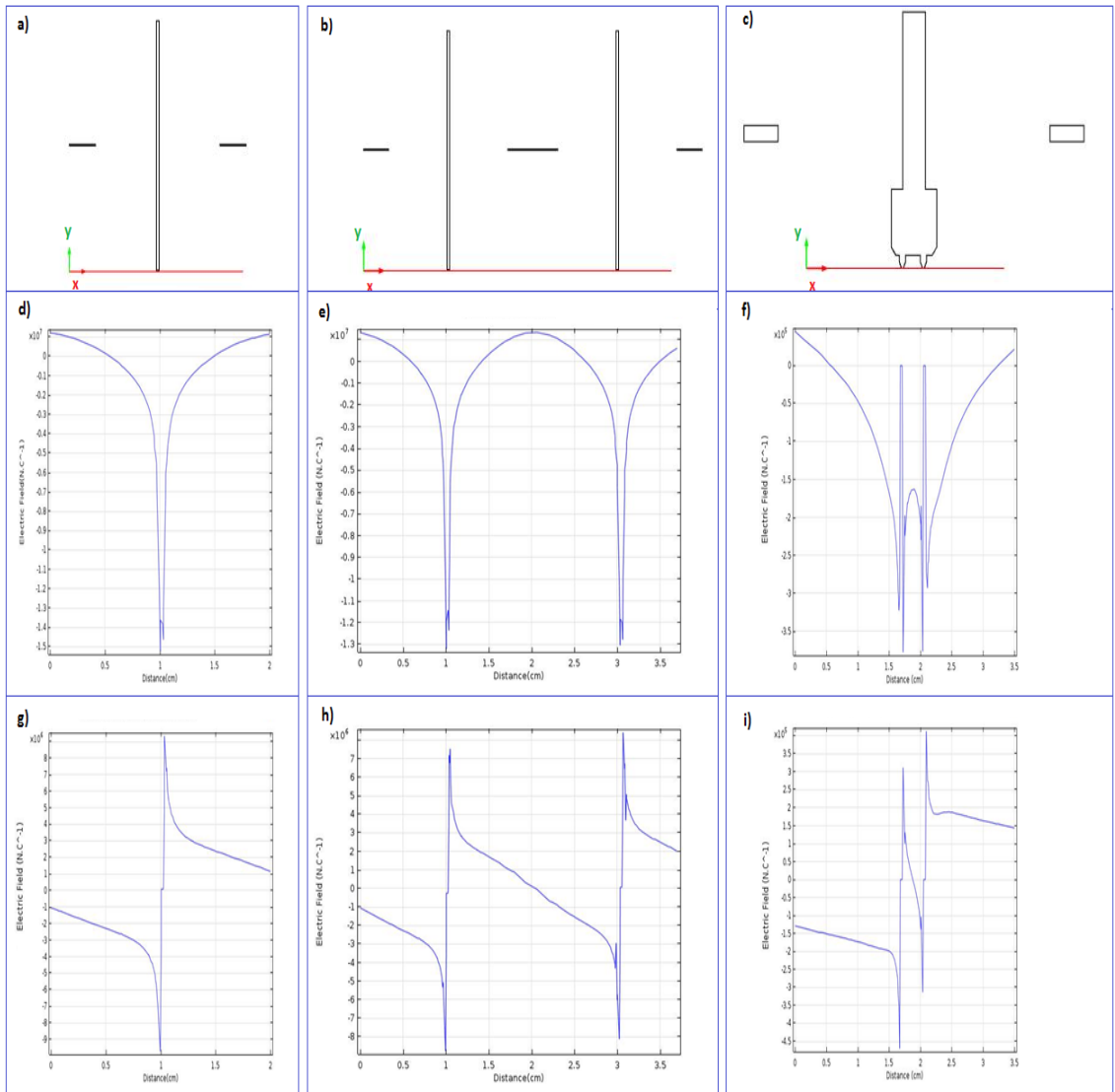
Figure 4.49: 2D Nozzle cross section (a, b and c), axial component of the electric field (d, e and f), the radial components of the electric field (g, h, and i) for each nozzle design. (All data related column-wise).

From the results obtained with the model, it was found that the overall behavior of the electric field component for all tested designs is similar. The design shows both radial and axial components lower than the other two configurations. This is as expected, due

to the fact that the single ring used in the new design has a much larger diameter than in other two designs. Comparing the magnitude of the axial to the radial component on each design, it can be seen that the magnitude of the radial component of the two designs reduced by a factor of 10 while in the single nozzle with four orifices design both remained almost equal. This shows azimuthal symmetry of an electric field in the single nozzle with four orifices. This can be seen in Figure 4.50 of the 3D model simulation carried out at two planes, one located at the nozzle tip and the other 2 mm below the nozzle. This suggests that the spray from each orifice is subjected to similar conditions. Hence, a similar breakup mechanism can be obtained.
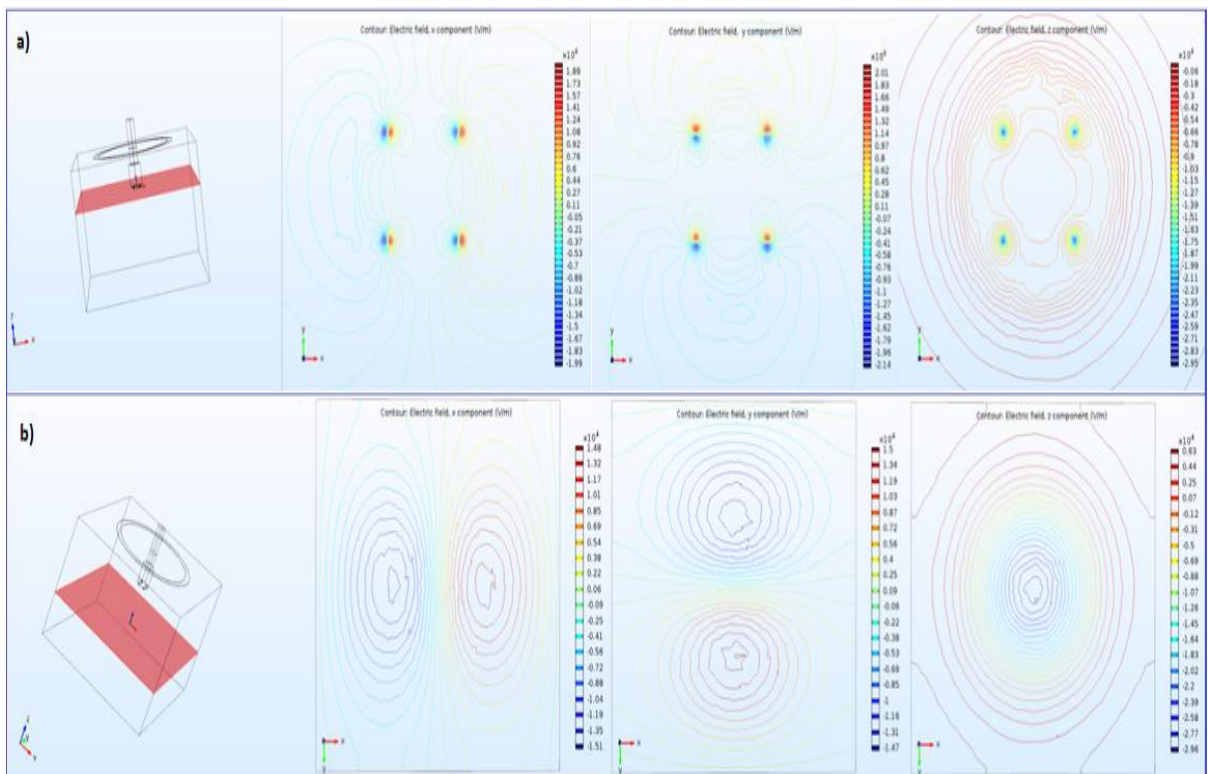
Figure 4.50: X-, Y-, and Z- electric field components at plane near the nozzle tip (a) and b) at 2 mm down the nozzle tip (b).

4.5.2 Electrospray Characteristics of 55% w/w IMF Solution

This section discusses the spray characteristics obtained using the single nozzle with four orifices.

4.5.2.1 Size Distribution

The experiments reported here were carried out at different total flow rates and different applied potentials. Here the total flow rate means the sum flow from the four orifices. For each flow rate in the uncharged situation, the droplet formation happened in the jetting regime and the applied electric potential was increased to a point where a whipping break-up was obtained for the selected flow rate. For each flow rate and applied potential droplets sizes and size distributions were evaluated. Figure 4.51 shows frequency histograms and corresponding cumulative frequency plots for the obtained droplet's populations at different operational parameters.
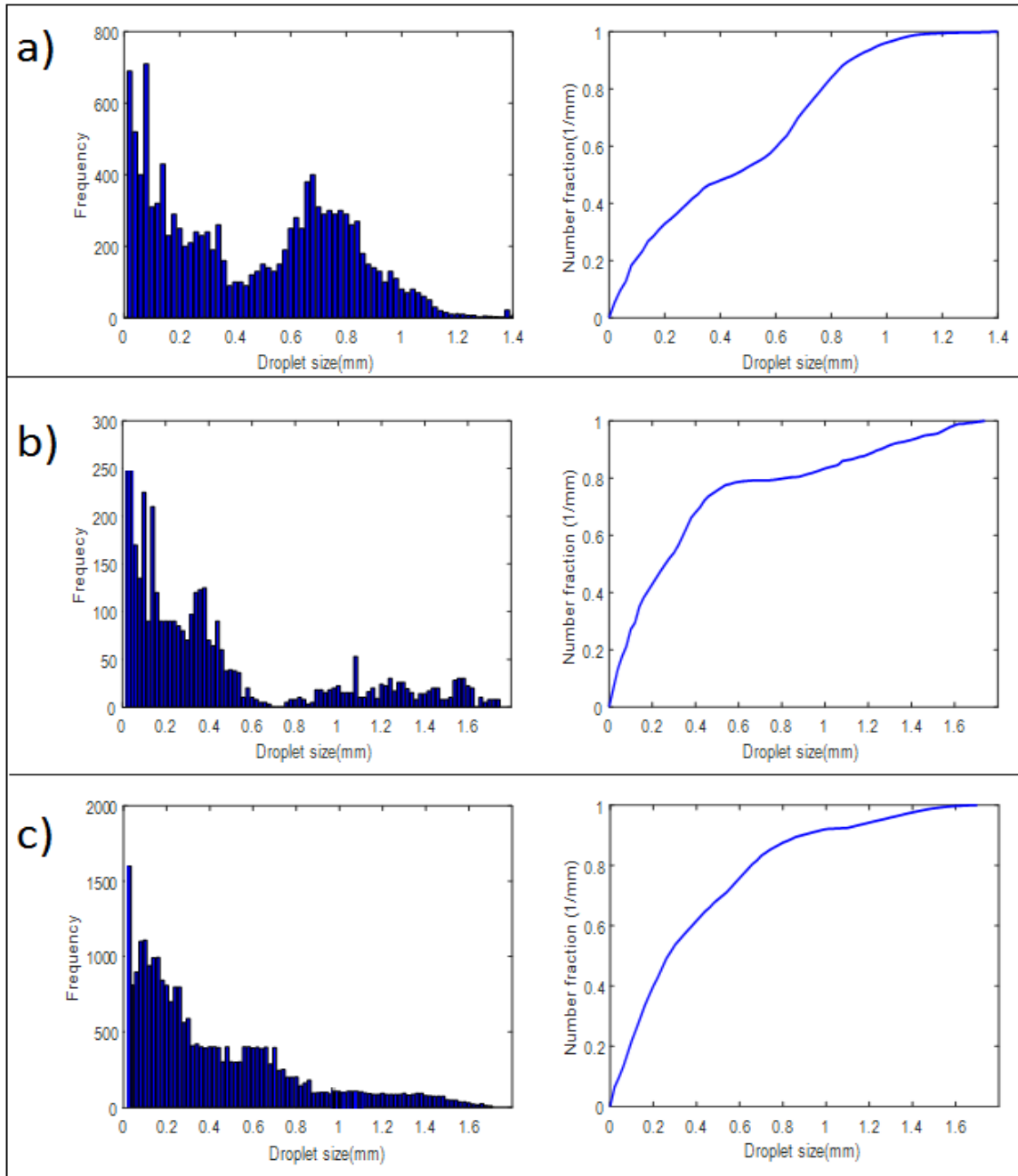
Figure 4.51: Frequency histograms and cumulative frequency plots for a) flow rate = 0.6 L h^{-1} and potential 18.6 kV, b) flow rate = 2.1 L h^{-1} and potential = 19.0 kV, and c) flow rate = 2.7 L h^{-1} and potential = 19.8 kV.

The obtained droplets size distributions were the characteristics of a whipping break up observed in previous section 4.4.2 with an exception of 0.6 L h⁻¹, in which a bimodal distribution was obtained with the main peak positioned at 0.6 mm. This shows that the droplets size was twice the nozzle diameter. From the images, the droplet formation process was a result of whipping break-up. The whipping, in this case, took a wavy shape. Therefore, during the motion, the liquid progressed to the leading end and then creating a thin filament at the curved surface. This becomes the breaking point which results in the formation of big and small droplets see Figure 4.52 (a). In the case of 2.1 L h⁻¹ and 2.7 L h⁻¹, the increased flow rate resulted in the formation of longer and thinner jets than in 0.6 L h⁻¹. Therefore, as jet progresses downward, the tip was observed to spray small droplets and at some point the jet break into ligaments. Such, ligaments proceeded to break into big and small droplets of different sizes. Figure 4.52 (b) shows a snapshot for the case of 2.7 L h⁻¹.
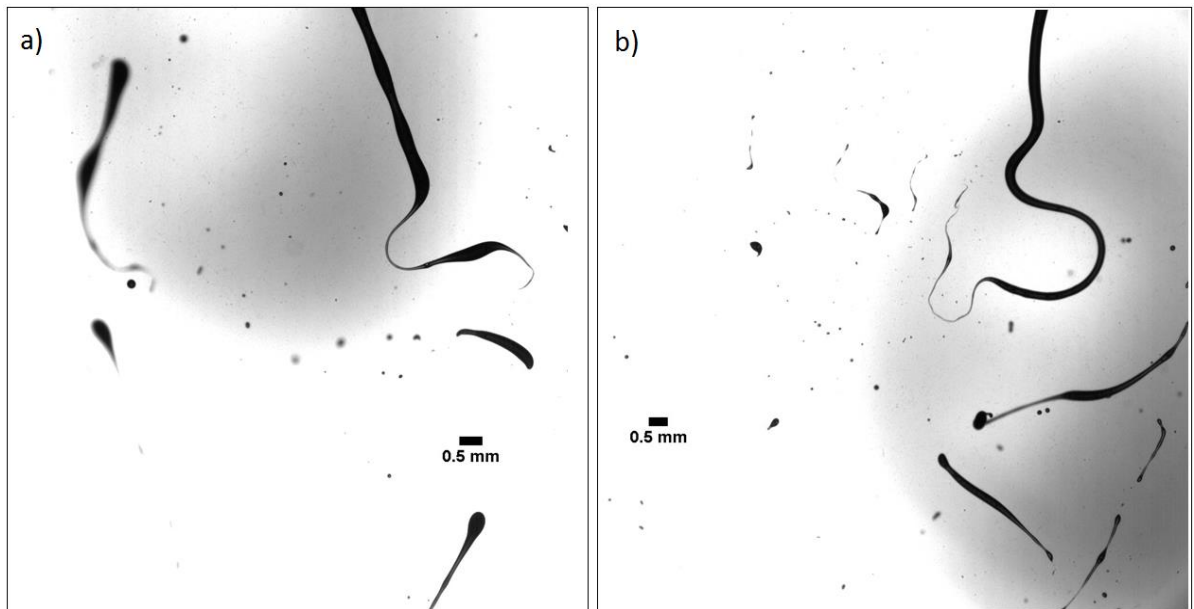
Figure 4.52: Jet break up and droplet formation for a) 0.6 L h⁻¹ (at 18.6 kV) and b) 2.7 L h⁻¹ (at 19.8 kV).

The minimum size of droplet obtained is 13 µm and the maximum size is 1.9 mm. From the cumulative curves, it can be noted that about 40-60% of the droplets population had their size less than the nozzle diameter (i.e. 300 µm). This suggested that, although EHDA led to the generation of small droplets while using high solid non-Newtonian liquid, their size distribution is wide.

An additional experiment was done using a flow rate of 2.7 L h^{-1} and an applied potential of 19.8 kV to quantify the droplet sizes for the individual nozzle tips. The tests were conducted by simply focusing the microscopic lens on each individual nozzle and recording high-speed movies independently. Figure 4.53 presents box plots, showing a comparison of the droplets sizes and size distributions obtained from the four orifices (here named as Jet). The red lines above the upper quartile are the outliers due to big droplets size produced that could not be contained within the fence. It can be seen that the spray characteristics obtained were more or less similar in terms of the droplets size distribution.
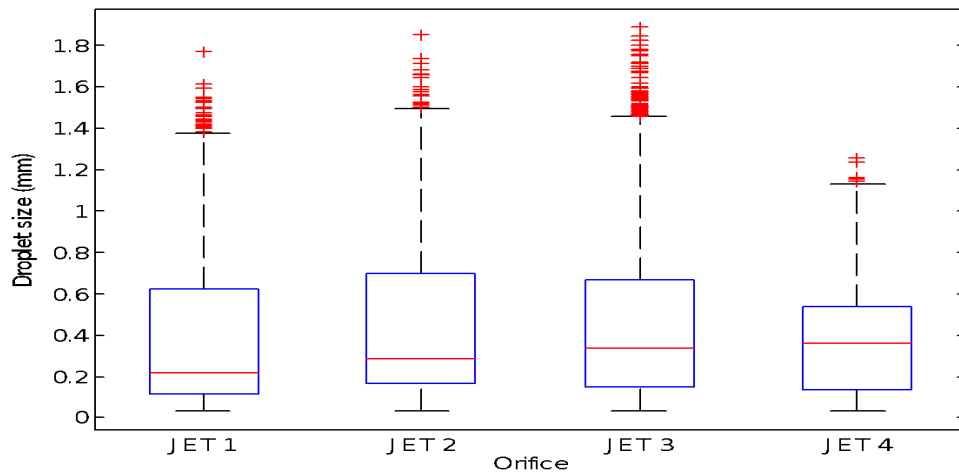
Figure 4.53: Comparison of droplet size obtained on four jets with a flow rate of 2.7 L h^{-1} and an applied potential of 19.8 kV.

94

4.5.2.2 Spray Dispersion

Figure 4.54 shows the influence of the electric field on the spatial dispersion of the four jets at different electric potentials and at a total flow rate of 1.7 L h^{-1}. From the figure, it can be observed that the effect of the electric field caused the jet to repel each other. This was an indication of a possibility for an electric potential to control the dispersion of droplets. Such observations have been noted in the case of multi-nozzle systems by Agostinho, 2013, Brouwer, 2011, Mwangi, 2013, and Yurteri et al., 2010.
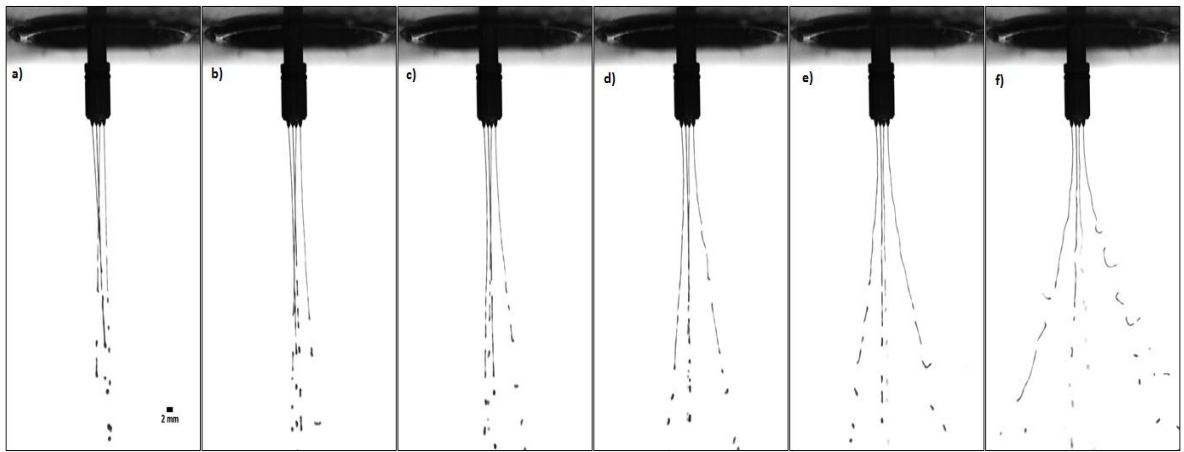
Figure 4.54: Spray envelope at 0 kV (a), 7 kV (b), 10 kV (c), 13 kV (d), 15 kV (e) and 19 kV (f) operated at a flow rate of 1.7 L h^{-1}.

Figure 4.55 is an image made by stacking a sequence of 200 snapshots. It shows the droplets spatial dispersion obtained at 19 kV when operated at a total flow rate of 2.1 L h^{-1}.

Figure 4.55: An image stack showing droplets dispersion obtained at a flow rate of 2.1 L h^{-1} and an applied potential of 19 kV (solid content = 55% w/w)

The image stack shows that the jets repel each other, their break up point starts at the same height, and the majority of droplets progresses downward along the path of the jet. However, a number of small droplets move away from the path and barely any droplet move to the center of the jets. This was attributed to the action of the charge created at the center of the jets and the charged droplets. The whipping breakup of the spray contributed to the wide spatial dispersion of small droplets, making them uncontrollable. This aspect is one of the considerations during the design of a spray drier evaporator.

Chapter 5
CONCLUSION AND RECOMMENDATIONS

5.1 **Conclusions**

The aim of this study was to investigate the intrinsic aspects of atomization by EHDA of non-Newtonian liquids with high solid content. With regard to electrospraying of IMF solutions in the dripping regime, the findings showed that only the spindle mode could be obtained for IMF solutions with solid content 30% and 40% w/w. While for solid content >40% w/w, the obtained modes could not be correlated to any of the conventional electrospray modes.

Electrospraying in the jetting regime seemed to be effective in the simple jet mode, which was obtained with the tested solutions (10-55% w/w). The spay characteristics showed variant droplets that were categorized into the main droplets, doubles, triples and satellite droplets. In addition to the recommendation of Agostinho (2013), that the simple jet mode is suitable for the process that requires large throughput, the results indicated that the whipping break up produced relatively small droplets compared to the varicose break-up. Due to increased solid content, the entrapment of air in the solution during preparation was inevitable, especially for solid content greater than 50% w/w. This contributed to the breaking process that generated ligaments instead of droplets as observed in Newtonian liquids. Such feed liquids are known to affect the morphology of the dried powder (Anandharamakrishnan, 2017). However, in the industry, the feed liquid is deaerated in a vacuum chamber reducing such occurrence (Carlsson and Jönnson, 2012).

The results of the spatial distribution of droplets showed that an applied potential led to droplet dispersion that can be controlled, but for a solution >50% w/w at high potential (i.e. 15 kV) the spray proved to be uncontrollable. This suggests that special

consideration needs to be undertaken in the design of an evaporator. One of the solutions could be employing charged plates alongside the drier chamber wall.

In an effort to apply EHDA to IMF solutions with a solid content of 55% w/w (interest in the industrial application), it led to designing and manufacturing of a nozzle with four orifices (ID = 300 mm). This nozzle enabled attaining of a throughput of ~3 L h^{-1}. The droplets obtained were in the range of ~13 μm to ~1.9 mm. Therefore, these results proved it difficult to obtain droplets with relatively narrow size distribution. But, based on these results and those obtained with whipping break up for 10% to 50% w/w IMF solution, EHDA atomization can successfully be applied to powder production, especially when high bulk density of the products is of concern.

5.2 Future Work

1. Additional studies are necessary to use solutions with high solid content to test the proposed EHDA system in a real- life evaporator with an aim to investigate the properties and morphology of the powder that would be produced after spray drying and to determine whether EHDA contribute to thermal efficiency of the production process.
2. Since the study shows that the atomization of Non-Newtonian liquids with high solid content using EHDA is possible, it would be important to investigate the rheological properties that influence break-up of droplets in these liquids to facilitate in the development of related EHDA scaling laws.

References

Agostinho, L. L. (2013). *Electrohydrodynamic atomization in the simple-jet mode: out-scaling and application (Doctoral dissertation)*. Delft University of Technology, Delft, The Netherlands.

Agostinho, L. L., Yurteri, C. U., Fuchs, E. C., Marijnissen, J. C. (2012). Monodisperse water microdroplets generated by electrohydrodynamic atomization in the simple-jet mode. *Applied Physics Letters, 100*(24), 1-4.

Agostinho, L. L., Yurteri, C. U., Wartena, J., Brouwer, S. P., Fuchs, E. C., Marijnissen, J. C. (2013). Insulated multinozzle system for electrohydrodynamic atomization in the simple-jet mode. *Applied Physics Letters, 102*(19), 1-5.

Almekinders, J. C., Jones, C. (1999). Multiple jet electrohydrodynamic spraying and applications. *Journal of Aerosol Science, 30*(7), 969-971.

Ambravaneswaran, B., Phillips, S. D., Basaran, O. A. (2000). Theoretical analysis of a dripping faucet. *Physical Review Letters, 85*(25), 5332-5335.

Ambravaneswaran, B., Subramani, H. J., Phillips, S. D., Basaran, O. A. (2004). Dripping-jetting transitions in a dripping faucet. *Physical Review Letters, 93*(3), 034501.

Anandharamakrishnan, C. (Ed.). (2017). *Handbook of drying for dairy products*. Hoboken, NJ: John Wiley & Sons.

Ashgriz, N., Yarin, A. L. (2011). Capillary instability of free liquid jets. In N. Ashgriz (ed.), *Handbook of atomization and sprays* (pp. 3-53). New York, NY: Springer.

Barnes, H. A. (2000). *A handbook of elementary rheology*. Wales: Institute of Non-Newtonian Fluid Mechanics.

Bhat, P. P., Appathurai, S., Harris, M. T., Pasquali, M., McKinley, G. H., Basaran, O. A. (2010). Formation of beads-on-a-string structures during break-up of viscoelastic filaments. *Nature Physics, 6*(8), 625-631.

Bienvenue, A., Jiménez-Flores, R., Singh, H. (2003). Rheological properties of concentrated skim milk: importance of soluble minerals in the changes in viscosity during storage. *Journal of Dairy Science, 86*(12) 3813-3821.

Bocanegra, R., Galán, D., Márquez, M., Loscertales, I. G., Barrero, A. (2005). Multiple electrosprays emitted from an array of holes. *Journal of Aerosol Science, 36*(12), 1387-1399.

Boger, D. V., Walters, K. (2012). *Rheological phenomena in focus* (vol. 4). New York, NY: Elsevier Science Publisher.

Bouman, S., Waalewijn, R., de Jong, P., van der Linden, J. H. (1993*).* Energy-efficient evaporators in the dairy industry. In P. A. Pilavachi (Ed.), *Energy efficiency in process technology* (pp. 455-464). New York, NY: Elsevier Science.

Bousfield, D. W., Keunings, R., Marrucci, G., Denn, M. M. (1986). Nonlinear analysis of the surface tension driven breakup of viscoelastic filaments. *Journal of Non-Newtonian Fluid Mechanics, 21*(1), 79-97.

Brouwer, S. P. (2011). *Design and characterization of a single-effect electrohydrodynamic desalinator (Masters dissertation)*. Delft University of Technology, Delft, The Netherlands.

Camelot, D. M. A., Hartman, R. P. A., Marijnissen, J. C. M., Scarlett, B., Brunner, D. (1999). Experimental study of the jet break up for ehda of liquids in the cone-jet mode. *Journal of Aerosol Science, 30*(7), 976-977.

Carlsson, H., & Jönsson, C. (2012). Separation of air bubbles from milk in a deaeration process. Retrieved from https://www.researchgate.net/profile/Christian_Joensson/publication/267687974_Separation_of_air_bubbles_from_milk_in_a_deaeration_process/links/5798df8d08aec89db7bb88f6/Separation-of-air-bubbles-from-milk-in-a-deaeration-process.pdf

Chen, D. R., Pui, D. Y. (1997). Experimental investigation of scaling laws for electrospraying: dielectric constant effect. *Aerosol Science and Technology, 27*(3), 367-380.

Chen, X. B. (2009). Modeling and control of fluid dispensing processes: a state-of-the-art review. The International Journal of Advanced Manufacturing Technology, 43(3), 276-286.

Chhabra, R. P. (2006). *Bubbles, drops, and particles in non-Newtonian fluids*. Boca Raton: CRC press.

Chhabra, R. P., Richardson, J. F. (2008). *Non-Newtonian flow and applied rheology: Engineering applications*. Oxford: Butterworth-Heinemann.

Chigier, N., Reitz, R. D. (1996). Regimes of jet breakup and breakup mechanisms-Physical aspects. Recent advances in spray combustion. *Spray Atomization and Drop Burning Phenomena, 1*, 109-135.

Christanti, Y., Walker, L. M. (2002). Effect of fluid relaxation time of dilute polymer solutions on jet breakup due to a forced disturbance. *Journal of Rheology, 46*(3), 733-748.

Clanet, C., Lasheras, J. C. (1999). Transition from dripping to jetting. *Journal of Fluid Mechanics, 383*, 307-326.

Clasen, C., Bico, J., Entov, V. M., McKinley, G. H. (2009). 'Gobbling drops': the jetting–dripping transition in flows of polymer solutions. *Journal of Fluid Mechanics, 636*, 5-40.

Cloupeau, M., Prunet-Foch, B. (1990). Electrostatic spraying of liquids: main functioning modes. *Journal of Electrostatics, 25*(2), 165-184.

Cloupeau, M., Prunet-Foch, B. (1989). Electrostatic spraying of liquids in cone-jet mode. *Journal of Electrostatics, 22*(2), 135-159.

De La Mora, J. F., Loscertales, I. G. (1994). The current emitted by highly conducting Taylor cones. *Journal of Fluid Mechanics, 260*, 155-184.

Eggers, J., Villermaux, E. (2008). Physics of liquid jets. *Reports on progress in physics, 71*(3), 036601.

Fenn, J. B., Mann, M., Meng, C. K., Wong, S. F., Whitehouse, C. M. (1989). Electrospray ionization for mass spectrometry of large biomolecules. *Science, 246*(4926), 64-71.

Fox, M., Akkerman, C., Straatsma, H., de Jong, P. (2010). Energy reduction by high dry matter concentration and drying. *New Food, 13*, 60-63.

Franck, A. (2004). Understanding rheology of structured fluids. *Book of TA Instruments,* 1-17. Retrieved from http://www.tainstruments.com/pdf/literature/AAN016_V1_U_StructFluids.pdf

Gamero-Casta-icirc, M., O, Hruby, V. (2001). Electrospray as a source of nanoparticles for efficient colloid thrusters. *Journal of Propulsion and Power, 17*(5), 977-987.

Ganan-Calvo, M, A., Davila, J., Barrero, A. (1997). Current and droplet size in the electrospraying of liquids. Scaling laws. *Journal of Aerosol Science, 28*(2), 249-275.

Goldin, M., Yerushalmi, J., Pfeffer, R., Shinnar, R. (1969). Breakup of a laminar capillary jet of a viscoelastic fluid. *Journal of Fluid Mechanics, 38*(04), 689-711.

Grace, J. M., Marijnissen, J. C. (1994). A review of liquid atomization by electrical means. *Journal of aerosol science, 25*(6), 1005-1019.

Hartman, R. P. A. (1998). *Electrohydrodynamic atomization in the cone-jet mode. From physical modeling to powder production (Doctoral dissertation).* Delft University of Technology, Tu Delft: The Netherlands.

Hartman, R. P., Brunner, D. J., Camelot, D. M., Marijnissen, J. C., Scarlett, B. (1999). Electrohydrodynamic atomization in the cone–jet mode physical modeling of the liquid cone and jet. *Journal of Aerosol Science, 30*(7), 823-849.

Hartman, R. P., Brunner, D. J., Camelot, D. M., Marijnissen, J. C., Scarlett, B. (2000). Jet break-up in electrohydrodynamic atomization in the cone-jet mode. *Journal of Aerosol Science, 31*(1), 65-95.

 Hendricks Jr, C. D. (1962). Charged droplet experiments. *Journal of Colloid Science, 17*(3), 249-259.

Hinds, W. C. (1999). *Aerosol technology: Properties, behavior, and measurement of airborne particles*. Canada: John Wiley & Sons.

Ijsebaert, J. C., Geerse, K. B., Marijnissen, J. C., Lammers, J. W. J., Zanen, P. (2001). Electro-hydrodynamic atomization of drug solutions for inhalation purposes. *Journal of Applied Physiology, 91*(6), 2735-2741.

Jaworek, A. T., Sobczyk, A. T. (2008). Electrospraying route to nanotechnology: an overview. *Journal of Electrostatics, 66*(3), 197-219.

Jaworek, A., Krupa, A. (1999). Classification of the modes of EHD spraying. *Journal of Aerosol Science, 30*(7), 975.

Kelly, A. L., Fox, P. F. ((2016). *Manufacture and properties of dairy powders*. In P. L. H. McSweeney, J. A. O'Mahony (Eds.), Advanced dairy chemistry (pp. 1-33). New York, NY: Springer.

Larson, R. G. (1999). *The structure and rheology of complex fluids* (vol. 150). New York: Oxford University Press.

Lefebvre, A. (1988). *Atomization and sprays* (vol. 1040, No. 2756). New York, NY: CRC Press.

Lin, S. P. (2003). *Breakup of liquid sheets and jets*. New York, NY: Cambridge University Press.

Lin, S. P., Reitz, R. D. (1998). Drop and spray formation from a liquid jet. Annual Review of Fluid Mechanics., 30(1), 85-105.

Loscertales, I. G., Barrero, A., Guerrero, I., Cortijo, R., Marquez, M., Ganan-Calvo, A. M. (2002). Micro/nano encapsulation via electrified coaxial liquid jets. *Science, 295*(5560), 1695-1698.

Macosko, C. W. (1994). *Rheology principles, measurements, and applications*. New York, NY: VCH Publ. Inc.

Marijnissen, J. C. (2004). Electro hydrodynamic atomization and its applications. *Journal of Aerosol Science*, (35), 3-4.

McKinley, G. H. (2005). Visco-elasto-capillary thinning and break-up of complex fluids. *Rheology Reviews*. 3.

Meesters, G. M., Vercoulen, P. H., Marijnissen, J. C., Scarlett, B. (1992). Generation of micron-sized droplets from the Taylor cone. *Journal of Aerosol Science, 23*(1), 37-49.

Middleman, S. (1965). Stability of a viscoelastic jet. *Chemical Engineering Science, 20*(12), 1037-1040.

Moghadam, H., Samimi, M., Samimi, A., Khorram, M. (2010). Electrospray modeling of highly viscous and non-Newtonian liquids. *Journal of Applied Polymer Science, 118*(3), 1288-1296.

Mun, R. P., Byars, J. A., Boger, D. V. (1998). The effects of polymer concentration and molecular weight on the breakup of laminar capillary jets. *Journal of Non-Newtonian Fluid Mechanics, 74*(1), 285-297.

Mutoh, M., Kaieda, S., Kamimura, K. (1979). Convergence and disintegration of liquid jets induced by an electrostatic field. *Journal of Applied Physics, 50*(5), 3174-3179.

Mwangi, M. A. (2017). *Design and characterisation of an electrohydrodynamic multinozzle atomizer for thermal desalination processes (Masters dissertation).* University of Nairobi, Nairobi, Kenya.

Notz, P. K., Basaran, O. A. (1999). Dynamics of drop formation in an electric field. *Journal of Colloid and Interface Science, 213*(1), 218-237.

Olson, E. (2011). Particle shape factors and their use in image analysis- Part 1: Theory. *Journal of GXP Compliance, 15*(3),85-86.

Orlu-Gul, M., Topcu, A. A., Shams, T., Mahalingam, S., Edirisinghe, M. (2014). Novel encapsulation systems and processes for overcoming the challenges of polypharmacy. *Current Opinion in Pharmacology, 18*, 28-34.

Pancholi, K., Ahras, N., Stride, E., Edirisinghe, M. (2009). Novel electrohydrodynamic preparation of porous chitosan particles for drug delivery. *Journal of Materials Science: Materials in Medicine, 20*(4), 917-923.

Reneker, D. H., Yarin, A. L. (2008). Electrospinning jets and polymer nanofibers. *Polymer, 49*(10), 2387-2425.

Scheideler, W. J., Chen, C. H. (2014). The minimum flow rate scaling of Taylor cone-jets issued from a nozzle. *Applied Physics Letters, 104*(2), 1-4.

Schramm, G. (1994). A practical approach to rheology and rheometry, 53-56. Germany: Karlsruhe: Haake.

Schuck, P., Jeantet, R., Dolivet, A. (2012). *Analytical methods for food and dairy powders*. West Sussex: John Wiley & Sons.

Shinjo, J., Umemura, A. (2010). Simulation of liquid jet primary breakup: Dynamics of ligament and droplet formation. *International Journal of Multiphase Flow, 36*(7), 513-532.

Shiryaeva, S. O., Grigor'ev, A. I. (1995). The semiphenomenological classification of the modes of electrostatic dispersion of liquids. *Journal of Electrostatics, 34*(1), 51-59.

Smith, D. P. (1986). The electrohydrodynamic atomization of liquids. IEEE Transactions on Industry Applications, (3), 527-535.

Stading, M. (2010). *Food rheology*. In C. Gallegos (Ed.), *Rheology, (Volume* II, pp. 283-306). Oxford: EOLSS Pulishers Co. Ltd.

Tang, K., Gomez, A. (1995). Generation of monodisperse water droplets from electrosprays in a corona-assisted cone-jet mode. *Journal of Colloid and Interface Science, 175*(2), 326-332.

Tatemoto, Y., Ishikawa, R., Takeuchi, M., Takeshita, T., Noda, K., Okazaki, T. (2007). An electrospray method using a multi-capillary nozzle emitter. *Chemical Engineering & Technology: Industrial Chemistry-Plant Equipment-Process Engineering-Biotechnology*, *30*(9), 1274-1279.

Taylor, G. I. (1964). Disintegration of water drops in an electric field. Proceedings of the Royal Society of London A: Mathematical, Physical and Engineering Sciences. *The Royal Society, 280*(1382), 383-397.

Trinh, B., Haisman, D., Trinh, K. T. (2007). Rheological characterisation of age thickening with special reference to milk concentrates. *Journal of Dairy Research, 74*(01), 106-115.

van Hoeve, W., Gekle, S., Snoeijer, J. H., Versluis, M., Brenner, M. P., Lohse, D. (2010). Breakup of diminutive Rayleigh jets. *Physics of Fluids, 22*(12), 122003.

Wu, W. D., Woo, M. W., Selomulya, C., Chen, X. D., Weeks, M. (2014). Towards spray drying of high solids dairy liquid: Effects of feed solid content on particle structure and functionality. *Journal of Food Engineering, 123*, 130-135.

Xie, J., Jiang, J., Davoodi, P., Srinivasan, M. P., Wang, C. H. (2015). Electrohydrodynamic atomization: A two-decade effort to produce and process micro-/nanoparticulate materials. *Chemical Engineering Science*, *125*, 32-57.

Xie, J., Marijnissen, J. C., Wang, C. H. (2006). Microparticles developed by electrohydrodynamic atomization for the local delivery of anticancer drug to treat C6 glioma in vitro. *Biomaterials, 27*(17), 3321-3332.

 Xie, J., Wang, C. H. (2007). Encapsulation of proteins in biodegradable polymeric microparticles using electrospray in the Taylor cone-jet mode. *Biotechnology and Bioengineering, 97*(5), 1278-1290.

Yıldırım, Ö. E., Basaran, O. A. (2006). Dynamics of formation and dripping of drops of deformation-rate-thinning and-thickening liquids from capillary tubes. *Journal of non-newtonian fluid mechanics*, *136*(1), 17-37.

Yurteri, C. U., Hartman, R. P., Marijnissen, J. C. (2010). Producing pharmaceutical particles via electrospraying with an emphasis on nano and nano structured particles-A review. *KONA Powder and Particle Journal*, *28*, 91-115.

Zeleny, J. (1917). Instability of electrified liquid surfaces. Physical Review, *10*(1), 1.

Zhang, H. B., Jayasinghe, S. N., Edirisinghe, M. J. (2006). Electrically forced microthreading of highly viscous dielectric liquids. Journal of electrostatics, *64*(6), 355-360.

Appendix

Dimensions and Connection of a Single Nozzle with Four Orifices
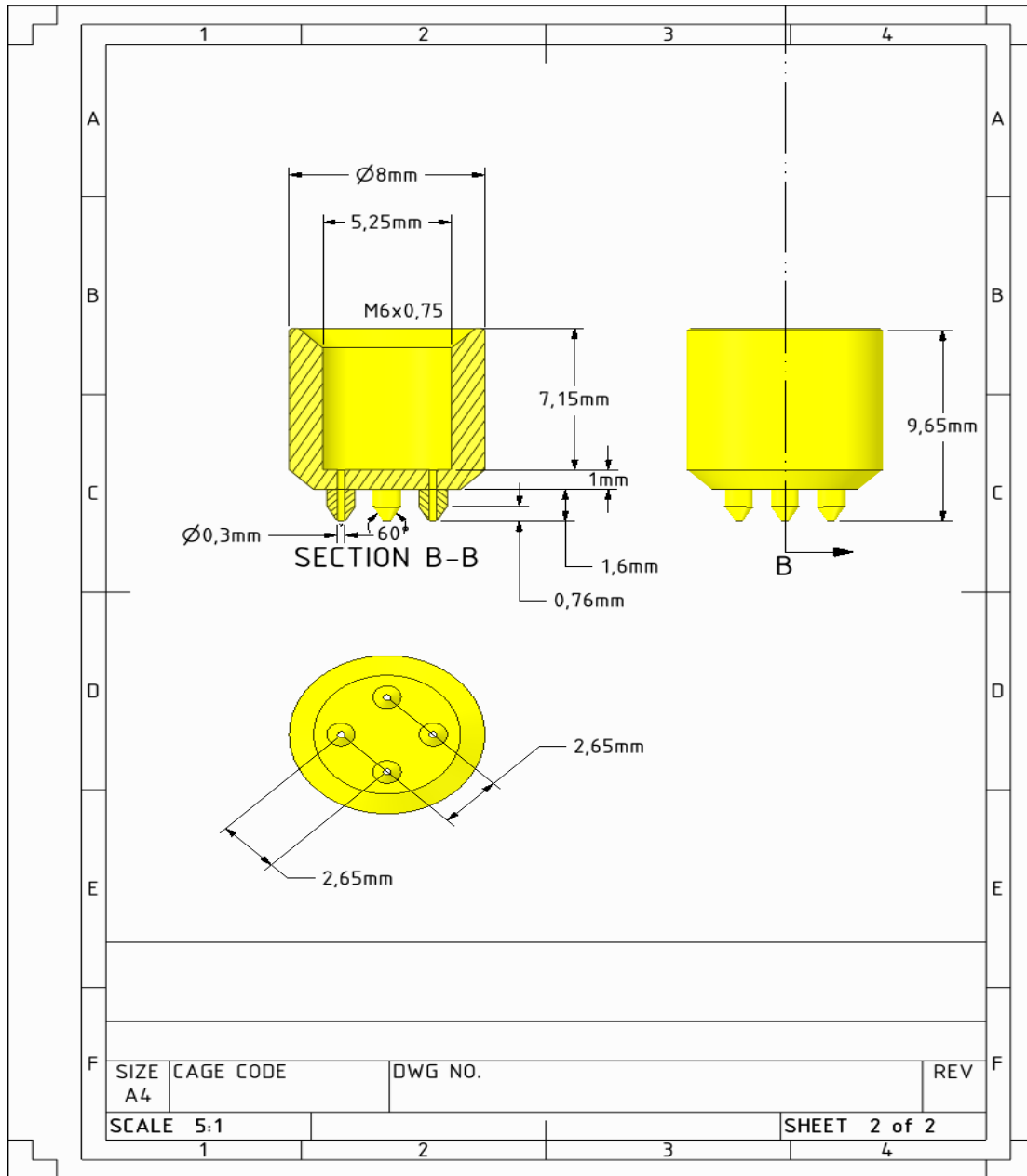
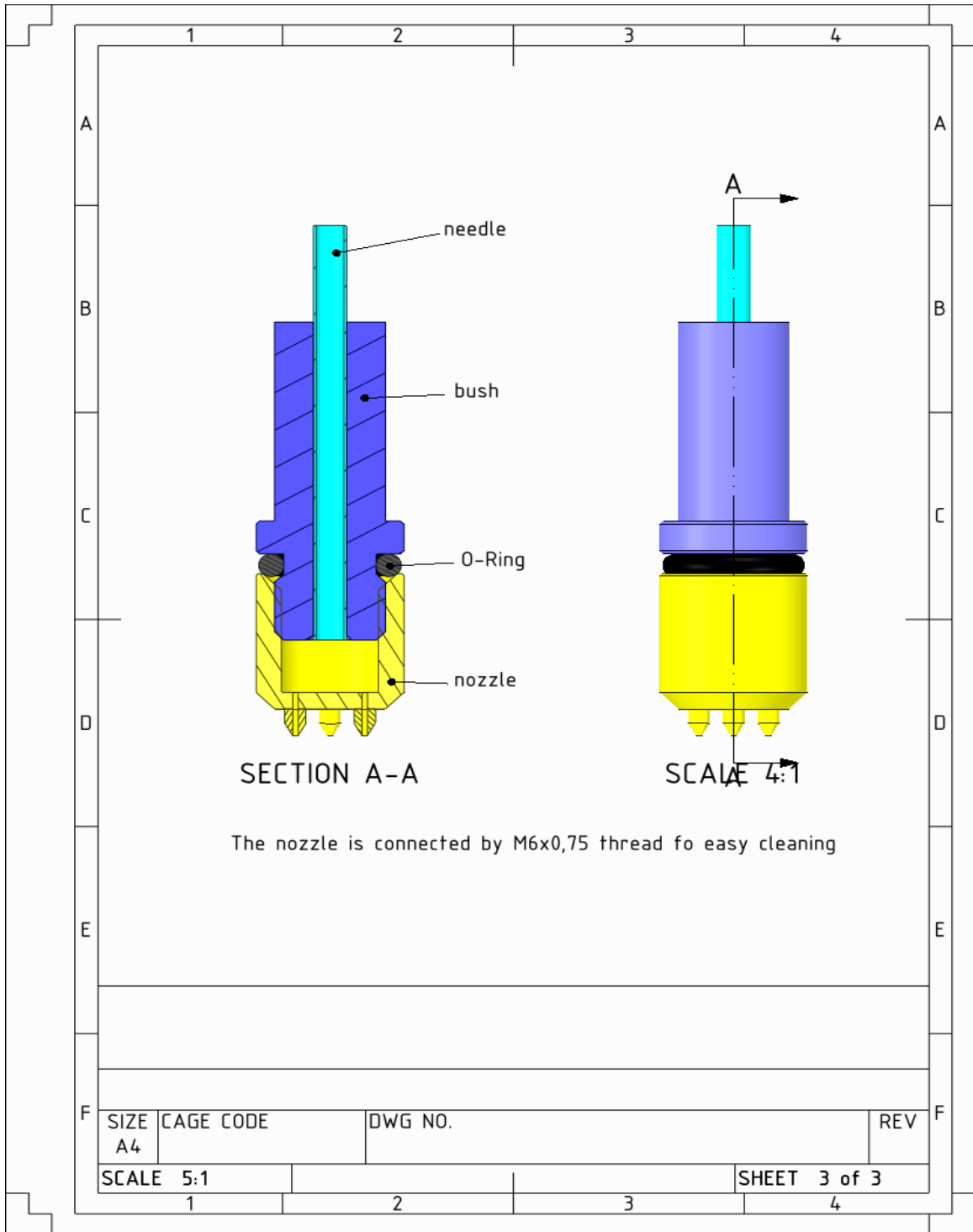

Figure 7.1: Dimensions of a single nozzle with four orifices.

Figure 7.2: Connections of the single nozzle with four orifices.